CRITICAL PROPERTIES OF THE DRIVEN-DISSIPATIVE ISING MODEL

By

Daniel Paz

A DISSERTATION

Submitted to
Michigan State University
in partial fulfillment of the requirements
for the degree of

Physics – Doctor of Philosophy

November 30, 2022

ABSTRACT

CRITICAL PROPERTIES OF THE DRIVEN-DISSIPATIVE ISING MODEL

By

Daniel Paz

Driven-dissipative quantum systems have become an important paradigm of nonequilibrium quantum systems, and aptly describe many common experimental setups in atomic, molecular, and optical physics. However, they are not understood as well as their equilibrium counterparts, and analytical solutions to the nonequilibrium dynamics are few and far between. Furthermore, phase transitions in driven-dissipative systems may host new universality classes, or connect to universality classes seen in equilibrium. In this work, we present a thorough analytical and numerical treatment of the driven-dissipative Ising model with infinite-range interactions and local spontaneous emission. This model is amenable to an exact field-theoretical solution via a quantum-to-classical mapping. We primarily focus on the critical properties, which show interesting similarities and differences in comparison with equilibrium and classical phase transitions. Notably, we identify two distinct universality classes in the phase diagram. A generic point on along the phase boundary falls under the same universality class as the infinite range classical Ising model with Glauber dynamics. However, in the weakly-dissipative limit we find that the system is in the same universality class as the finite-temperature equilibrium transition of the quantum Ising model. Furthermore, we discover a new notion of time-reversal symmetry which occurs near the phase boundary due to the interplay of drive and dissipation. Finally, we characterize various measures of entanglement in the model throughout the phase diagram by calculating the quantites known as the quantum Fisher information, the logarithmic negativity, and spin squeezing. We complement these findings by also calculating measures of total correlations in the system such as the von Neumann entropy and the mutual information.

Dedicated to Caley Harris and our two cats, Kubo and Hedwig

ACKNOWLEDGEMENTS

I would first like to thank my advisor and mentor, Mohammad Maghrebi. Your tutelage has helped mold me into the physicist and person I am today. I am grateful for the patience and understanding you have showed me over the past 6 years. To my parents, Deborah and Alexander Paz, thank you for teaching me how to learn and keep an open mind, for supporting my education, and always showing interest in whatever I am doing. I would also like to thank all of the wonderful friends I have made while in the physics program at MSU, namely Isaac Yandow, Abbie Cathcart, Tamas Budner, Kyle Krowpman, Thomas Chuna, Corey Cooling, and Alyssa Turcsak. Their friendship and camaraderie over the past six years is something I will always treasure. A big shoutout to the Michigan Super Smash Bros. Melee Community, with whom I spent a lot of my free time, and are now some of my closest friends. Alec Russell, Will Portnoy, Colin Anderson, Fred Lee, Alex Gamero and the rest of the gang who's names I omit purely due to lack of space, I want to thank you for welcoming me into your community and treating me like one of your own from day one. This would not be an acknowledgement section without mentioning my closest friend of almost two decades, Tony Pietra. We have grown alongside each other since middle school, and to this day you have supported me and stood by me through all of the good and the bad despite being separated by many states. Finally, thank you to Caley Harris, my partner of 6 years and love of my life. I would not have made it through graduate school, or the pandemic, without you. You showed patience with me when I was in crunch time for work, and listened to my many rants about physics (and everything else!) with open ears.

TABLE OF CONTENTS

KEY TO ABBREVIATIONS

NESS nonequilibrium steady state

DDIM Driven-dissipative Ising model

CPTP Completely positive trace-preserving map

AMO Atomic, molecular & optical

TRS Time-reversal symmetry

TRS* Modified time-reversal symmetry observed near the phaseboundary of the DDIM

CHAPTER 1

INTRODUCTION

1.1 Quantum Many-Body Physics and Critical Phenomena

A system of one or several atoms may be solved exactly. In contrast, realistic physical systems are composed of a macroscopic number of particles that are *interacting* with one another, and it is this fact that makes many-body systems difficult to solve but just as interesting in the phenomena they produce.

A principal feature of interest in quantum many-body systems is the *phase transition*, where a system transitions from one phase of matter to another. This transition may give rise to a critical behavior. The object that distinguishes these two phases is the *order parameter*, which is typically defined to be zero on one side while it assumes a finite value on the other. Second-order phase transitions, the primary focus of this work, are accompanied by spontaneous symmetry breaking, where a symmetry of the state is broken upon crossing the phase boundary. The symmetry-breaking is driven by the interactions of the model, not an external field. In addition, the fluctuations of the order parameter diverge at the phase boundary and the dynamics slows to a crawl, a primary signal of the phase transition.

Systems that exhibit the above properties are deemed *critical*. However, most critical phenomena is understood from the perspective of thermal equilibrium, where a many-body system is weakly coupled to a bath, and the state ρ is given by the Gibbs state

$$\rho_{\mathrm{EQ}} = e^{-H/T}\,, \tag{1.1}$$

where H is the system Hamiltonian and T is the bath temperature. In this work, we will instead be focusing on the phase transitions of nonequilibrium systems, where the state is no longer described by the thermal state in Eq. (1.1), and the dynamics is not governed by a hermitian, time-independent Hamiltonian (or a Hamiltonian at all!).

1.2 Driven-Dissipative Systems

Equilibrium physics describes many systems of interest, yet it only occupies a small corner of the space of physics. There are various nonequilibrium paradigms such as non-hermitian Hamiltonians, Floquet systems, and quench dynamics, each yielding their own plethora of rich physics. Of interest to us are *driven-dissipative systems*, or open quantum systems, where a Hamiltonian system is externally driven by a classical drive while weakly coupled to a bath. In this paradigm, the competition between the external drive and the dissipation due to the bath lead to a nonequilibrium steady state (NESS) at long times, which we denote as ρ_{SS}. In general, this state is not equivalent to the thermal state, i.e. $\rho_{\mathrm{SS}} \neq \rho_{\mathrm{EQ}}$.

Open quantum systems have received much attention both experimentally and theoretically in the past decade due to recent experimental advancements in AMO systems that allow for precise control over physical systems and, therefore, enable the engineering of various kinds of Hamiltonian and non-Hamiltonian dynamics. Dissipation is naturally present in any physical system. While dissipation is commonly considered detrimental to quantum behavior, together with specific drive fields, it can even lead to quantum coherence and entanglement. In this thesis, we will explore this point further by investigating the entanglement in a many-body NESS of dissipative dynamics.

The dynamics of open quantum systems is governed, under generic approximations, by a quantum master equation. Hence, these systems are more difficult to treat both analytically and numerically, and necessitate new techniques such as Keldysh field theory, which we discuss next.

1.3 Keldysh Field Theory

Many-body systems have a macroscopic number of degrees of freedom, and thus have a large Hilbert space. Specifically, the interaction leads to complicated many-body states. One cannot generally solve these systems exactly in a fashion similar to one, or few, particle systems. Therefore, many-body systems require a different framework. The natural language for a broad range of quantum many-body systems is quantum field theory, a description of the system that encodes the individual degrees of freedom into coarse-grained fields. This powerful representation significantly reduces

the variables one needs to keep track of. Field theory also has the added advantage of making many concepts of phase transitions and criticality explicit in the formalism. For example, the symmetry corresponding to the phase transition can always be made apparent at the level of the action. Furthermore, perturbative expansions with respect to the interaction strength can be made systematic, and semi-classical approximations are readily available. In addition to these benefits, field theory provides access to correlation and response functions, the principle objects of interest in many-body systems.

We will investigate nonequilibrium dynamics of driven-dissipative systems. This requires a more general kind of field theory, known as Keldysh field theory, to tackle. This field theory can be seen as the real-time path integral formulation, as opposed to the imaginary time formulation commonly used in equilibrium. While we gain the advantage of working in real time, and thus straightforward access to dynamics, we pay the price in additional degrees of freedom and a sign problem. More explicitly, Keldysh field theory requires twice the number of fields when compared with the imaginary time and Feynman path integral formulations. In addition to this, the field theory comes with additional properties and quirks which we will discuss later in the text.

1.4 Thesis Overview

The thesis will be organized as follows: Chapter 2 will introduce the fundamental concepts required to understand the rest of the thesis. These fundamental concepts range from the density matrix formalism, necessary to treat open systems, to Keldysh field theory and mapping open quantum system to Keldysh path integrals. In Ch. 3, we discuss the relevant models that we will be investigating, namely the open Dicke model and the driven-dissipative Ising model. Furthermore, we show how one would map the driven-dissipative Ising model to a field theory as well as the tools necessary to treat such a field theory. Our primary tools will be the saddle-point solution of the Keldysh action, a quadratic expansion of said action, and diagrammatics. Up to this point, we have only discussed analytical techniques, however, it is important to utilize numerical simulations to supplement analytical results; we introduce the required numerical techniques in Ch. 4. In this

chapter, we discuss exact diagonalization and quantum trajectories, and show how they are modified to take advantage of the system's permutation symmetry. Chapter 5 utilizes the concepts developed in Ch. 3 and Ch. 4 to investigate the critical properties of the driven-dissipative Ising model. We focus on the effective temperature of the steady state, as well as the critical exponents and finite-size scaling of the correlation and response functions near the phase boundary. Next, we shift focus in Ch. 6 to the emergent modified time-reversal symmetry exhibited by the driven-dissipative Ising model near the phase transition. We show how this symmetry emerges by constructing an effective field theory. Finally, Ch. 7 reports the entanglement features of the steady state in the driven-dissipative Ising model throughout the entire phase diagram. We calculate entanglement quantities such as the logarithmic negativity, the quantum Fisher information, and the spin squeezing parameter. These quantities are compared with measures of total correlations, i.e. the von Neumann entropy and the mutual information.

CHAPTER 2

OPEN SYSTEMS FUNDAMENTALS

In this chapter we introduce the reader to the fundamental concepts upon which the rest of the thesis is built upon. We begin by introducing the density matrix, a powerful representation of a quantum state, and discuss its important properties. Next, we discuss the dynamical equation governing the time-evolution of a subsystem of a larger quantum system, the so-called Lindblad equation. The Lindblad equation will describe the dynamics of all models considered in this thesis. Finally, we require the tools to handle open many-body quantum systems and so we provide a compact introduction to Keldysh field theory. This field theory is capable of describing nonequilibrium dynamics of open many-body systems and will prove necessary for our analysis. Before proceeding, we note that most of what we will be covering in this chapter is more thoroughly described in the textbooks of the field. Extensive discussions on density matrices and open quantum systems can be found in Refs. [1–3], and a comprehensive text on Keldysh field theory in Ref. [4].

2.1 The Density Matrix

The dynamics of any closed system in Quantum Mechanics is governed by the Schrodinger equation,

$$i\partial_t|\psi(t)\rangle = H|\psi(t)\rangle\,, \tag{2.1}$$

where $|\psi(t)\rangle$ is a state at time t, and H is a general Hamiltonian. This equation governs the dynamics of the quantum state at all times, and (for a time-independent Hamiltonian) has the solution

$$|\psi(t)\rangle = e^{-iHt}|\psi(0)\rangle\,. \tag{2.2}$$

Quantum states have the unique property of posibbly being *entangled*, where a wavefunction describing two or more particles cannot be separated into a product state. As an example, consider two particles where each particle can be in either the $|1\rangle$ state or the $|0\rangle$ state. The wavefunction of the two-particle state can be a product state

$$|\psi\rangle = |\psi_1\rangle\,|\psi_2\rangle\ , \tag{2.3}$$

where $|\psi_{1/2}\rangle$ is the wavefunction for particle 1 or 2. However, it is also possible for $|\psi\rangle$ to be an entangled state, where $|\psi\rangle \neq |\psi_1\rangle\,|\psi_2\rangle$. An example of an entangled state is

$$|\psi\rangle = \frac{1}{\sqrt{2}}(|1\rangle\,|1\rangle + |0\rangle\,|0\rangle)\,. \tag{2.4}$$

Equation (2.4) cannot be separated into a product of single-particle states like we see in Eq. (2.3), which is the definition of entangled. It is important to emphasize that there exists no analogue of this phenomena in classical systems, and that entanglement is a signature feature of quantum mechanics and the source of much of the interesting physics observed in quantum systems.

At the level of the wavefunction, we learn that the expectation value of an operator O with respect to a state $|\psi\rangle$ is given by

$$\langle O\rangle_t = \langle\psi(t)|O|\psi(t)\rangle\,. \tag{2.5}$$

However, this is a specific case of a more general form of the expectation value. More generally, the expectation value can be written in terms of the *density matrix* ρ as

$$\langle O(t)\rangle = \mathrm{Tr}(O(t)\rho)\,. \tag{2.6}$$

In the case that

$$\rho(t) = |\psi(t)\rangle\langle\psi(t)|\,, \tag{2.7}$$

the density matrix is in a *pure* state, and we reproduce the expectation value in Eq. (2.5). Density matrices can also be *mixed*,

$$\rho = \sum_i p_i\,|p_i\rangle\langle p_i|\,, \tag{2.8}$$

where p_i and $|p_i\rangle$ are the eigenvalues and eigenvectors of ρ respectively. The density matrix has three important properties: it is

1. Hermitian: $\rho^\dagger = \rho$, where we have taken the adjoint of the density matrix.

2. Positive semi-definite: All eigenvalues p_i of the density matrix satisfy $p_i \geq 0\,\forall i$.

3. Unit trace: $\mathrm{Tr}(\rho) = \sum_i p_i = 1$, i.e. the state is normalized.

Properties 2 & 3 imply that the eigenvalues of the density matrix can be interpreted as probabilities of being in the corresponding quantum state. In other words, the density matrix is a classical mixture over quantum states, where the probability of being in the eigenstate $|p_i\rangle$ is the corresponding eigenvalue p_i. For a pure state like we have in Eq. (2.7), we only have one non-zero eigenvalue which equals one. We can take this as the definition of a pure state. In the more general case of a mixed state, there will be more than one non-zero eigenvalue of the density matrix. Taking the time derivative of Eq. (2.7), we obtain the equation that governs the dynamics of the density matrix,

$$\partial_t \rho = -i[H, \rho]\,, \tag{2.9}$$

where the brackets denote the commutator. This equation is known as the von Neumann equation, and is essentially the Schrodinger equation for density matrices. It has the same form as the Heisenberg equation that describes operator dynamics, up to a minus sign,

$$\partial_t O = i[H, O]\,, \tag{2.10}$$

where O is a generic operator.

It is often the case that the entire quantum system is composed of multiple subsystems, however, we are typically only interested in one of the subsystems. More formally, suppose we had two subsystems denoted by A and B with the state $|\psi_{AB}\rangle$ and Hamiltonian H_{AB}, and we chose the basis states $|i_A\rangle \in \mathcal{H}_A\,, |j_B\rangle \in \mathcal{H}_B$, where $\mathcal{H}_A, \mathcal{H}_B$ are the Hilbert spaces for subsystems A and B respectively. The basis states of the composite system reside in the composite space spanned by $|i_A\rangle \otimes |j_B\rangle \in \mathcal{H}_A \otimes \mathcal{H}_B$. If we are interested in only subsystem A, then we must introduce some operation that integrates over the degrees of freedom in subsystem B. To perform this operation, we require the density matrix picture. When starting from a wavefunction describing the entire system, the density matrix is a pure state given by

$$\rho = |\psi_{AB}\rangle\langle\psi_{AB}|\,, \tag{2.11}$$

where

$$|\psi_{AB}\rangle = \sum_{i_A, j_B} c_{i_A, j_B} |i_A\rangle |j_B\rangle\,. \tag{2.12}$$

In the case that ρ already describes a subsystem entangled with a larger quantum system, we instead have a *mixed* state. We now introduce the *partial trace* operation, which traces over the Hilbert space of one subsystem,

$$\rho_A = \mathrm{Tr}_B(\rho) = \sum_{i_A, i'_A} \left(\sum_{j_B} c_{i_A, j_B} c^*_{i'_A, j_B} \right) |i_A\rangle\langle i'_A| \ . \tag{2.13}$$

The resultant reduced density matrix ρ_A is still a bonafide density matrix that satisfies properties 1 through 3. However, the density matrix describing subsystem A is, in general, a mixed state, as opposed to the pure state in Eq. (2.11) describing the entire system. This is a common feature of tracing out degrees of freedom. We reduce the size of the state and the number of degrees of freedom to keep track of, but lose the explicit information pertaining to the traced out degrees of freedom. Furthermore, correlations between the two subsystems appear as a classical mixture of different quantum states in the resultant reduced density matrix. Once can see this final point by supposing that $\rho = \rho_A \otimes \rho_B$ is a product state and tracing out subsystem B. It is straightforward to see that the state of the subsystem A remains unchanged, which is purely due to the absence of correlations between the two subsystems.

Expectation values are handled straightforwardly when the Hilbert space is composed of multiple subsystems. For operators $O_A : \mathcal{H}_A \to \mathcal{H}_A$ (and similarly for subsystem B), we have

$$\langle O_A \rangle = \mathrm{Tr}\big((O_A \otimes I_B)\rho\big) \,, \qquad \langle O_B \rangle = \mathrm{Tr}\big((I_A \otimes O_B)\rho\big) \,. \tag{2.14}$$

Most importantly, the reduced density matrix defined in Eq. (2.13) preserves the expectation values of the original density matrix,

$$\langle O_A \rangle = \mathrm{Tr}(O_A \rho_A) = \mathrm{Tr}\big((O_A \otimes I_B)\rho\big) \,. \tag{2.15}$$

This shows that we still have access to all observables in system A once we trace out system B.

2.2 Lindblad Equation

To determine the dynamics of the reduced density matrix, we must take the partial trace of Eq. (2.9). In general, this is a non-trivial task for interacting subsystems. To make analytical progress,

let us take subsystem B to consist of a bath or a reservoir of many degrees of freedom. Furthermore, we assume that the bath and our system of interest are weakly coupled (the Born approximation) and that the bath has a short-time memory of its interactions with the system of interest (the Markov approximation). We define $H = H_A + H_B + H_I$, where H_A and H_B are the system and bath Hamiltonians respectively, and H_I characterizes the interactions between the bath and the system. Taking the partial trace over subsystem B in Eq. (2.9), in combination with the above approximations, leads to the well-known Lindblad equation [5, 6],

$$\partial_t \rho \equiv \mathcal{L}[\rho] = -i[H, \rho] + \sum_\alpha L_\alpha \rho L_\alpha^\dagger - \frac{1}{2}\{L_\alpha^\dagger L_\alpha, \rho\}\,. \tag{2.16}$$

In an abuse of notation, we denote the density matrix of subsystem A as ρ. We also neglect the Lamb shift, which is typically small compared to the energy scales of the Hamiltonian [3].

In its entirety, the Lindblad equation is composed of two parts: the first term is simply the von Neumann term for subsystem A and characterizes the coherent dynamics of the state, and the sum over α is the dissipative contribution that was introduced after tracing out the bath. The operators L_α are called Lindblad operators, or jump operators, in the literature, and they represent dissipative processes whose origin lies in the interaction between the environment and the system. The exact form of the Lindblad operators depends on the form of the system Hamiltonian, as well as the system-bath interaction. A microscopic derivation of the master equation may be found in many textbooks; see for example [3, 5, 7].

The object $\mathcal{L}$ is called the Liouvillian and is what is known as a superoperator, an object that takes operators to operators and acts on them from both sides. It is the principle object of interest in open quantum systems that satisfy the Born-Markov approximation, including many quantum optical systems and those with light-matter interactions; examples are cavity QED and circuit QED [8–11].

The Liouvillian generates non-unitary dynamics, as seen by the dissipative terms, but still preserves the three important properties of the density matrix:

1. Hermiticity: $\mathcal{L}[\rho]^\dagger = \mathcal{L}[\rho]$.

2. (Complete) Positivity: $\mathcal{L}[\rho] \geq 0$.

3. Unit Trace: $\mathrm{Tr}(e^{t\mathcal{L}}[\rho]) = 1$.

In fact, Eq. (2.16) is the most general equation that satisfies these requirements [12]. Complete positivity (Point 2 above) states that $\mathcal{L}$ is completely positive if $(\mathcal{L} \otimes 1_B)[\rho] \geq 0$, where we have enlarged the Hilbert space to include subsystem B, and 1_B is the identity in this new subspace. The three properties listed above make $\mathcal{L}$ a completely positive trace preserving (CPTP) map.

As an operator of operators, the Liouvillian has *eigenoperators* with corresponding eigenvalues, as opposed to eigenvectors in the case of the Hamiltonian, such that $\mathcal{L}[\rho_i] = \lambda_i \rho_i$. The eigenvalues of the Liouvillian always have $\mathrm{Re}[\lambda_i] \leq 0$, and are purely real or come in complex conjugate pairs. The condition on the real part of the eigenvalues tells us that most of the eigenoperators are short-lived and decay away, as any state evolving under Liouvillian dynamics can be written as $\rho(t) = \sum_i c_i e^{\lambda_i t} \rho_i$ where c_i are constants. Most notably, the Liouvillian typically has at least one eigenoperator with a corresponding eigenvalue of zero, i.e. $\mathcal{L}[\rho_{\mathrm{ss}}] = 0$. This is the steady state of the system, and is what we will be focusing on in the rest of this thesis.

2.2.1 Vectorization

It is difficult, in general, to solve a many-body Hamiltonian system due to interactions as well as the size of the Hilbert space. For example, for a Hamiltonian comprised of N 2-level systems, the Hilbert space will have dimension 2^N. This limits numerical techniques like exact diagonalization to a system size of about $N = 25$ with state of the art methods. Analytically, if we are interested in ground state physics, then we must deal with the non-trivial problem of finding the ground state eigenvector of the Hamiltonian (or use many-body methods such as field theory or statistical mechanics). Now consider the Liouvillian superoperator $\mathcal{L}$. To learn about its long-time behavior we must now solve for the steady state eigenoperator as opposed to a vector, for which the Hamiltonian toolbox does not necessarily apply. However, we can transform the superoperator into a matrix (albeit a non-hermitian one!) by performing a simple procedure called vectorization. There are different

ways to define vectorization. Here, we define the following operation

$$\rho = \sum_{i,j} c_{i,j} \left|i\right\rangle \left\langle j\right| \rightarrow \left|\rho\right\rangle\!\right\rangle = \sum_{i,j} c_{i,j} \left|i\right\rangle \left|j\right\rangle \ , \qquad A\rho B \rightarrow A \otimes B^T \left|\rho\right\rangle\!\right\rangle \ , \tag{2.17}$$

where A and B are any operator. Applying this operation to $\mathcal{L}$, we find

$$\mathbb{L} = -i(H \otimes I - I \otimes H^T) + \sum_{\alpha} L_\alpha \otimes L_\alpha^* - \frac{1}{2}\left(L_\alpha^\dagger L_\alpha \otimes I + I \otimes L_\alpha^T L_\alpha^*\right) . \tag{2.18}$$

For the rest of this work, we use the double angle brackets on vectorized states which we call superkets, and we use the blackboard font to denote vectorized superoperators that now take the form of matrices in a larger space. From now on, we also define the "upper" and "lower" branches of the vectorized Liouvillian, such that $O^{(u)} = O \otimes I$ and $O^{(l)} = I \otimes O$ denote operators on the upper and lower branches respectively.

With this transformation, we have successfully converted the Liouvillian into a matrix but at the cost of *doubling* the size of the Hilbert space. This means that numerical simulations are restricted to roughly half of the system size available to Hamiltonian systems. In addition, the matrix $\mathbb{L}$ can be viewed as a non-hermitian Hamiltonian, $\mathbb{L}^\dagger \neq \mathbb{L}$, which prohibits the use of certain numerical techniques that require hermiticity. The vectorization procedure, however, does make analytical treatment easier as it makes the mapping of Hamiltonian/equilibrium tools to this nonequilibrium setting straightforward. We will see this explicitly when we take advantage of the form in Eq. (2.18) to map the system to a field theory using a quantum-to-classical mapping in Sec. 2.3.

Expectation values of operators take on a different form in this vectorized representation. We first note that the space of operators acting on $\mathcal{H}_A$ can also be interpreted as a vector space for the space of superoperators (i.e. $\mathcal{L}$ or $\mathbb{L}$). This interpretation is directly related to the vectorized picture, as exhibited by the inner prodcut,

$$\mathrm{Tr}(A^\dagger B) = \langle\langle A|B\rangle\rangle \ , \tag{2.19}$$

for two operators A and B. It is simple to prove this equality by vectorization of the left-hand side. Applying this to the relation $\mathrm{Tr}(\rho) = 1$, we find that we can alternatively represent the trace condition as

$$\mathrm{Tr}(\rho) = 1 \rightarrow \langle\langle I|\rho\rangle\rangle = 1 \, , \tag{2.20}$$

where $|I\rangle\rangle$ is the vectorized Identity matrix. Applying the same procedure to Eq. (2.6), we find

$$\langle O \rangle = \langle\langle O|\rho\rangle\rangle \ , \tag{2.21}$$

the vectorized representation of the expectation value of the operator O. However, we can construct two other, equivalent, forms for the expectation value of O in the vectorized representation. Recalling that $O\rho \rightarrow O^{(u)} |\rho\rangle\rangle$ and $\rho O \rightarrow O^{(l)T} |\rho\rangle\rangle$, we can equivalently define the expectation value as

$$\langle O \rangle = \langle\langle I| O^{(u)} |\rho\rangle\rangle = \langle\langle I| O^{(l)T} |\rho\rangle\rangle \ . \tag{2.22}$$

In the rest of the thesis, we will use whichever of the three definitions is most suitable.

2.3 Keldysh Field Theory Crash Course

The treatment of nonequilibrium many-body systems demands powerful tools. The presence of interactions drastically increases the complexity of the many-body states due to non-trivial correlations between system constituents. One such tool is Keldysh field theory, a field theory designed to handle nonequilibrium dynamics of a density matrix. In this section we will describe the damped quantum harmonic oscillator with a field theory in the form of a path integral, and discuss some basic properties of Keldysh field theories. Most of this section will be taken from the review in [13] as well as section III of [14]. Also helpful is the bible of Keldysh field theory, Kamenev's thorough textbook [4].

Our starting point is the Lindblad equation for a single cavity mode coupled to the external vacuum. The QED vaccuum is to be taken as the bath and is assumed to satisfy the Born-Markov approximation. In this case, the Hamiltonian $H = \omega_0 a^\dagger a$ is simply that of a harmonic oscillator with detuning ω_0, and the Lindblad operator $L = \sqrt{\kappa} a$ represents the dissipative process of the cavity leaking a photon out to the environment at a rate κ. The resultant Lindblad equation takes the form

$$\mathcal{L}[\rho] = -i\omega_0 [a^\dagger a, \rho] + \kappa (a\rho a^\dagger - \frac{1}{2}\{a^\dagger a, \rho\}) \, . \tag{2.23}$$

The operators a and $a^\dagger$ are the bosonic raising and lowering operators, and satisfy the bosonic commutation relation $[a^\dagger, a] = 1$.

The density matrix at time t is given by $\rho(t) = e^{t\mathcal{L}}[\rho]$, where the exponential of the superoperator is defined with the usual power series. We define the nonequilibrium partition function $Z = \mathrm{Tr}(\rho(t)) = 1$, different from the equilibrium partition function which could take any (positive) value. Our goal now is to map Z to a path integral over the fields. We apply our vectorization process to the nonequilibrium partition function to find

$$Z = \langle\langle I|\, e^{t\mathbb{L}}\, |\rho\rangle\rangle \ . \tag{2.24}$$

The vectorized form of the Liouvillian is

$$\mathbb{L} = -i\omega_0(a^{(u)\dagger}a^{(u)} - a^{(l)T}a^{(l)*}) + \kappa\left(a^{(u)}a^{(l)*} - \frac{1}{2}(a^{(u)\dagger}a^{(u)} + a^{(l)T}a^{(l)*})\right) \tag{2.25}$$

The form of this equation should be reminiscent of the starting point for the derivation of the Feynman path integral. Following a similar process, we perform a Trotter decomposition [15] of the time translation generator

$$\langle\langle I|\, e^{t\mathbb{L}}\, |\rho\rangle\rangle = \lim_{M\to\infty} \langle\langle I|\left(e^{\delta t\mathbb{L}}\right)^M |\rho\rangle\rangle \ , \tag{2.26}$$

where $\delta t = t/M$. This relation is exact. After every time step k we introduce a resolution of the identity in the basis of the coherent states,

$$\mathbb{I}_k = \int \frac{d\phi_k^{(u)} d\phi_k^{(u)*}}{\pi} \int \frac{d\phi_k^{(l)} d\phi_k^{(l)*}}{\pi} e^{-\phi_k^{(u)*}\phi_k^{(u)}} e^{-\phi_k^{(l)*}\phi_k^{(l)}}\, |\phi_k^{(u)}\rangle\langle\phi_k^{(u)}| \otimes |\phi_k^{(l)*}\rangle\langle\phi_k^{(l)*}| \ , \tag{2.27}$$

where the coherent states are defined by $a\,|\phi\rangle = \phi\,|\phi\rangle$ and, through complex conjugation, $a^*\,|\phi^*\rangle = \phi^*\,|\phi^*\rangle$. In writing Eq. (2.27), we have used the (over)completeness relation of the coherent states [13]. While it is not convention to define coherent states with a conjugate parameter as $|\phi^*\rangle$, we do so for future convenience.

Now the partition function looks like

$$\begin{aligned} Z = \lim_{M\to\infty} \prod_{k=0}^{M} \left(\int \mathcal{D}[\phi_k^{(u)}] \int \mathcal{D}[\phi_k^{(l)}] e^{-\phi_k^{(u)*}\phi_k^{(u)}} e^{-\phi_k^{(l)*}\phi_k^{(l)}}\right) \\ \times \langle\langle I|\, \phi_M^{(u)}, \phi_M^{(l)*}\rangle \prod_{k=1}^{M} \left(\langle\phi_k^{(u)}, \phi_k^{(l)*}|\, e^{\delta t\mathbb{L}}\, |\phi_{k-1}^{(u)}, \phi_{k-1}^{(l)*}\rangle\right) \langle\phi_0^{(u)}, \phi_0^{(l)*}\, |\rho\rangle\rangle \ , \end{aligned} \tag{2.28}$$

where we use the $\mathcal{D}$ to denote the measures of the integrals in Eq. (2.27). Consider one factor of the exponential and expand to linear order in δt, i.e. $e^{t\mathbb{L}} \sim 1 + \delta t\mathbb{L} + O(\delta t^2)$. This expansion is valid in the $M \to \infty$ limit, which is identical to taking $\delta t \to 0$. Then, using the overlap between two coherent states $\langle\phi|\psi\rangle = e^{\phi^*\psi}$, we evaluate the matrix element between the coherent states at time step k and $k-1$,

$$\begin{aligned}\langle\phi_k^{(u)}, \phi_k^{(l)*}|\,(1+\delta t\mathbb{L})\,|\phi_{k-1}^{(u)}, \phi_{k-1}^{(l)*}\rangle &= e^{\phi_k^{(u)*}\phi_{k-1}^{(u)}} e^{\phi_k^{(l)}\phi_{k-1}^{(l)*}} (1+\delta t\mathbb{L}[\phi_k^{(u)*}, \phi_k^{(l)}, \phi_{k-1}^{(u)}, \phi_{k-1}^{(l)*}]) \\ &\approx e^{\phi_k^{(u)*}\phi_{k-1}^{(u)} + \phi_k^{(l)}\phi_{k-1}^{(l)*} + \delta t\mathbb{L}[\phi_k^{(u)*}, \phi_k^{(l)}, \phi_{k-1}^{(u)}, \phi_{k-1}^{(l)*}]}\,.\end{aligned} \tag{2.29}$$

We have taken advantage of the fact that Eq. (2.25) is normal ordered so that the operators can be replaced by the corresponding coherent state fields. Inserting Eq. (2.29) into Eq. (2.28) we find,

$$Z = \int \mathcal{D}[\phi^{(u)}, \phi^{(l)}] \prod_{k=1}^{M} e^{i\delta t\left(-i\phi_{k-1}^{(u)}\partial_t\phi_{k-1}^{(u)*} + i\phi_{k-1}^{(l)}\partial_t\phi_{k-1}^{(l)*} - i\mathbb{L}[\phi_k^{(u)*}, \phi_k^{(l)}, \phi_{k-1}^{(u)}, \phi_{k-1}^{(l)*}]\right)} \times \text{const.} \tag{2.30}$$

We have used the notation $\partial_t\phi_k = (\phi_k - \phi_{k-1})/\delta t$ and have grouped the boundary terms (which will soon be neglected) into the constant multiplicative factor at the end.

We may now take the continuum limit, extend the range of time evolution from $(0, t) \to (-\infty, \infty)$, and push the boundaries out to infinity. As we are interested in the steady state which is assumed to be unique, we ignore the initial conditions. The contribution from the final state that connects the two branches at $t = \infty$ (i.e. enforces the trace) is also negligible as the boundary has been pushed out to infinity. This leaves us with the (almost) final form of our Keldysh path integral

$$Z = \int \mathcal{D}[\phi^{(u)}, \phi^{(l)}] e^{i\int_{-\infty}^{\infty} dt\left(-i\phi^{(u)}\partial_t\phi^{(u)*} - i\phi^{(l)*}\partial_t\phi^{(l)} - i\mathbb{L}[\phi^{(u)*}, \phi^{(l)}, \phi^{(u)}, \phi^{(l)*}]\right)}\,, \tag{2.31}$$

where

$$\mathbb{L}[\phi^{(u)*}, \phi^{(l)}, \phi^{(u)}, \phi^{(l)*}] = (-i\omega_0 - \frac{\kappa}{2})\phi^{(u)*}\phi^{(u)} + (i\omega_0 - \frac{\kappa}{2})\phi^{(l)*}\phi^{(l)} + \kappa\phi^{(u)}\phi^{(l)*}\,. \tag{2.32}$$

The partition function retains its normalization, $Z = 1$, as we have done nothing but map the trace to a path integral. This path integral, due to the limits on the time integral, describes the field theory of the steady state of the system (which we have assumed to be unique).

2.3.1 Keldysh Action

The final ingredient necessary to bring the path integral into our desired form is the Keldysh rotation, $\phi^{(u/l)} = (\phi_c \pm \phi_q)/\sqrt{2}$. The field ϕ_c is called the "classical" field as it is allowed to have a finite expectation value $\langle\phi_c\rangle \neq 0$. On the other hand, the field ϕ_q is called the "quantum" field as it is related to fluctuations and always obeys $\langle\phi_q\rangle = 0$. We also introduce the Fourier transform of the fields $\phi(t) = \frac{1}{2\pi}\int d\omega\phi(\omega)e^{-i\omega t}$. After the Keldysh rotation and Fourier transform, we arrive at the Keldysh action for a single mode cavity coupled to the vacuum,

$$S = \int_\omega \begin{pmatrix}\phi_c \\ \phi_q\end{pmatrix}^\dagger_\omega \begin{pmatrix}0 & P^A \\ P^R & P^K\end{pmatrix}_\omega \begin{pmatrix}\phi_c \\ \phi_q\end{pmatrix}_\omega \tag{2.33}$$

where

$$P^R(\omega) = P^A(\omega)^* = \omega - \omega_0 + \frac{i\kappa}{2}\,, \qquad P^K(\omega) = i\kappa\,, \tag{2.34}$$

and we have used the compact notation $\int_\omega = \int \frac{d\omega}{2\pi}$. The path integral now takes the concise form

$$Z = \int \mathcal{D}[\phi_c, \phi_q] e^{iS} = 1\,. \tag{2.35}$$

We note that the measure of the path integral has changed according to the Keldysh rotation, while we still have $Z = 1$. The mapping to the path integral preserves the partition function's value of unity. Furthermore, the Keldysh action exhibits a general feature that $S[\phi_c, \phi_q = 0] = 0$. This is equivalent to the statement that the Liouvillian dynamics conserves the probabilities of the density matrix. One can see this by realizing that $\phi_q = 0 \longleftrightarrow \phi^{(u)} = \phi^{(l)}$, which is identical to taking the trace. A consequence of this feature is that every term in the action has at least one quantum field, and therefore it is a property of all quadratic Keldysh actions that the $\phi_c^*\phi_c$ element is zero.

The matrix elements of the kernel in Eq. (2.33) take on the typical Keldysh structure [4, 13, 14]. The retarded/advanced elements $P^{R/A}$ characterize the dynamics of the field, while the Keldysh element P^K represents the noise. The inverse of this kernel yields the Green's functions

$$G^R(\omega) = G^A(\omega)^* = -i\langle\phi_c(\omega)\phi_q^*(\omega)\rangle = \frac{1}{P^R(\omega)} \tag{2.36}$$

$$G^K(\omega) = -i\langle\phi_c(\omega)\phi_c(\omega)^*\rangle = -G^R(\omega)P^K(\omega)G^A(\omega)\,. \tag{2.37}$$

The Green's functions $G^{R/A}$ are the retarded/advanced response functions, and G^K is the Keldysh correlation function. These can be recast in terms of the original operators we started with. Going back to the time domain,

$$G^R(t-t') = -i\Theta(t)\langle[a(t), a^\dagger(t')]\rangle \tag{2.38}$$

$$G^K(t-t') = -i\langle\{a(t), a^\dagger(t')\}\rangle\,. \tag{2.39}$$

We have used the fact that the steady state is time translation invariant in time to write the Green's functions as functions of only the time difference. A derivation of these relations can be found in Ref. [13]. Returning to the frequency domain for a moment, we can compute the Keldysh Green's function:

$$G^K(\omega) = \frac{\kappa}{(\omega-\omega_0)^2 + \kappa^2/4}\,. \tag{2.40}$$

Performing the frequency integral, we find $\frac{1}{2\pi}\int_{-\infty}^{\infty} d\omega\, iG^K(\omega) = iG^K(t=0) = 1$. Recalling that $G^K(0) = \langle\{a, a^\dagger\}\rangle$, we use the bosonic commutation relation to find $G^K(0) = 2\langle a^\dagger a\rangle + 1 = 1$ which implies $\langle a^\dagger a\rangle = 0$. In other words, the steady state of the cavity is the vacuum state! This result is intuitive. The dissipation from the environment, taking of the form of photons leaking from the cavity, always depletes the cavity in the long-time limit.

This simple exercise, while overkill for a single mode cavity, demonstrates the use of the Keldysh formalism. We have been able to translate the Liouvillian superoperator into a classical action in a path integral that makes the correlation and response functions readily apparent. Once we include interactions, the field theory will contain terms beyond quadratic order, complicating the analysis. In this thesis, we focus on a nontrivial model which is, however, amenable to an exact field-theoretical description.

2.3.2 Source Fields

Because the nonequilibrium partition function always takes the value $Z = 1$, there is no functional dependence on the system's parameters to take derivatives w.r.t. and generate expectation values as one does in equilibrium. In other words, there is no object like the free energy as $\ln(Z) = 0$. To

circumvent this, we introduce source terms $j^{(u)}(t)$ and $j^{(l)}(t)$ into the Liouvillian, which couple to an operator (a or $a^\dagger$ for example) which we are interested in. The new terms arise in the coherent part of the Liouvillian, and modify the commutator:

$$\mathbb{L}[j^{(u)}, j^{(l)}] = -i\left(H^{(u)} + j^{(u)}O^{(u)} - H^{(l)T} - j^{(l)}O^{(l)T}\right), \tag{2.41}$$

where O is the operator whose expectation values we are interested in. These source terms have the crucial property of being distinct on each branch of the vectorized Liouvillian, i.e. $j^{(u)} \neq j^{(l)}$. This spoils the conservation of probability of the dynamics and directly implies that $Z[j^{(u)}, j^{(l)}] \neq 1$. The advantage now is that we may take derivatives of Z with respect to these source fields to generate correlation and response functions. This connection is made transparent after applying the Keldysh rotation to the source fields in the path integral representation. Introducing source fields for the bosonic annihilation operator a, we may write [13]

$$Z[j_c, j_q] = \left\langle e^{-i\int_t j_c^*(t)\phi_q(t) + i\int_t j_q^*(t)\phi_c(t)} \right\rangle, \tag{2.42}$$

where the expectation value is taken with respect to the Keldysh path integral. One could also introduce source fields for the conjugate bosonic fields if desired. Equation (2.42) is the so called characteristic function. We can define a more convenient quantity akin to a free energy, which we call the generating function:

$$W[j_c, j_q] = -i \ln Z[j_c, j_q]. \tag{2.43}$$

Functional derivatives of the generating function produce connected correlation functions. For example, $\delta^2 W/\delta j_q^*(t)\delta j_q^*(t')| = \langle(\phi_c(t) - \langle\phi_c\rangle)(\phi_c(t') - \langle\phi_c\rangle)\rangle = \langle\phi_c(t)\phi_c(t')\rangle_c$. Connected correlation functions subtract out the contribution from lower order averages (in this case the first moment). This is relevant when one is interested in the fluctuations in a system and wants to remove the trivial extensive contribution.

2.4 Keldysh Field Theory for a Spin Coupled to a Cavity

In the previous section we derived the path integral for a single bosonic mode. Here, we introduce a mapping to represent a dissipative two-level system coupled to a cavity as a Keldysh path integral

over a real field. We take a spin-cavity system coupled to the vacuum with The Lindblad equation

$$\mathcal{L}[\rho] = -i[H, \rho] + \Gamma \mathcal{D}_{\sigma^-}[\rho] + \kappa \mathcal{D}_a[\rho] \,, \tag{2.44}$$

$$\mathcal{D}_L[\bullet] = L \bullet L^\dagger - \frac{1}{2}\{L^\dagger L, \bullet\} \,, \tag{2.45}$$

$$H = \omega_0 a^\dagger a + \Delta \sigma^z + g\sigma^x (a^\dagger + a) \,. \tag{2.46}$$

The operators $\sigma^\alpha, \alpha \in \{x, y, z\}$ are the Pauli matrices

$$\sigma^x = \begin{pmatrix} 1 & 0 \\ 0 & -1 \end{pmatrix} \quad \sigma^y = \begin{pmatrix} 0 & i \\ -i & 0 \end{pmatrix} \quad \sigma^z = \begin{pmatrix} 0 & 1 \\ 1 & 0 \end{pmatrix} , \tag{2.47}$$

with $\sigma^- = (\sigma^+)^T = (\sigma^x - i\sigma^y)/2$. The Hamiltonian is known as the Tavis-Cummings model [5]. We can take this model to be phenomenological. The only jump operator for the spin is the lowering operator corresponding to spontaneous emission at a rate Γ. Photons leak out of the cavity to the environment at a rate κ. We denote the spin-cavity interaction strength as g. Following the same procedure as before, we vectorize the Liouvillian to obtain

$$\begin{aligned} \mathbb{L} = -i\left(H \otimes I - I \otimes H^T\right) + \Gamma\left(\sigma^- \otimes \sigma^- - \frac{1}{2}\sigma^-\sigma^+ \otimes I - \frac{1}{2} I \otimes \sigma^-\sigma^+\right) \\ + \kappa\left(a^{(u)} a^{(l)*} - \frac{1}{2}(a^{(u)\dagger} a^{(u)} + a^{(l)T} a^{(l)*})\right) . \end{aligned} \tag{2.48}$$

This Liouvillian can be interpreted as a non-hermitian Hamiltonian describing two spins coupled through the dissipative terms, and these spins are each separately coupled to their own cavity. These cavities are also interacting with each other through the dissipative coupling. This is a feature of vectorization that the doubled degrees of freedom interact with each other through the dissipative terms in the Liouvillian.

Now we repeat the process of of obtaining the path integral by trotterizing the partition function as before, $Z = \lim_{M\to\infty} \langle\langle I| \left(e^{\delta t \mathbb{L}}\right)^M |\rho_0\rangle\rangle$. Furthermore, we can split the exponential into two parts, $e^{\delta t \mathbb{L}} \to e^{\delta t \mathbb{L}_0} e^{\delta t \mathbb{L}_1}$, where $\mathbb{L}_0$ contains the atom-cavity interaction term and $\mathbb{L}_1 = \mathbb{L}_{\text{spin}} + \mathbb{L}_{\text{cav}}$ all of the non-interacting terms. This split is exact due to the $M \to \infty$ limit. Separating the exponentials this way allows us to insert resolutions of the identity in a basis that makes treating $\mathbb{L}_0$ easy, i.e. we expand in the basis $\mathbb{I}_{\text{spin},k} \otimes \mathbb{I}_{\text{cav},k}$, where

$$\mathbb{I}_{\text{spin},k} = \sum_{\sigma^{(u)}, \sigma^{(l)}} |\sigma_k^{(u)}, \sigma_k^{(l)}\rangle\langle\sigma_k^{(u)}, \sigma_k^{(l)}| \,, \tag{2.49}$$

with $\sigma^{x(u/l)}\,|\sigma^{(u)},\sigma^{(l)}\rangle = \sigma^{(u/l)}\,|\sigma^{(u)},\sigma^{(l)}\rangle$; the quantity $\mathbb{I}_{\text{cav},k}$ is given by Eq. (2.27). Once again, we label each resolution with the time-step k. Inserting these resolutions after every time-step, we find

$$\begin{aligned} Z = \lim_{M\to\infty} \sum_{\{\sigma\}} \int \mathcal{D}[\phi^{(u)},\phi^{(l)}] f_m f_0 \prod_{k=0}^{M-1} e^{-ig\left(\sigma_{k+1}^{(u)}(\phi_{k+1}^{(u)}+\phi_{k+1}^{(u)*})-\sigma_{k+1}^{(l)}(\phi_{k+1}^{(l)}+\phi_{k+1}^{(l)*})\right)} \\ \times \langle \sigma_{k+1}^{(u)},\sigma_{k+1}^{(l)}|\, e^{\delta t \mathbb{L}_{\text{spin}}}\,|\sigma_k^{(u)},\sigma_k^{(l)}\rangle\, e^{i\delta t\left(-i\phi_k^{(u)}\partial_t\phi_k^{(u)*}-i\phi_k^{(l)*}\partial_t\phi_k^{(l)}-i\mathbb{L}_{\text{cav}}[\phi_{k+1}^{(u)*},\phi_{k+1}^{(l)},\phi_k^{(u)},\phi_k^{(l)*}]\right)}\,. \end{aligned} \tag{2.50}$$

The coefficients f_m, f_0 are the the boundary terms for both the spin and the cavity. Now, we can pull the exponential factor that is linear in $\sigma^{(u/l)}$ into the $\langle \sigma_{k+1}^{(u)},\sigma_{k+1}^{(l)}|\, e^{\delta t\mathbb{L}_{\text{spin}}}\,|\sigma_k^{(u)},\sigma_k^{(l)}\rangle$ matrix element, and turn it back into an operator while absorbing it into $e^{\delta t\mathbb{L}_{\text{spin}}}$. We define this new matrix as $\mathbb{T}_k$. At this intermediate step, our partition function takes the form

$$Z = \lim_{M\to\infty}\int \mathcal{D}[\phi^{(u)},\phi^{(l)}] e^{iS_{\text{cav}}}\,\langle\langle I_{\text{spin}}|\prod_k\left(\mathbb{I}_{\text{spin},k}e^{\delta t\mathbb{T}_k}\right)|\rho_{\text{spin},0}\rangle\rangle\,. \tag{2.51}$$

The action S_{cav} is given by Eq. (2.33). We have assumed that the initial state is a product state between the spin and the cavity. Furthermore, we have resummed the resolution of identities, allowing us to return back to an operator form. Removing the identities and taking the $M\to\infty$ limit (i.e. the continuum limit) while extending the integration limits to infinity, we find

$$Z = \int \mathcal{D}[\phi_c,\phi_q] e^{iS}\,, \tag{2.52}$$

where we have recalled the Keldysh rotation and defined the action

$$S = S_{\text{cav}} - i\ln\text{Tr}\left(\mathcal{T}e^{\int_t \mathbb{T}(t)}\right)\,. \tag{2.53}$$

The object $\mathcal{T}$ is the time-ordering operator and is required as $\mathbb{T}$ is a function of time. The matrix $\mathbb{T}(t)$, in our chosen basis that diagonalizes σ^x, is given by

$$\mathbb{T}(t) = \begin{pmatrix} -\frac{\Gamma}{4}-i\sqrt{2}gx_q & i\Delta & -i\Delta & \frac{\Gamma}{4} \\ i\Delta-\frac{\Gamma}{2} & -\frac{3\Gamma}{4}-i\sqrt{2}gx_c & -\frac{\Gamma}{4} & -i\Delta-\frac{\Gamma}{2} \\ -i\Delta-\frac{\Gamma}{2} & -\frac{\Gamma}{4} & -\frac{3\Gamma}{4}+i\sqrt{2}gx_c & i\Delta-\frac{\Gamma}{2} \\ \frac{\Gamma}{4} & -i\Delta & i\Delta & -\frac{\Gamma}{4}+i\sqrt{2}gx_q \end{pmatrix}, \tag{2.54}$$

with $x_{c/q} = (\phi_{c/q} + \phi^*_{c/q})/\sqrt{2}$ the classical and quantum components of the cavity quadrature. We have also made the simplification of setting $\langle\langle I|\bullet|\rho_0\rangle\rangle \to \mathrm{Tr}(\bullet)$, which is valid due to expanding the integration limits out to infinity in combination with the fact that $\mathbb{T}$ captures dissipative dynamics and will take any initial state to a unique steady state. Furthermore, in making this simplification we have assumed the initial state of the cavity and spin is separable.

Equation (2.53) represents our mapping of the Liouvillian dynamics of a single spin coupled to a cavity to a path integral over a pair of fields, and at this point is exact. We will see that the action for the driven-dissipative Ising model takes a very similar form and is obtained using almost exactly the same procedure. The action in Eq. (2.53) is a formal expression, but it can be expanded in powers of the cavity quadrature. If there is some small expansion parameter, it is possible to truncate this expansion and obtain a relatively simpler description of the field theory that well describes the original model. While there is no obvious expansion parameter in the present model, we show in Sec. 3.2 how this would be done on a closely related model.

CHAPTER 3

MODELS AND FIELD THEORY

In this chapter we will introduce the relevant models to our work. While this thesis primarily focus on the DDIM, we will begin this chapter by first introducing the closely related open Dicke model as it provides experimental motivation and is required in the derivation of the DDIM. Then, the equilibrium properties of the Ising model will be discussed; they provide a useful point of comparison for the nonequilibrium results we obtain later. We then elaborate on the various symmetries of the model, their physical significance, as well as how we can take advantage of these symmetries when studying these models. Finally, we will map the DDIM Liouvillian to a Keldysh path integral using the techniques established in the previous chapter. This path integral will serve as the starting point for the rest of our analysis.

3.1 Open Dicke Model

The Dicke model [16, 17] is a paradigmatic model of light-matter interactions. It describes a cavity mode coupled to atoms modeled as 2-level systems. At sufficiently large coupling strengths, this system exhibits a phase transition from a normal phase to a *superradiant* phase where the cavity is macroscopically occupied and the spins spontaneously align. In principle, the cavity and the atoms are coupled through the underlying dipole coupling, but the coupling strength would be much smaller than the cavity frequency and the atom energy splitting. Furthermore, there is the subtlety known as the diamagnetic term (or the A^2 term) which has sparked much debate on the existence of a no-go theorem [18] for the superradiant transition. However, both of these problems can be circumvented by utilizing driving schemes [17, 19] to generate the atom-cavity coupling. These schemes have the added benefit of bringing the detuned cavity frequency (in the rotating frame of the drive) within the same order of magnitude as the coupling strength. Using this scheme, in the rotating frame of the drive the Hamiltonian can be modeled as [17]

$$H_{\text{Dicke}} = \omega_0 a^\dagger a + \Delta S_z + \frac{2g}{\sqrt{N}} S_x (a^\dagger + a) \tag{3.1}$$

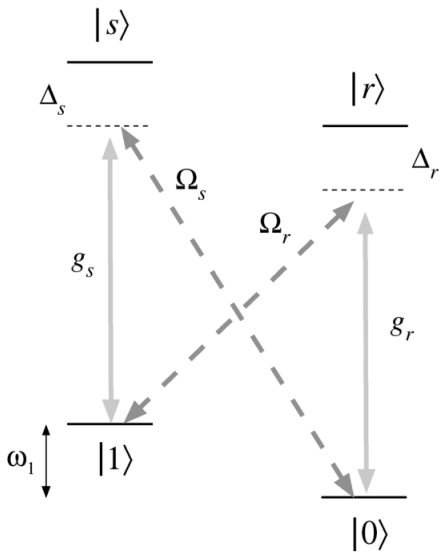

Figure 3.1 (Note: From Ref. [19]) Balanced Raman channels used to derive the Dicke Hamiltonian in [19]. The cavity couples two sets of levels, $1 \leftrightarrow s$ and $0 \leftrightarrow r$. Two drives of frequency Ω_s and Ω_r couple $0 \leftrightarrow s$ and $1 \leftrightarrow r$. By detuning the drive frequencies from the excited states, these states can be adiabatically eliminated to leave an effective two level system consisting of $|1\rangle$ and $|0\rangle$ with level splitting ω_1.

where $S_\alpha = \sum_i \sigma_i^\alpha$ are the collective spin operators. We have ω_0 the detuned cavity frequency, Δ the atom level splitting, and g is the atom-cavity coupling generated by the drive (time-independent as we are in the rotating frame).

There are different microscopic physical systems that yield Eq. (3.1) in certain regimes. One of the primary examples was proposed by Charmichael et. al. [19], where the system consists of actual atoms with two pairs of internal levels coupled to the cavity. In addition, two driving lasers are applied to the atoms that couple these two pairs of internal levels; see Fig. 3.1. The lasers are detuned such that the higher excited states of each pair of levels can be adiabatically eliminated, and we are left with an effective two level system comprised of the ground state of each original pair. This scheme was experimentally realized in [20]. A different scheme involves using a Bose-Einstein condensate (BEC) in a driven cavity, where at high enough pump strengths the BEC self-organizes into even and odd checkerboard lattices [8, 21]. The cavity couples to the motional states of the BEC, and this interaction can be mapped to a similar type of Dicke model as in Eq. (3.1).

Now we consider the more general case where the atom and the cavity are coupled to the QED vacuum. The atom-vacuum coupling (i.e. sponteaneous emission of the individual atoms) was typically assumed to be negligible in comparison with photon leakage from the cavity, however, it has been shown to have observable effects on the behaviour of system [20, 22]. Therefore, we consider both types of coupling here. Assuming that the bath satisfies the Born-Markov approximation discussed in Sec. 2.2, and that the driving strength is weak compared to the bare cavity frequency and internal level splittings of the atom, we can justifiably write down the Lindblad equation for the open Dicke model (ODM) [8, 14, 17, 19, 22–25]

$$\mathcal{L}[\rho] = -i[H_{\text{Dicke}}, \rho] + \Gamma \sum_i \mathcal{D}_{\sigma_i^-}[\rho] + \kappa \mathcal{D}_a[\rho] \,. \tag{3.2}$$

We have included the most probable kinds of dissipation, namely photon loss and spontaneous emission.

The Liouvillian has a $\mathbb{Z}_2$ symmetry, which can be seen by its invariance under the transformation $a \to -a, \sigma^x \to -\sigma^x$. However, in contrast to Hamiltonian systems this does not imply conservation of parity [26]. At large enough atom-cavity coupling strengths, the system undergoes a superradiant phase transition which is of the Ising type, i.e. it is a second-order phase transition that corresponds to a broken $\mathbb{Z}_2$ symmetry. In the normal phase $\langle a \rangle = \langle \sigma^x \rangle = 0$, and in the ordered phase these quantities become finite and spontaneously choose to be positive or negative in accordance with the broken symmetry. It has been shown [22] that spontaneous emission is non-negligible in determining the location of the critical point in the ODM. Furthermore, there is a permutation symmetry that can be seen by swapping $i \leftrightarrow j$ for any two spins i and j which leaves the Liouvillian invariant. This symmetry will prove useful when performing numerical simulations as it reduces the dimensionality of the steady state Hilbert space from 4^N to $O(N^3)$ (for details on how this is done see Sec. 4.1).

3.2 Driven-Dissipative Ising Model

In this work, we are interested in the critical properties of the NESS as it undergoes the phase transition. However, the ODM can actually be simplified further to an atom-only description that

still captures much of the essential physics; see Sec. 3.4. In other words, we seek a minimal model with which we can perform our analysis. There are various limits that can be taken to yield an atom-only description, most of them yielding non-Lindbladian dynamics [27], but we will be focusing on the large-detuning limit ($\omega_0, \kappa \gg g, \Gamma, \Delta$) which preserves the Lindblad form. In this case, the cavity dynamics occur on a much shorter timescale than that of the spins and therefore can be adiabatically eliminated. This yields a new Liouvillian,

$$\mathcal{L}[\rho] = -i[H, \rho] + \Gamma \sum_i \mathcal{D}_{\sigma_i^-}[\rho] + \Gamma_x \mathcal{D}_{S_x}[\rho] \,, \tag{3.3}$$

with the Hamiltonian

$$H = \frac{-J}{N} S_x^2 + \Delta S_z \,, \tag{3.4}$$

where $J = 16g^2\omega_0/(\kappa^2 + 4\omega_0^2)$ and $\Gamma_x = J\kappa/\omega_0$. We see that elimination of the cavity mode introduces collective dephasing in the x-direction. In the limit that $\omega_0 \gg \kappa$, we can neglect this term to arrive at the final form of the DDIM,

$$\mathcal{L}[\rho] = -i[H, \rho] + \Gamma \mathcal{D}_{\sigma^-}[\rho] \,. \tag{3.5}$$

This represents the minimal many-body model that is host to a phase transition and will be the focus of the rest of this thesis. We emphasize that Eq. (3.5) is a driven-dissipative model despite the absence of an explicit driving term. We are several steps removed from the microscopic dynamics and are operating in the rotating frame of the drive. Furthermore, one can check that a system is driven-dissipative when the Lindblad operators do not take you between eigenstates of the Hamiltonian. This is equivalent to the condition $[H, L(\omega)] = -\omega L(\omega)$, where $L(\omega)$ are Lindblad operators that take you between all eigenstates with energy difference ω [6].

In the absence of dissipation, the Hamiltonian in Eq. (3.4) is known as the Lipkin-Meshkov-Glick (LMG) model and has been studied extensively [28–33]. This model is integrable, i.e. it has infinitely many conserved quantities in the thermodynamic limit, and is therefore exactly solvable. The infinite-ranged nature of the interactions means that the collection of spins can be interpreted as a single large spin, and can be treated semi-classically in the thermodynamic limit [28, 34]. The

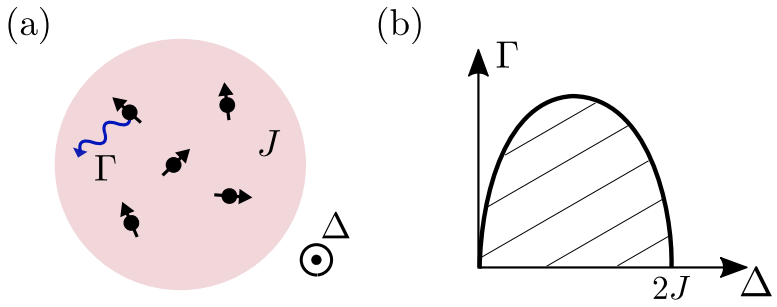

Figure 3.2 (a) Schematic diagram of the DDIM. There is an infinite-range interaction of strength J between the all of the spins, while each spin experiences spontaneous emission at a rate Γ. In addition, the spins experience a transverse field of strength Δ. (b) The phase diagram of the DDIM. Shaded regions represent the ordered phase where $\langle S_x \rangle \neq 0$. The weakly-dissipative point at $\Delta = 2J$ represents a unique limit of the model and coincides with the critical point of the equilibrium model at zero temperature.

most important conserved quantity is the total spin operator $S^2 = S_x^2 + S_y^2 + S_z^2$, which satisfies $[H, S] = 0$. However, this feature of the model is spoiled by spontaneous emission which does not conserve total spin. The lack of conservation of total spin in the DDIM can be interpreted as a positive as it enriches the possible space of states. Despite this, Eq. (3.5) is still exactly solvable.

Equation (3.5) is a descendent of the ODM and, therefore, has the same symmetries, namely the $\mathbb{Z}_2$ and permutation symmetries. It also experiences the same Ising phase transition from a normal phase, where $\langle S_x \rangle = 0$, to an ordered phase with $\langle S_x \rangle \neq 0$; see Fig. 3.2(b). In equilibrium, at zero temperature, this model has a quantum phase transition at $\Delta = 2J$ [28] as shown in Fig. 5.11(b). The driven-dissipative model instead has the ordered phase extend outwards in the parameter space to finite Γ. We note that the nature of phase transitions in driven-dissipative systems is distinct from those of equilibrium. Driven-dissipative phase transitions occur in the NESS of the dynamics, while zero-temperature phase transitions occur in the ground state and finite-temperature phase transitions in the thermal state. As we will show in Ch. 5, the steady state of the DDIM is host to two different universality classes. The system exhibits different sets of critical exponents when Γ is finite compared to the weakly-dissipative critical point where $\Gamma \to 0, \Delta = 2J$.

3.2.1 Mean-Field Theory

Mean-field theory is the simplest analysis one can perform on an interacting theory. It is based on the notion that the interaction may be replaced by a single field proportional to the single-particle expectation value of a spin. In other words, mean-field theory reduces a many-body theory to a single-particle theory, a tremendous simplification. The DDIM is what is known as a "mean-field" type model, meaning that the phase diagram is exactly given by the mean-field solution in the thermodynamic limit. Before proceeding with an exact treatment of the model that includes fluctuations, we perform a simple mean-field analysis.

The standard mean-field equations of motion are obtained by calculating the expectation values $\langle \sigma_i^\alpha \rangle$ and assuming that the density matrix is factorized in space and is uniform:

$$\rho = \bigotimes_i \rho_i = \rho_{\mathrm{MF}}^{\otimes N}, \tag{3.6}$$

where ρ_{MF} is the mean-field density matrix, uniform across all sites. Using this approximation, we find the mean-field Heisenberg equations of motion (in the $N \to \infty$ limit)

$$\partial_t \langle \sigma^x \rangle = -2\Delta \langle \sigma^y \rangle - \frac{\Gamma}{2} \langle \sigma^x \rangle, \tag{3.7a}$$

$$\partial_t \langle \sigma^y \rangle = (4J \langle \sigma^z \rangle + 2\Delta) \langle \sigma^x \rangle - \frac{\Gamma}{2} \langle \sigma^y \rangle, \tag{3.7b}$$

$$\partial_t \langle \sigma^z \rangle = -4J \langle \sigma^y \rangle \langle \sigma^x \rangle - \Gamma (1 + \langle \sigma^z \rangle), \tag{3.7c}$$

where we have dropped the spatial index due to the uniform ansatz. By setting the LHS to zero, we can solve for the nonequilibrium steady-state values of the three observables. In the normal phase, the only solution is the trivial one: $\langle \sigma^x \rangle_{\mathrm{ss}} = 0, \langle \sigma^y \rangle_{\mathrm{ss}} = 0, \langle \sigma^z \rangle_{\mathrm{ss}} = -1$ with the subscript indicating the steady state. In the ordered phase, we identify two stable solutions as

$$\langle \sigma^x \rangle_{\mathrm{ss}} = \pm \frac{\sqrt{32J\Delta - 16\Delta^2 - \Gamma^2}}{4\sqrt{2}J}, \tag{3.8a}$$

$$\langle \sigma^y \rangle_{\mathrm{ss}} = \mp \frac{\Gamma \sqrt{32J\Delta - 16\Delta^2 - \Gamma^2}}{16\sqrt{2}J\Delta}, \tag{3.8b}$$

$$\langle \sigma^z \rangle_{\mathrm{ss}} = -\frac{\Gamma^2 + 16\Delta^2}{32J\Delta}, \tag{3.8c}$$

from which the phase boundary follows as

$$\Gamma^2 + 16\Delta^2 - 32J\Delta = 0\,. \tag{3.9}$$

The phase diagram defined by this equation is given in Fig. 3.2(b). The mean-field solution is exact in the thermodynamic limit due to the collective interactions. However, to characterize fluctuations and to identify the critical behavior of the model, we must go beyond mean field. Using a quantum-to-classical mapping, we shall provide an exact field-theoretical description, allowing us to perform a systematic study of fluctuations beyond mean field.

3.3 DDIM Field Theory

The DDIM Liouvillian, given by Eq. (3.5), is a many-body system and is better described in the field-theoretical framework. Mapping the system to a field-theory will allow us to go beyond the simple mean-field treatment performed in Sec. 3.2.1. In this section, we will map the nonequilibrium partition function to a Keldysh path integral using the techniques developed in Ch. 2. Our starting point is the vectorized partition function

$$Z = \langle\langle I|\, e^{\delta t \mathbb{L}}\, |\rho_0\rangle\rangle\ . \tag{3.10}$$

We trotterize the evolution operator and split the Liouvillian into interacting terms (i.e. the Ising term), $\mathbb{L}_0$, and non-interacting terms, $\mathbb{L}_1$,

$$Z = \lim_{M\to\infty} \langle\langle I|\left(e^{\delta t \mathbb{L}_0} e^{\delta t \mathbb{L}_1}\right)^M |\rho_0\rangle\rangle\ . \tag{3.11}$$

Next, we introduce resolutions of the identity $\mathbb{I}_k$ labeled in accordance with the time steps, their form is given by Eq. (2.49), but expanded to include all N spins. Inserting these resolutions of the identity and taking advantage of the fact that $\mathbb{L}_0$ is diagonalized by our chosen basis, we find

$$Z = \lim_{M\to\infty} \sum_{\{\sigma\}} f_m f_0 \prod_{k=1}^{M-1} e^{i\frac{J}{N}\left((S_k^{(u)})^2 - (S_k^{(l)})^2\right)} \langle\{\sigma_k^{(u)}\}, \{\sigma_k^{(l)}\}|\, e^{\delta t \mathbb{L}_1}\, |\{\sigma_{k-1}^{(u)}\}, \{\sigma_{k-1}^{(l)}\rangle\}\,, \tag{3.12}$$

where $S^{(u/l)} = \sum_i \sigma_i^{(u/l)}$ is the classical collective spin and $f_0 = \langle\langle\{\sigma_0^{(u)}\}, \{\sigma_0^{(l)}\}|\rho_0\rangle\rangle\,, f_m = \langle\langle I|\{\sigma_M^{(u)}\}, \{\sigma_M^{(l)}\}\rangle\rangle$ arise from the boundary terms. The curly brackets around spins, $\{\sigma\}$, represent

the collection of all N spins. At this point we require one additional ingredient to proceed with the recipe established in Sec. 2.4. We introduce the Hubbard-Stratonovich transformation [4, 15],

$$e^{i\frac{J}{N}\left((S_k^{(u)})^2-(S_k^{(l)})^2\right)} = \frac{1}{\mathcal{N}}\int_{-\infty}^{\infty} dm_k^{(u)} dm_k^{(l)} e^{-i\delta t JN[(m_k^{(u)})^2-(m_k^{(l)})^2]+i2J\delta t(m_k^{(u)}S_k^{(u)}-m_k^{(l)}S_k^{(l)})}, \tag{3.13}$$

where $\mathcal{N}$ is an unimportant normalization factor such that we retrieve the left hand side after performing the Gaussian integration over the real fields $m^{(u/l)}$.

The Hubbard-Stratonovich transformation allows us to decouple the Ising interaction at the cost of introducing new fields, and linearizes the argument of the exponential with respect to the classical spins. This allows us to proceed with the usual recipe and pull the now linearized exponential inside of the inner product $\langle\{\sigma_k^{(u)}\},\{\sigma_k^{(l)}\}|\, e^{\delta t\mathbb{L}_1}\,|\{\sigma_{k-1}^{(u)}\},\{\sigma_{k-1}^{(l)}\}\rangle$ and absorb the new term into $\mathbb{L}_1$; we call this new matrix $\overline{\mathbb{T}}_k$. We point out that $\overline{\mathbb{T}}_k = \sum_i \mathbb{T}_{k,i}$ is actually a sum of identical terms,

$$\begin{aligned}\mathbb{T}_{k,i} =& i2J\left((m_k^{(u)}\sigma_i^{x(u)} - m_k^{(l)}\sigma_i^{x(l)}\right) - i\Delta\left(\sigma_i^{z(u)} - \sigma_i^{z(l)}\right)\\ &+\Gamma\sigma_i^{-(u)}\sigma_i^{-(l)} - \frac{\Gamma}{2}\left(\sigma_i^{+(u)}\sigma_i^{-(u)} + \sigma_i^{+(l)}\sigma_i^{-(l)}\right).\end{aligned} \tag{3.14}$$

After we sum up and remove the resolution of identities, we can take advantage of the above fact to write

$$Z = \lim_{M\to\infty}\int \mathcal{D}[m^{(u)},m^{(l)}]e^{-i\delta t JN[(m_k^{(u)})^2-(m_k^{(l)})^2]}\left(\langle\langle I|\prod_k e^{\delta t\mathbb{T}_k}\,|\rho_0\rangle\rangle\right)^N \tag{3.15}$$

where we have replaced $\mathbb{T}_{k,i}$ with $\mathbb{T}_k$ as they are all equivalent. In writing the above equation, we have assumed that the initial state is a product state of identical spin states which is valid considering we are only interested in the steady state. We have also defined the measure for the Hubbard-Stratonovich fields, $\mathcal{D}[m^{(u)},m^{(l)}] = \prod_k \frac{dm_k^{(u)}dm_k^{(l)}}{\mathcal{N}}$.

Taking the continuum limit, extending the initial and final times out to infinity, and performing the Keldysh rotation on the Hubbard-Stratonovich fields, we arrive at the DDIM Keldysh path integral $Z = \int \mathcal{D}[m_c,m_q]e^{iS}$, where

$$S = -2JN\int_t m_c(t)m_q(t) - iN\ln\mathrm{Tr}\left(\mathcal{T}e^{\int_t\mathbb{T}(t)}\right). \tag{3.16}$$

We have repeated the simplification made in Sec. 2.4, where extending the initial time out to infinity allows us to make the replacement $\langle\langle I|\bullet|\rho_0\rangle\rangle \to \mathrm{Tr}(\bullet)$ as the matrix $\mathbb{T}$ will yield a unique

steady state no matter the initial state. The matrix $\mathbb{T}$ is almost identical to Eq. (2.54),

$$\mathbb{T}(t) = \begin{pmatrix} -\frac{\Gamma}{4} + i2\sqrt{2}Jm_q & i\Delta & -i\Delta & \frac{\Gamma}{4} \\ i\Delta - \frac{\Gamma}{2} & -\frac{3\Gamma}{4} + i2\sqrt{2}Jm_c & -\frac{\Gamma}{4} & -i\Delta - \frac{\Gamma}{2} \\ -i\Delta - \frac{\Gamma}{2} & -\frac{\Gamma}{4} & -\frac{3\Gamma}{4} - i2\sqrt{2}Jm_c & i\Delta - \frac{\Gamma}{2} \\ \frac{\Gamma}{4} & -i\Delta & i\Delta & -\frac{\Gamma}{4} - i2\sqrt{2}Jm_q \end{pmatrix}. \tag{3.17}$$

This matrix is akin to a transfer matrix for two spins on the upper and lower branch of the Keldysh contour respectively. Imaginary matrix elements describe coherent evolution, and real matrix elements describe dissipation. This matrix will be an important object in the rest of our analysis, and we will show how to manipulate it and the ln Tr term of the action. Most importantly, we will be able to truncate an expansion of the action thanks to the overall factor of N. In the thermodynamic limit, this overall factor of N makes the saddle-point solution exact and only allows for quadratic fluctuations, which we will show in the following sections.

3.3.1 Field-Spin Relationship

The quantum-to-classical mapping utilizes the Hubbard-Stratonovich transformation to introduce a real field $m^{(u/l)}$ in place of the classical total spin $S^{(u/l)}$. Therefore, expectation values of $m_{c/q}$ should be naturally related to those of the original spin operator S_x. To derive this relationship, we introduce time-dependent source fields $\alpha^{(u/l)}(t)$ coupled to S_x on both the upper and lower branches of the vectorized DDIM Liouvillian, $i(\alpha^{(u)}S_x^{(u)} - \alpha^{(l)}S_x^{(l)})$, where we can have $\alpha^{(u)} \neq \alpha^{(l)}$ so that the nonequilibrium partition function $Z \neq 1$ as discussed in Sec. 2.3.2 [13]. The source fields do not alter the mapping to the field theory, they simply introduce new elements to the matrix $\mathbb{T}$ as

$$\mathbb{T}'(t) = \mathbb{T}(t) + i\sqrt{2}\begin{pmatrix} \alpha_q & 0 & 0 & 0 \\ 0 & \alpha_c & 0 & 0 \\ 0 & 0 & -\alpha_c & 0 \\ 0 & 0 & 0 & -\alpha_q \end{pmatrix}, \tag{3.18}$$

where we have performed the Keldysh rotation $\alpha_{c/q} = (\alpha^{(u)} \pm \alpha^{(l)})/\sqrt{2}$ on the source fields. The fields $m_{c/q}$ are dummy variables under the path integral. Making the change of variables

$m_{c/q}(t) \to m_{c/q}(t) + \alpha_{c/q}(t)/2J$, we can move the source terms out into the quadratic portion of the action to find (using the same field variables)

$$S = N \int_t \left(m_c(t)\alpha_q(t) + m_q(t)\alpha_c(t) - \frac{\alpha_q(t)\alpha_c(t)}{2J} \right) + S_0[m_{c/q}], \tag{3.19}$$

where S_0 is the original action without the source fields in Eq. (3.16). Taking derivatives of the generating functional $Z[\alpha(t)]$ with respect to the source fields generates correlation functions [13]. Specifically, taking a derivative with respect to α_q yields

$$\frac{\sqrt{2}}{N}\langle S_x(t)\rangle = -i\frac{\partial Z}{\partial \alpha_q(t)}\bigg|_{\alpha_{c/q}=0} = \langle m_c(t)\rangle\,, \tag{3.20}$$

which provides a clear translation between the two descriptions (the factor of $\sqrt{2}$ arises due to the Keldysh rotation). Next, we consider the two-point correlation function and response function, respectively:

$$\begin{aligned} \frac{1}{N^2}\langle\{S_x(t), S_x(t')\}\rangle &= -\frac{\delta Z}{\delta\alpha_q(t)\delta\alpha_q(t')}\bigg|_{\alpha_{c/q}=0} \\ &= \langle m_c(t)m_c(t')\rangle, \end{aligned} \tag{3.21}$$

and

$$\begin{aligned} \frac{1}{N^2}\langle[S_x(t), S_x(t')]\rangle &= -\left(\frac{\delta Z}{\delta\alpha_q(t)\delta\alpha_c(t')} - \frac{\delta Z}{\delta\alpha_c(t)\delta\alpha_q(t')}\right)\bigg|_{\alpha_{c/q}=0} \\ &= \langle m_c(t)m_q(t')\rangle - \langle m_q(t)m_c(t')\rangle\,. \end{aligned} \tag{3.22}$$

This establishes the relationships between the spin operator and the fields. The Hubbard-Stratonovich fields essentially represent S_x/N, which could have been inferred from the Hubbard-Stratonovich transformation in Eq. (3.13). It is straightforward to find the analogs of these relations at higher orders by taking appropriate derivatives with respect to the source fields.

Source fields can also be introduced to calculate expectation values of S_y and S_z, however, the procedure is more complicated as the relationship between $m_{c/q}$ and these expectation values is not straightforward. These calculations will be expanded upon in Ch. 6.

3.3.2 Saddle-Point Solution

The overall factor of N in Eq. (3.16) signifies that the saddle-point solution to the path integral is valid when N is large [13]. While the saddle-point solution is essentially equivalent to the mean-field solution and neglects fluctuations, it provides a good starting point for further analysis. More importantly, we will expand the action around the saddle-point solution. First, we take the functional derivative of the action with respect to both m_c and m_q and set them to zero:

$$\left.\frac{\delta S}{\delta m_c(t)}\right|_{\substack{m_c=m\\m_q=0}} = 0\,, \qquad \left.\frac{\delta S}{\delta m_q(t)}\right|_{\substack{m_c=m\\m_q=0}} = 0\,. \tag{3.23}$$

The solutions for the fields $\langle m_c\rangle = m, \langle m_q\rangle = 0$ that satisfy these conditions are the saddle-point solutions. Because we are interested in the steady state, we are guaranteed that m is a constant, and $\langle m_q\rangle$ is always zero by definition of the Keldysh path integral as discussed in Sec. 2.3. Furthermore, because every term in the action contains at least one quantum field, the first condition in Eq. (3.23) is trivially zero. The second condition will give us the saddle-point solution m,

$$\begin{aligned}\left.\frac{\delta S}{\delta m_q(t)}\right|_{\substack{m_c=m\\m_q=0}} &= -2JNm - iN\frac{\mathrm{Tr}\left(e^{(t_f-t)\mathbb{T}_0}\mathbb{T}_q e^{(t-t_i)\mathbb{T}_0}\right)}{\mathrm{Tr}\left(e^{(t_f-t_i)\mathbb{T}_0}\right)}\\ &= -2JNm - iN\,\langle\langle I|\,\mathbb{T}_q\,|\rho_{\mathrm{ss}}\rangle\rangle = 0\,.\end{aligned} \tag{3.24}$$

There are quite a few important points to take into account when going from the first to the second line of Eq. (3.24). First, we take the derivative of the time-ordered exponential which inserts the matrix $\partial\mathbb{T}/\partial m_q(t)$ at time t in the product of the resultant time-ordered exponentials. For clarity, we define the three matrices

$$\mathbb{T}_0 = \mathbb{T}(m_c = m, m_q = 0) \tag{3.25}$$

$$\mathbb{T}_c = \left.\frac{\partial\mathbb{T}}{\partial m_c(t)}\right|_{\substack{m_c=m\\m_q=0}} = i2\sqrt{2}J\,\mathrm{diag}\{0,1,-1,0\}\,, \tag{3.26}$$

$$\mathbb{T}_q = \left.\frac{\partial\mathbb{T}}{\partial m_q(t)}\right|_{\substack{m_c=m\\m_q=0}} = i2\sqrt{2}J\,\mathrm{diag}\{1,0,0,-1\}\,. \tag{3.27}$$

Next, we take advantage of the fact that $\mathbb{T}_0$ is non-hermitian and has a left and right eigenvector with eigenvalue zero (i.e. the steady states). We know that it must have such an eigenvalue because $\mathbb{T}_0$ is

equivalent to a fully-fledged single-particle Liouvillian. The left eigenvector with eigenvalue zero is simply the vectorized identity matrix $\langle\langle I| = (1,0,0,1)^T$. The right eigenvector is the mean-field steady state

$$|\rho_{\rm ss}\rangle\rangle = \left(\frac{1}{2} + \frac{8\sqrt{2}\Delta J m}{\Gamma^2+16\Delta^2+16J^2m^2}, -\frac{\Gamma^2+16\Delta^2+4i\sqrt{2}\Gamma J m}{2(\Gamma^2+16\Delta^2+16J^2m^2)}, -\frac{\Gamma^2+16\Delta^2-4i\sqrt{2}\Gamma J m}{2\left(\Gamma^2+16\Delta^2+16J^2m^2\right)}, \frac{1}{2} - \frac{8\sqrt{2}\Delta J m}{\Gamma^2+16\Delta^2+16J^2m^2}\right)^T. \tag{3.28}$$

Using the property of the steady state, $\lim_{t\to\infty} e^{t\mathbb{T}_0}|i\rangle = |\rho_{\rm ss}\rangle\rangle$ for the right eigenvector in addition to $\lim_{t\to\infty}\langle i|e^{t\mathbb{T}_0} = \langle\langle I|$ for some vector $|i\rangle$, we can simplify the trace in the numerator of Eq. (3.24). The trace in the denominator simplifies to unity because the left and right eigenvectors of $\mathbb{T}_0$ are bi-orthonormal, i.e. $\langle\langle I|\rho_{\rm ss}\rangle\rangle = 1$. The second line of Eq. (3.24) may be solved for m, where we find three solutions:

$$m = \begin{cases} 0 & \text{Normal Phase} \\ \pm\sqrt{-\Gamma^2-16\Delta^2+32\Delta J}/4J & \text{Ordered Phase} \end{cases}. \tag{3.29}$$

We see that this solution agrees with Eq. (3.7) up to a factor of $\sqrt{2}$ which comes from the Keldysh rotation. Equipped with the saddle-point solutions, we are now able to expand the action.

3.3.3 Quadratic Expansion

Equipped with the saddle-point solutions, we can now investigate Gaussian fluctuations; i.e. the quadratic terms in the expansion of the action around the saddle-point solution. Expanding Eq. (3.16) to second-order around the saddle-point solutions in the normal phase ($m = 0$), we have

$$S^{(2)} = \frac{1}{2}\int_{t,t'} \begin{pmatrix} m_c, & m_q \end{pmatrix}_t \begin{pmatrix} 0 & P^A \\ P^R & P^K \end{pmatrix}_{t-t'} \begin{pmatrix} m_c \\ m_q \end{pmatrix}_{t'}, \tag{3.30}$$

where a factor of $\sqrt{N}$ has been absorbed into the fields for convenience. Note that the kernel is a function of the time difference only, reflecting the fact that time translation symmetry is restored in the NESS. The kernel also exhibits the Keldysh structure [4, 13, 14] as discussed in Sec. 2.3.1, therefore the elements $P^{R/A}$ can be interpreted as the retarded/advanced inverse Green's functions

and P^K as the Keldysh component. These terms are given by

$$\begin{aligned} P^R(t) = P^A(-t) &= \left.\frac{\delta \mathcal{S}}{\delta m_q(t)\delta m_c(0)}\right|_{\substack{m_c=0\\ m_q=0}} \\ &= -2J\delta(t) - i\Theta(t)\,\langle\langle I|\,\mathbb{T}_q e^{t\,\mathbb{T}_0}\mathbb{T}_c\,|\rho_{\rm ss}\rangle\rangle \\ &= -2J\delta(t) + \Theta(t) 8J^2 e^{-\frac{\Gamma}{2}t}\sin(2\Delta t)\,, \end{aligned} \tag{3.31a}$$

and

$$\begin{aligned} P^K(t) = \left.\frac{\delta \mathcal{S}}{\delta m_q(t)\delta m_q(0)}\right|_{\substack{m_c=0\\ m_q=0}} &= -i\,\langle\langle I|\,\mathbb{T}_q e^{|t|\,\mathbb{T}_0}\mathbb{T}_q\,|\rho_{\rm ss}\rangle\rangle \\ &= i8J^2 e^{-\frac{\Gamma}{2}|t|}\cos(2\Delta t)\,. \end{aligned} \tag{3.31b}$$

The above elements take a relatively simple form, with the dissipation leading to the exponential decay and the transverse field to oscillations. In addition, a delta function emerges in (3.31a) as a remnant of the Hubbard-Stratonovich transformation and ensures the proper normalization of the partition function. This delta function dissapears when calculating correlations of the original spin operators, as seen in Eq. (3.22) where it is subtracted out. The step function in the second and third line comes from $\langle\langle I|\,\mathbb{T}_c e^{t\mathbb{T}_0}\mathbb{T}_q\,|\rho_{ss}\rangle\rangle = 0$, and enforces the proper time ordering of the matrices. Because we absorbed a factor of $\sqrt{N}$ into the fields, higher-order terms in the expansion are at least of the order $O(1/N)$, rendering Eq. (3.30) exact in the thermodynamic limit.

It will be convenient to recast these expressions in frequency space. With the Fourier transform $m_{c/q}(t) = \int \frac{d\omega}{2\pi} m_{c/q}(\omega)e^{-i\omega t}$, the kernel elements are

$$P^R(\omega) = -2J - 4iJ^2\left(\frac{1}{-\Gamma/2 - i(2\Delta-\omega)} - \frac{1}{-\Gamma/2 + i(2\Delta+\omega)}\right), \tag{3.32a}$$

and

$$P^K(\omega) = 4iJ^2\Gamma\left(\frac{1}{\Gamma^2/4 + (\omega-2\Delta)^2} + \frac{1}{\Gamma^2/4 + (\omega+2\Delta)^2}\right). \tag{3.32b}$$

These analytic expressions follow from the simple form of the steady-state vector in the normal phase, $|\rho_{ss}\rangle\rangle = (1,-1,-1,1)^T/2$.

An advantage of our quantum-to-classical mapping and resultant exact action, is that we are not limited to the normal phase, we can instead explore the entire phase diagram. In the ordered

phase, evaluating expressions like Eq. (3.31) becomes difficult as they require the nontrivial form of $|\rho_{ss}\rangle\rangle$ shown in Eq. (3.28), as well as the fact that the $\mathbb{T}$ matrix is now evaluated at finite m. We nevertheless derive formal expressions for the above functions as follows. We first decompose the exponential matrix $e^{t\mathbb{T}_m}$, where $\mathbb{T}_m = \mathbb{T}\left(m_c(t) = m, m_q(t) = 0\right)$, into its spectral form

$$\begin{aligned} e^{t\mathbb{T}_m} &= \sum_{i=0}^{3} e^{\lambda_i t} \, |\lambda_i^R\rangle\rangle \, \langle\langle \lambda_i^L| \\ &= |\rho_{ss}\rangle\rangle \, \langle\langle I| + \sum_{i=1}^{3} e^{\lambda_i t} \, |\lambda_i^R\rangle\rangle \, \langle\langle \lambda_i^L| \ . \end{aligned} \tag{3.33}$$

The vectors $\langle\langle \lambda_i^L|$ and $|\lambda_i^R\rangle\rangle$ denote the i'th left and right eigenvectors of $\mathbb{T}_m$ with eigenvalue λ_i, respectively, and are normalized as $\langle\langle \lambda_i^L | \lambda_j^R\rangle\rangle = \delta_{ij}$; the bi-orthonormal structure is due to $\mathbb{T}_m$ being non-Hermitian. The expressions for the inverse response and Keldysh components in the frequency domain are then

$$P^R(\omega) = -2J - i \sum_{i=1}^{3} C_i \int_t e^{i\omega t} \Theta(t) e^{\lambda_i t} = -2J + i \sum_{i=1}^{3} C_i \frac{1}{\lambda_i + i\omega} \, , \tag{3.34a}$$

and

$$P^K(\omega) = -i \sum_{i=1}^{3} \tilde{C}_i \int_t e^{i\omega t} e^{\lambda_i |t|} = 2i \sum_{i=1}^{3} \tilde{C}_i \frac{\lambda_i}{\lambda_i^2 + \omega^2} \, . \tag{3.34b}$$

The accompanying coefficients are given by

$$C_i = \langle\langle I| \, \mathbb{T}_q \, |\lambda_i^R\rangle\rangle \, \langle\langle \lambda_i^L| \, \mathbb{T}_c \, |\rho_{ss}\rangle\rangle \, , \tag{3.35a}$$

$$\tilde{C}_i = \langle\langle I| \, \mathbb{T}_q \, |\lambda_i^R\rangle\rangle \, \langle\langle \lambda_i^L| \, \mathbb{T}_q \, |\rho_{ss}\rangle\rangle \, . \tag{3.35b}$$

$P^R(\omega)$ and $P^K(\omega)$ can be obtained by numerically solving for the eigenvalues and the eigenvectors of $\mathbb{T}_m$.

3.3.4 Diagrammatics

Despite the quadratic action being exact in the thermodynamic limit, we need to include quartic terms when considering finite-size effects. It is also at times necessary to calculate terms beyond

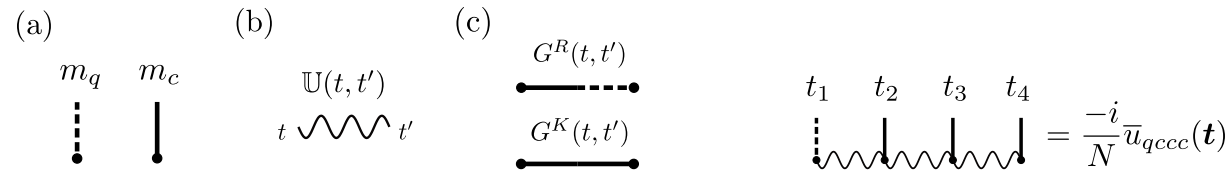

Figure 3.3 Left: Diagrammatic representation of the action expansion. (a) The solid and dashed legs in (a) represent classical (m_c) and quantum (m_q) fields, respectively. (b) The wavy line represents the time evolution where time ordering is understood from right to left. (c) Connected legs correspond to Green's functions with G^R the response function and G^K the Keldysh correlation function. Right: A representative (classical) vertex. The interaction coefficient $\overline{u}_{qccc}(\boldsymbol{t})$ is time ordered such that $t_1 \geq t_2 \geq t_3 \geq t_4$, and is given explicitly by Eq. (3.38).

quartic when performing perturbative expansions about the critical point in the ordered phase. To go beyond the quadratic action, we introduce a diagrammatic representation of the interaction terms in the expansion of the action. These terms can be found by first expanding the argument of the logarithm in Eq. (3.16) in powers of the fields as

$$S = -2J \int_t m_c(t) m_q(t) - iN \ln\left(1 + \sum_{i,\boldsymbol{\alpha}} \mathcal{D}_{i,\boldsymbol{\alpha}}\right), \tag{3.36}$$

where, as stated before, a factor of $\sqrt{N}$ has been absorbed into $m_{c/q}$, and $\mathcal{D}_{i,\boldsymbol{\alpha}}$ is the i'th-order connected diagram:

$$\mathcal{D}_{i,\boldsymbol{\alpha}} = \frac{1}{N^{\frac{i}{2}}} \int_{\boldsymbol{t}} \overline{u}_{\boldsymbol{\alpha}}(\boldsymbol{t}) m_{\alpha_1}(t_1) \cdots m_{\alpha_{i-1}}(t_{i-1}) m_{\alpha_i}(t_i). \tag{3.37}$$

Here, we have used $\boldsymbol{t}$ as a shorthand for $\{t_1, \cdots, t_{i-1}, t_i\}$ and $\boldsymbol{\alpha} = (\alpha_1, \cdots, \alpha_i)$ with $\alpha_k \in \{c, q\}$. The sum over $\boldsymbol{\alpha}$ in Eq. (3.36) is only over distinct orderings of c/q to avoid overcounting. The rules for constructing these diagrams can be found in Fig. 3.3. Connected diagrams are time ordered from right to left, therefore the interaction coefficient $\overline{u}_{\boldsymbol{\alpha}}$ is time ordered too with $t_1 \geq \cdots \geq t_{i-1} \geq t_i$. These coefficients are given by

$$\overline{u}_{\boldsymbol{\alpha}} = \overline{\mathrm{Tr}}\left(\mathbb{T}_{\alpha_1} \mathbb{U}(t_1, t_2) \mathbb{T}_{\alpha_2} \cdots \mathbb{U}(t_{i-1}, t_i) \mathbb{T}_{\alpha_i}\right), \tag{3.38}$$

where we have defined the "trace" operation $\overline{\mathrm{Tr}}(\bullet) = \langle\langle I| \bullet |\rho_{ss}\rangle\rangle$, have utilized the matrices $\mathbb{T}_{c/q}$ defined earlier, and have introduced the *propagators* $\mathbb{U}(t - t') = e^{(t-t')\mathbb{T}_0}$ with $\mathbb{T}_0 = \mathbb{T}(m = 0)$. The latter propagators are depicted as wavy lines in our diagrammatic notation; see Fig. 3.3(b). This

time-ordered representation of the interaction coefficients (and diagrams) is best understood in a scattering picture. The superket $|\rho_{ss}\rangle\rangle$ describes the nonequilibrium steady state of a pair of spins on the upper and lower branch of the vectorized space, and is taken as the "in" state. This state propagates freely (via $\mathbb{U}$) while scattering off the mean-field ($m_{c/q}$) intermittently. In other words, the interaction coefficients follow from the time-dependent perturbation theory in the expansion of the evolution operator $\mathcal{T}e^{\int_t \mathbb{T}(t)}$, with $\mathbb{T}(t) = \mathbb{T}_0 + m_c(t)\mathbb{T}_c + m_q(t)\mathbb{T}_q$, in powers of the scattering potentials $m_{c/q}\mathbb{T}_{c/q}$.

The scattering interpretation becomes manifest in Fourier space. Let's first consider the free propagator in Fourier space:

$$\mathbb{U}(\omega) = \int_{t>0} e^{-i\omega t} e^{t\mathbb{T}_0} = -\frac{1}{\mathbb{T}_0 - i\omega}. \tag{3.39}$$

Here, we have used the fact that the matrix $\mathbb{T}_0$ is diagonalizable, and that the real part of its eigenvalues λ is non-positive. For an eigenvalue with a zero real part, we substitute $\omega \to \omega - i\epsilon$ due to causality with the understanding that the limit $\epsilon \to 0$ is taken at the end of the calculation. The above expression is reminiscent of the Lippmann-Schwinger equation with $\mathbb{T}_0$ taking the role of the Hamiltonian, though we must recall that $\mathbb{T}_0$ is non-Hermitian and acts on two copies of a spin. It is often convenient to compute the interaction coefficient in the Fourier space. Some algebra yields

$$\overline{u}(\boldsymbol{\omega})_{\boldsymbol{\alpha}} = \overline{\mathrm{Tr}}\left(\mathbb{T}_{\alpha_1}\mathbb{U}(\tilde{\omega}_1)\mathbb{T}_{\alpha_2}\cdots\mathbb{U}(\tilde{\omega}_i)\mathbb{T}_{\alpha_i}\right), \tag{3.40}$$

where $\widetilde{\omega}_j = \omega_1 + \ldots + \omega_j - \omega_{j+1} - \ldots - \omega_i$.

So far, we have considered the connected diagrams that arise inside the logarithm in Eq. (3.36). However, the full diagrammatic expansion of the action requires an expansion of the logarithm too. Expanding Eq. (3.36) in powers of the connected diagrams, we obtain all interaction vertices comprising connected as well as disconnected diagrams. Formally, a multi-legged diagram with $M = \sum_{j=1}^{p} l_j$ disconnected parts is given by

$$i\frac{(M-1)!(-1)^M}{N^{-1}\prod_j^p l_j!}(\mathcal{D}_{i_1,\boldsymbol{\alpha}_1})^{l_1}(\mathcal{D}_{i_2,\boldsymbol{\alpha}_2})^{l_2}\cdots(\mathcal{D}_{i_p,\boldsymbol{\alpha}_p})^{l_p} \tag{3.41}$$

where each $\mathcal{D}_{i,\alpha}$, integrated over the corresponding time coordinates, represents one of the p unique connected diagrams with multiplicity l_j. The combinatorial factor $\frac{1}{M}\frac{M!}{\prod_j^p l_j!} = \frac{(M-1)}{\prod_j^p l_j!}$ is included, where the factor of $\frac{1}{M}$ is due to the expansion of the logarithm, and $\frac{M!}{\prod_j^p l_j!}$ accounts for each set of identical disconnected diagrams with multiplicity l_j. As an example, Fig. 3.3 depicts the diagrammatic representation of the "classical vertex" $\frac{-i}{N}\int_{\boldsymbol{t}} \overline{u}_{qccc}(\boldsymbol{t}) m_q(t_1) m_c(t_2) m_c(t_3) m_c(t_4)$ with the time integral constrained as $t_1 \geq t_2 \geq t_3 \geq t_4$. We remark that the disconnected diagrams discussed here emerge at the level of the action, before expanding the exponential factor in the partition function. Expanding the latter exponential factor will further generate disconnected diagrams whose coefficients should be properly determined from the combinatorial factors reported above. In this sense, we must keep track of the origin of various disconnected diagrams (whether they appear in the action itself or result from the expansion of the exponential factor). This pattern is in contrast with the standard diagrammatic representation and is a unique feature of our nonequilibrium setting.

The diagrams discussed here have certain causal properties. First, each diagram must come with at least one quantum leg (dashed line), reflecting the property of the Keldysh action that $S(m_c, m_q = 0) = 0$. Furthermore, the last leg of all connected diagrams is *always* a quantum field which enforces causality and ensures that the partition function retains its normalization ($Z = 1$). Curiously, only certain orderings of classical and quantum legs are allowed. The diagrammatic notation developed here will prove very useful when calculating quantities such as self-energy corrections as well as expanding the action in the ordered phase. The former can be determined systematically by contracting quantum and classical fields in these diagrams.

3.4 Mapping ODM to DDIM

Here, we show that the model in Eq. (3.5) exactly follows from the open Dicke model given by Eq. (3.2) in the limit of large cavity detuning. We emphasize that this procedure is exact and does not rely on any assumptions about the cavity mode. Beginning with Eq. (3.2), the full quantum master

equation takes the form

$$\begin{aligned}\frac{d\rho}{dt} =& -i[H_{\text{Dicke}},\rho] + \kappa\left(a\rho a^\dagger - \frac{1}{2}\{a^\dagger a,\rho\}\right)\\ &+ \Gamma\sum_i\left(\sigma_i^-\rho\sigma_i^+ - \frac{1}{2}\{\sigma_i^+\sigma_i^-,\rho\}\right).\end{aligned} \tag{3.42}$$

Following the same steps as outlined in Sec. 2.4, we obtain an action that consists of cavity, atomic and interaction terms:

$$S_D = S_{\text{cav}} + S_{\text{int}} + S_{\text{spin}}\,. \tag{3.43}$$

The cavity term in the action is given by

$$S_{\text{cav}} = \int_\omega \begin{pmatrix} a_c \\ a_q\end{pmatrix}^\dagger \begin{pmatrix} 0 & \omega-\omega_0-i\frac{\kappa}{2} \\ \omega-\omega_0+i\frac{\kappa}{2} & i\kappa\end{pmatrix}\begin{pmatrix} a_c \\ a_q\end{pmatrix}. \tag{3.44}$$

Defining $a = (x - ip)/2$, we can integrate out the imaginary component of the cavity field, p, exactly as S_{int} does not depend on p. Tracing out the spins (see Sec. **??**), we then find an *exact* expression for the action

$$S_D = \int_\omega \mathbf{x}^T(-\omega)\mathbf{D}(\omega)\mathbf{x}(\omega) - iN\ln\text{Tr}\left(\mathcal{T}e^{\int_t \mathbb{T}_D(x_{c/q}(t)}\right), \tag{3.45}$$

where $\mathbf{x}(\omega) = (x_c(\omega), x_q(\omega))^T$ and the kernel $\mathbf{D}(\omega)$ is given by

$$\begin{aligned}\mathbf{D}(\omega) &\equiv \begin{pmatrix} 0 & D^A(\omega) \\ D^R(\omega) & D^K(\omega)\end{pmatrix}\\ &= \begin{pmatrix} 0 & \frac{1}{4}\left(-\frac{(\kappa+2i\omega)^2}{4\omega_0}-\omega_0\right) \\ \frac{1}{4}\left(-\frac{(\kappa-2i\omega)^2}{4\omega_0}-\omega_0\right) & \frac{i\kappa(\kappa^2+4(\omega^2+\omega_0^2))}{16\omega_0^2}\end{pmatrix}.\end{aligned} \tag{3.46}$$

The matrix $\mathbb{T}_D$ is rather similar to that in Eq. (2.54):

$$\mathbb{T}_D(x_c(t),x_q(t)) = \begin{pmatrix} -\frac{\Gamma}{4}-i\frac{2\sqrt{2}g}{\sqrt{N}}x_q(t) & i\Delta & -i\Delta & \frac{\Gamma}{4} \\ i\Delta-\frac{\Gamma}{2} & -\frac{3\Gamma}{4}-i\frac{2\sqrt{2}g}{\sqrt{N}}x_c(t) & -\frac{\Gamma}{4} & -i\Delta-\frac{\Gamma}{2} \\ -i\Delta-\frac{\Gamma}{2} & -\frac{\Gamma}{4} & -\frac{3\Gamma}{4}+i\frac{2\sqrt{2}g}{\sqrt{N}}x_c(t) & i\Delta-\frac{\Gamma}{2} \\ \frac{\Gamma}{4} & -i\Delta & i\Delta & -\frac{\Gamma}{4}+i\frac{2\sqrt{2}g}{\sqrt{N}}x_q(t)\end{pmatrix}. \tag{3.47}$$

We then make the transformation $m_c \equiv D_0^R x_c/\sqrt{N}g$ and $m_q \equiv D_0^R x_q/\sqrt{N}g$ with $\mathbf{D}_0 \equiv \mathbf{D}(\omega = 0)$, and further define $J \equiv -g^2/D_0^R = 16g^2\omega_0/(\kappa^2 + 4\omega_0^2)$ and $\Gamma_x \equiv J\kappa/\omega_0$. The action is then cast as

$$S_D = \int_\omega \mathbf{m}^T(-\omega)\mathbf{P}(\omega)\mathbf{m}(\omega) - iN \ln \mathrm{Tr}\left(\mathcal{T} e^{\int_t \mathbb{T}(m_{c/q}(t))}\right), \tag{3.48}$$

where $\mathbf{m}(\omega) = (m_c(\omega), m_q(\omega))^T$, the kernel $\mathbf{P}$ is given by

$$\mathbf{P}(\omega) = N \begin{pmatrix} 0 & -J(1 + \frac{4i\kappa\omega - 4\omega^2}{\kappa^2+\omega_0^2}) \\ -J(1 - \frac{4i\kappa\omega+4\omega^2}{\kappa^2+\omega_0^2}) & i\Gamma_x(1 + \frac{4\omega^2}{\kappa^2+4\omega_0^2}) \end{pmatrix}, \tag{3.49}$$

and the matrix $\mathbb{T}(m_c(t), m_q(t))$ is identical to that in Eq. (3.17).

Now we consider the limit of large ω_0 and κ, in which case we can ignore those terms in Eq. (3.49) that are suppressed by a factor of $1/(\kappa^2 + \omega_0^2)$. This eliminates the frequency-dependent terms and yields the kernel

$$\mathbf{P}(\omega) \approx N \begin{pmatrix} 0 & -J \\ -J & i\Gamma_x \end{pmatrix}. \tag{3.50}$$

Using the quantum-to-classical mapping, one can show that the diagonal term ($\sim i\Gamma_x$) can be identified with dephasing in the form of the Lindblad operator $L_x = \sqrt{\Gamma_x/N}S_x$. Indeed, this agrees with the large-detuning limit discussed in Ref. [27]. Our model is different, however, due to the atomic spontaneous emission, which allows for a nontrivial nonequilibrium steady state. Finally, to obtain the DDIM, we consider the detuning ω_0 to be the largest frequency frequency scale, even compared to κ. In this limit, we can neglect the dephasing term, since $\Gamma_x = J\kappa/\omega_0 \ll J$, and recover the driven-dissipative Ising model introduced in Eq. (3.16). The advantage of this process compared to the usual adiabatic elimination procedure, is that we have not discarded any information about the cavity. We are simply showing that the action of the open Dicke model in the large detuning limit is exactly identical to the DDIM action.

CHAPTER 4

NUMERICAL METHODS

In the previous chapter, we developed a field theoretical description of the DDIM that will prove useful for analytical calculations. At the same time, it is important to benchmark analytical results against numerical simulations. This is done for a variety of reasons: the analytics often involves approximations and we want to make sure these approximations are valid and produce correct results which can be becnhmarked against numerics, or perhaps the analytics describe an effective theory of a microscopic system and we need numerics to simulate the microscopics for comparison. In our case, the analytics are performed in the thermodynamic limit, but we are also interested in finite-size scaling effects. For this, we utilize numerical simulation to obtain explicit results for finite system sizes and compare these with our scaling predictions and results in the thermodynamic limit.

In this chapter, we will discuss the two main numerical techniques we used to calculate observable quantities such as dynamical correlations and entanglement. The first is the standard exact diagonalization which makes no approximations beyond machine error, however, we take advantage of the permutation symmetry of the DDIM which requires a special basis. The second technique is the well established quantum trajectories [35], but with the added twist of using different jump operators that incorporate the permutation symmetry. Although both numerical techniques used in this work are prevalent in the literature, we must adapt them to our specific model and its symmetries. A reader mainly interested in analytical techniques and/or the physics and results, may skip this chapter without issue.

4.1 Exact Diagonalization

The simplest approach to solving for eigenstates in any quantum system is to construct the matrix governing the dynamics, e.g. a Hamiltonian or a vectorized Liouvillian, and decompose it into its eigenvectors and eigenvalues using freely available linear algebra packages in any standard

computational language. Equipped with the eigenvectors and eigenvalues, we know everything about the system and can compute any quantity we wish. A fundamental issue is that exact diagonalization must deal with the entire Hilbert space, which grows exponentially with the system size. Typically, this would heavily limit the maximum possible system size that can be ran on even high-performance computing clusters. In certain cases, we can take advantage of the system's symmetries to reduce the size of the relevant Hilbert space.

As discussed in Sec. 3.2, Eq. (3.5) has a permutation symmetry, which means that the Liouvillian remains invariant under permutation of the site indices. More rigorously, we have

$$\mathrm{P}_{\mathscr{P}}^{-1}\mathcal{L} = \mathcal{L}\,, \tag{4.1}$$

where $\mathrm{P}_{\mathscr{P}}$ is the permutation operator that permutes the site indices according to the permutation $\mathscr{P} \in S_N$, and S_N is the permutation group (or symmetric group) [36]. This symmetry lends structure to the form of the vectorized Liouvillian, breaking it into block-diagonal matrices where each block corresponds to a different permutation symmetry sector. This is analogous to Hamiltonian systems where symmetries of the Hamiltonian lead to separate sectors defined by the eigenvalues of the symmetry operator.

We are only interested in the sector that contains the steady state, which we reasonably assume (and later prove) belongs in the totally-symmetric sector, i.e. the sector where $\mathrm{P}_{\mathscr{P}}[\rho] = \rho$ for all $\mathscr{P}$ and eigenstate ρ. An example of another sector is the completely anti-symmetric sector, where $\mathrm{P}_{\mathscr{P}}[\rho] = \rho$ for even permutations and $\mathrm{P}_{\mathscr{P}}[\rho] = -\rho$ for odd permutations. The totally symmetric sector of the Liouvillian must have eigenstates that respect this symmetry, therefore, we introduce a permutation symmetric basis

$$\begin{aligned}\rho_{N_x,N_y,N_z} = \frac{1}{\mathcal{N}}\sum_{\mathscr{P}}\mathrm{P}_{\mathscr{P}}(&\sigma_1^x \otimes \ldots \otimes \sigma_{N_x}^x \otimes \sigma_{N_x+1}^y \otimes \ldots \otimes \sigma_{N_x+N_y}^y \\ &\otimes \sigma_{N_x+N_y+1}^z \otimes \ldots \otimes \sigma_{N_x+N_y+N_z}^z \otimes I_{N_x+N_y+N_z+1} \otimes \ldots \otimes I_N)\,,\end{aligned} \tag{4.2}$$

with the normalization factor $\mathcal{N} = \sqrt{N!N_x!N_y!N_z!N_I!}$. The sum is over all permutations $\mathscr{P}$ of the indices, making the overall state clearly symmetric under any permutation. These basis elements are

normalized as $\mathrm{Tr}(\rho_\mu \rho_\nu)/2^N = \delta_{\mu,\nu}$ where $\mu = (N_x, N_y, N_z)$, and the Liouvillian matrix elements are given by

$$\mathcal{L}_{\mu,\nu} = \frac{1}{2^N}\mathrm{Tr}\left(\rho_\mu \mathcal{L}[\rho_\nu]\right) . \tag{4.3}$$

In this basis, the dimensionality of totally symmetric subspace grows polynomially with the system size as $(N+1)(N+2)(N+3)/6 \sim O(N^3)$ in contrast with the exponential growth in a generic many-body system. This scaling can also be contrasted with the $O(N^4)$ growth of the angular-momentum basis with basis elements $\langle J, m | J'.m' \rangle$; each of the quantum numbers is proportional to N.

Because the Liouvillian is permutation symmetric, action of $\mathcal{L}$ on this basis will keep us in the fully symmetric subspace. To efficiently construct the matrix $\mathcal{L}_{\mu\nu}$ from the permutation symmetric basis given by Eq. (4.2), we should identify how the basis itself is transformed by $\mathcal{L}$ defined in Eq. (3.5). The action of the Liouvillian on a state can be determined analytically by inspecting how the total-spin operators act on one of our basis elements:

$$\begin{aligned} S_x \rho_{N_x,N_y,N_z} =& \sqrt{N_x(N_I+1)}\,\rho_{N_x-1,N_y,N_z} + i\sqrt{N_y(N_z+1)}\,\rho_{N_x,N_y-1,N_z+1} \\ & - i\sqrt{(N_y+1)N_z}\,\rho_{N_x,N_y+1,N_z-1} + \sqrt{(N_x+1)N_I}\,\rho_{N_x+1,N_y,N_z} , \end{aligned} \tag{4.4}$$

$$\begin{aligned} S_y \rho_{N_x,N_y,N_z} =& \sqrt{N_y(N_I+1)}\,\rho_{N_x,N_y-1,N_z} + i\sqrt{N_z(N_x+1)}\,\rho_{N_x+1,N_y,N_z-1} \\ & - i\sqrt{(N_z+1)N_x}\,\rho_{N_x-1,N_y,N_z+1} + \sqrt{(N_y+1)N_I}\,\rho_{N_x,N_y+1,N_z} , \end{aligned} \tag{4.5}$$

$$\begin{aligned} S_z \rho_{N_x,N_y,N_z} =& \sqrt{N_z(N_I+1)}\,\rho_{N_x,N_y,N_z-1} + i\sqrt{N_x(N_y+1)}\,\rho_{N_x-1,N_y+1,N_z} \\ & - i\sqrt{(N_x+1)N_y}\,\rho_{N_x+1,N_y-1,N_z} + \sqrt{(N_z+1)N_I}\,\rho_{N_x,N_y,N_z+1} , \end{aligned} \tag{4.6}$$

where $N_I = N - N_x - N_y - N_z$, and the action from the right can be found by taking the adjoint of the RHS. The only other non-trivial term is the dissipative term $\sum_i \sigma_i^- \rho \sigma_i^+$, whose action on the basis elements is given by

$$\sum_i \sigma_i^- \rho_{N_x,N_y,N_z} \sigma_i^+ = \frac{1}{2}\left[(N_I - N_z)\rho_{N_x,N_y,N_z} + \sqrt{N_z(N_I+1)}\rho_{N_x,N_y,N_z-1} - \sqrt{N_I(N_z+1)}\rho_{N_x,N_y,N_z+1}\right] . \tag{4.7}$$

Using the above relations, we find the action of the Liouvillian on our basis as

$$\begin{aligned}\mathcal{L}[\rho_{N_x,N_y,N_z}] =&\frac{4J}{N}\Big(\sqrt{(N_x+1)(N_y+1)N_zN_I}\,\rho_{N_x+1,N_y+1,N_z-1}+\sqrt{N_x(N_y+1)N_z(N_I+1)}\rho_{N_x-1,N_y+1,N_z-1}\\&-\sqrt{N_xN_y(N_z+1)(N_I+1)}\,\rho_{N_x-1,N_y-1,N_z+1}-\sqrt{(N_x+1)N_y(N_z+1)N_I}\,\rho_{N_x+1,N_y-1,N_z+1}\Big)\\&+2\Delta\Big(\sqrt{N_x(N_y+1)}\,\rho_{N_x-1,N_y+1,N_z}-\sqrt{N_y(N_x+1)}\,\rho_{N_x+1,N_y-1,N_z}\Big)\\&+\frac{\Gamma}{2}\Big((N_I-N_z-N)\rho_{N_x,N_y,N_z}-2\sqrt{(N_z+1)N_I}\rho_{N_x,N_y,N_z+1}\Big)\,.\end{aligned} \tag{4.8}$$

Using this equation, it is possible to construct the Liouvillian matrix as defined in Eq. (4.3). In the rest of this section, we take $\mathcal{L}$ to mean the matrix constructed in the numerics using Eq. (4.3), not the superoperator form.

Equipped with Eq. (4.2), we can efficiently construct the Liouvillian matrix. However, for large system sizes it is still prohibitive to store the entire matrix in memory, so it must be stored as a sparse matrix. Furthermore, finding the full spectrum of a sparse matrix is not efficient. We are only interested in the extremal state of the spectrum, namely the steady state with eigenvalue zero. In this case we can more efficiently find the steady state by employing the so-called shifted-inverse power method [37]. This technique consists of performing the iteration

$$|\rho_{k+1}\rangle\rangle = \frac{(\mathcal{L}')^{-1}\,|\rho_k\rangle\rangle}{\left\|(\mathcal{L}')^{-1}\,|\rho_k\rangle\rangle\right\|} \tag{4.9}$$

where k is the iteration step, $\mathcal{L}' = \mathcal{L} - \epsilon I$, and $|\rho\rangle\rangle = \sum_\mu c_\mu\,|\rho_\mu\rangle\rangle$, $\mu = (N_x, N_y, N_z)$ are the states represented in our permutation symmetric basis. The quantity ϵ is chosen such that the iteration converges on the eigenstate with eigenvalue closest to ϵ, i.e. the state $|\lambda_j\rangle\rangle$ where $(\lambda_j - \epsilon)^{-1}$ is the largest. While this procedure is iterative, it typically converges after only one iteration as we know that the desired state has eigenvalue zero, so we choose $\epsilon \sim 10^{-14}$.

The iterative procedure showed in Eq. (4.9) involves the inversion of the Liouvillian matrix $\mathcal{L}$. Inverting a matrix is resource intensive, especially if needed at every step of the iteration, however, we can instead equivalently solve the linear equation $\mathcal{L}'\,|v\rangle\rangle = |\rho_k\rangle\rangle$ for some vector $|v\rangle\rangle$. There are a myriad of linear solvers in every popular coding language. For systems sizes $N < 90$, it is

efficient to solve this linear equation by direct LU decomposition [38], but for larger system sizes more approximate methods are required (such as BICGSTAB [39]).

To characterize the dynamics, we typically investigate correlation and response functions of the collective spin operators $S_{x/y/z}$. As an example, we will consider observables of S_x only. We define the correlation function $C(t) = \langle\{S_x(t), S_x(0)\}\rangle/N$ and response function $\chi(t) = -i\langle[S_x(t), S_x(0)]\rangle/N$. The two-time expectation values can be calculated as [5]

$$\langle\{S_x(t), S_x(0)\}\rangle = \mathrm{Tr}\left(S_x e^{t\mathcal{L}}[S_x\rho_{ss}] + S_x e^{t\mathcal{L}}[\rho_{ss}S_x]\right) = 2\mathrm{ReTr}\left(S_x e^{t\mathcal{L}}[S_x\rho_{ss}]\right), \tag{4.10}$$

$$\frac{1}{i}\langle[S_x(t)S_x(0)]\rangle = \frac{1}{i}\mathrm{Tr}\left(S_x e^{t\mathcal{L}}[S_x\rho_{ss}] - S_x e^{t\mathcal{L}}[\rho_{ss}S_x]\right) = 2\mathrm{ImTr}\left(S_x e^{t\mathcal{L}}[S_x\rho_{ss}]\right), \tag{4.11}$$

with ρ_{ss} being the steady state density matrix. We can instead represent the above equations in a vectorized form using our permutation symmetric basis:

$$C(t) = \frac{2}{N}\mathrm{ReTr}\left(S_x e^{t\mathcal{L}}[S_x\rho_{ss}]\right) = \frac{2}{N}\mathrm{Re}\frac{\langle\langle S_x| e^{t\mathcal{L}} |S_x\rho_{ss}\rangle\rangle}{\langle\langle I|\rho_{ss}\rangle\rangle}, \tag{4.12}$$

$$\chi(t) = \frac{2}{N}\mathrm{ImTr}\left(S_x e^{t\mathcal{L}}[S_x\rho_{ss}]\right) = \frac{2}{N}\mathrm{Im}\frac{\langle\langle S_x| e^{t\mathcal{L}} |S_x\rho_{ss}\rangle\rangle}{\langle\langle I|\rho_{ss}\rangle\rangle}, \tag{4.13}$$

where we have defined the vectorized state

$$|\rho(t)\rangle\rangle = \sum_\mu c_\mu(t)\,|\rho_\mu\rangle\rangle\ . \tag{4.14}$$

The denominator in Eq. (4.12) is due to the normalization of the steady state (this is equivalent to dividing the state by $c_{0,0,0}$). In the case of static correlations, one can see that the auto-correlation function takes the simple form

$$C(0) = \frac{2}{Nc_{0,0,0}}\left(\sqrt{2N(N-1)}c_{2,0,0} + Nc_{0,0,0}\right). \tag{4.15}$$

Using these techniques, we are able to numerically investigate dynamical correlations with system sizes up to $N \sim 200$. However, this permutation symmetric basis does not provide the density matrix elements, only the vector of coefficients c_μ. This means we do not have access to entanglement quantities that require eigenvalues of the density matrix. We will introduce another numerical technique in the next section to remedy this.

4.2 Quantum Trajectories for a Permutation Symmetric Liouvillian

We wish to calculate various entanglement measures that each require explicit access to the density matrix and its eigenvalues. To do this, we utilize the numerical technique known as quantum trajectories [35, 40]. This technique simulates the dynamics of open systems through stochastic evolution of the wavefunction. To do this, it utilizes an effective non-hermitian Hamiltonian in addition to stochastic quantum jumps taking the place of the Lindblad operators from the Lindblad equation. Formally, given a Liouvillian of the form Eq. (2.16) with Lindblad operators L_α, we can write an equivalent dynamics as follows: we evolve the wavefunction according to the Schrödinger equation

$$i\partial_t |\psi\rangle = H_{\text{eff}} |\psi\rangle \ , \tag{4.16}$$

where the effective Hamiltonian is given by

$$H_{\text{eff}} = H - \frac{i}{2} \sum_\alpha L_\alpha^\dagger L_\alpha \ . \tag{4.17}$$

We discretize this differential equation and have $\partial_t |\psi(t)\rangle = (|\psi(t+\delta t)\rangle - |\psi(t)\rangle)/\delta t$, where δt is chosen to be smaller than all other timescales in the system. A quantum jump occurs at each timestep with probability

$$p = \delta t \sum_\alpha \langle\psi(t)| L_\alpha^\dagger L_\alpha |\psi(t)\rangle = \sum_\alpha p_\alpha \ , \tag{4.18}$$

and leaves the wave function in the state

$$|\psi(t+\delta t)\rangle = \frac{L_\alpha |\psi(t)\rangle}{\sqrt{p_\alpha/\delta t}} \tag{4.19}$$

where the specific Lindblad operator that acts on the state is chosen with probability p_α/p. No jump occurs with probability $1-p$, in which case we simply renormalize the wave function that has been evolved with respect to the effective Hamiltonian,

$$|\psi(t+\delta t)\rangle = \frac{1}{\sqrt{1-p}} (1 - i\delta t H_{\text{eff}}) |\psi(t)\rangle \ . \tag{4.20}$$

The renormalization is necessary because the norm of the wavefunction decays as the state evolves with respect to a non-hermitian Hamiltonian.

This procedure can be repeated for as many timesteps as desired, and produces the dynamics for a single trajectory of the quantum state. Clearly, we must repeat this dynamics for many initial states to generate enough trajectories such that we sufficiently sample the entire state space. With enough trajectories, we can average over them to produce an approximate density matrix,

$$\rho_M(t) = \frac{1}{M}\sum_k^M |\psi_k(t)\rangle\langle\psi_k(t)|\,, \tag{4.21}$$

which equals the exact density matrix given by the original Lindblad equation in the limit $M \to \infty$. This final density matrix can then be used to calculate desired observables.

In this work, we aim to take advantage of the permutation symmetry of the DDIM Liouvillian in the context of quantum trajectories. This has been established in previous works [40–42], so we will briefly introduce it here for the convenience of the reader.

Consider the angular momentum basis $|J, m, i\rangle$ where J is the total angular momentum quantum number, m is the projection along the z-axis, and i is the degeneracy label of the state. Any state of N spin-1/2's may be represented completely in this basis, we simply have $J \in \{N/2, N/2-1, \cdots, 0\}$ (assuming N is even), $m \in -J, -J+1, \cdots, J$, and the degeneracy of each total angular moment sector is given by

$$d_N^J = \frac{N!(2J+1)}{(N/2-J)!(N/2+J+1)!}\,. \tag{4.22}$$

As shown in Ref. [41], for a Liouvillian that exhibits permutation symmetry it is convenient to introduce the so-called collective basis

$$|J, m\rangle = \frac{1}{\sqrt{d_N^J}}\sum_i^{d_N^J} |J, m, i\rangle\ , \tag{4.23}$$

which groups together all states with the same J and m, but different degeneracy labels i. The insight here is that permutation symmetric processes do not distinguish between the different degenerate sectors, and therefore allows for a more compact representation by utilizing the collective basis. With this representation, we can represent a quantum state as

$$|\psi\rangle = \sum_{J,m,i} c_{J,m,i}\,|J, m, i\rangle = \sum_{J,m}\sqrt{d_N^J}c_{J,m}\,|J, m\rangle\ , \tag{4.24}$$

where we have taken advantage of the fact that different degenerate sectors are indistinguishable to enforce $c_{J,m} = c_{J,m,i}\ \forall\ i$. This representation can be extended to density matrices as well,

$$\rho = \sum_J \sum_{m,m'} d_N^J c_{J,m;m'} \left|J,m\right\rangle\!\left\langle J,m'\right| , \quad \left|J,m\right\rangle\!\left\langle J,m'\right| = \frac{1}{d_N^J} \sum_i \left|J,m,i\right\rangle\!\left\langle J,m',i\right| . \tag{4.25}$$

The factor of d_N^J in the definition of the collective states preserves normalization, and can actually be omitted when performing calculations until expectation values or traces or performed. We note that the density matrix element $\left|J,m\right\rangle\!\left\langle J,m'\right|$ in the collective basis is *not* the outer product of Eq. (4.24) with itself, as that would lead to two sums over the degeneracy label. We are abusing notation for convenience.

In Ref. [41], it was shown that a permutation symmetric Liouvillian preserves collective states, i.e.

$$\mathcal{L}[\left|J,m\right\rangle\!\left\langle J,m'\right|] = \sum_{J',m_1,m_2} f^{J,m,m'}_{J',m_1,m_2} \left|J',m_1\right\rangle\!\left\langle J',m_2\right| , \tag{4.26}$$

where f is simply a function of its indices. Note that after action by the Liouvillian we retrieve a linear combination of collective states, and that the Liouvillian does not introduce coherence's between sectors of different J. Therefore, the collective states are a good basis with which to characterize the dynamics of the state with respect to the permutation symmetric Liouvillian. In fact, this basis represents the same subspace as the permutation symmetric basis introduced in Eq. (4.2), as they both scale with system size as $(N+1)(N+2)(N+3)/6$.

We aim to utilize this representation in the context of quantum trajectories, which means we need to determine how the jump operators behave in this collective basis representation. In Ref. [40], it was shown that the permutation symmetric decay channels of the form

$$\mathcal{D}_{\sigma^-}[\bullet] = \Gamma \sum_i \sigma_i^- \bullet \sigma_i^+ - \frac{1}{2}\{\sigma_i^+\sigma_i^-, \bullet\} \tag{4.27}$$

can be described by three separate jump operators which transform the state amplitudes as follows

$$c_{J+q,m-1}(t+\delta t) = \sqrt{\delta t \Gamma} P_q^{J,m} c_{J,m}(t) , \tag{4.28}$$

where $q \in \{-1, 1, 0\}$ and each channel occurs with probability $p_q = \delta t \Gamma d_N^J \sum_m |P_q^{J,m} c_{J,m}(t)|^2$. The coefficients $P_q^{J,m}$ are given by

$$P_{-1}^{J,m} = -\sqrt{\frac{(N+2J+2)(J+m)(J+M-1)}{4J(2J+1)}} \tag{4.29}$$

$$P_0^{J,m} = \sqrt{\frac{(2+N)(J+m)(J-m+1)}{4J(J+1)}} \tag{4.30}$$

$$P_1^{J,m} = \sqrt{\frac{(N-2J)(J-m+1)(J-m+2)}{4(J+1)(2J+1)}}\,. \tag{4.31}$$

These are all the ingredients necessary to evaluate the quantum trajectory dynamics of the DDIM Liouvillian in the collective state basis. Furthermore, we can see from Eq. (4.28) the origin of the properties of Eq. (4.26). Most notably, the wavefunction has one definite value of J at any given time such that when the outer product is taken to obtain the density matrix, there are no coherences generated between states with different J's.

In this work, we apply this formalism to the case where we split the system in to two subsystems. Consider the case where we have N spins, and we wish to divide the system into to two equally sized subsystems A and B. It is straightforward to define the split system collective spin operators $S_\alpha = S_\alpha^A + S_\alpha^B$ for $\alpha \in \{x, y, z\}$, and to write the Liouvillian in terms of the two subsystems:

$$\mathcal{L}[\bullet] = -i[H, \bullet] + \mathcal{D}_{\sigma^-}^A + \mathcal{D}_{\sigma^-}^B\,, \tag{4.32}$$

where

$$H = -\frac{J}{N}\left(S_x^A + S_x^B\right)^2 + \Delta\left(S_z^A + S_z^B\right)\,. \tag{4.33}$$

Each of the dissipators $\mathcal{D}^{A/B}$ strictly act on their respective subsystem. We now introduce the split system collective basis,

$$|\psi\rangle = \sum_{J_A,J_B}\sum_{m_A,m_B} c_{m_A;m_B}^{J_A,J_B}\,|J_A, m_A\rangle\,|J_B, m_B\rangle\,, \quad \sum_{J_A,J_B}\sum_{m_A,m_B} d^{J_A} d^{J_B} |c_{m_A;m_B}^{J_A,J_B}|^2 = 1 \tag{4.34}$$

where we have defined $d_{N/2}^J = d^J$ for each of the multiplicities as it is always understood that we have divided the system in half. The density matrix follows straightforwadly,

$$\rho = \sum_{J_A,J_B}\sum_{m_A,m_A'}\sum_{m_B,m_B'} c_{m_A,m_A';m_B,m_B'}^{J_A,J_B}\,|J_A, m_A\rangle\langle J_A, m_A'| \otimes |J_B, m_B\rangle\langle J_B, m_B'|\,, \tag{4.35}$$

with normalization

$$\sum_{J_A,J_B} \sum_{m_A,m_B} d^{J_A} d^{J_B} c^{J_A,J_B}_{m_A,m_A;m_B,m_B} = 1 \,. \tag{4.36}$$

Now, it is easy to see that Eq. (4.32) preserves the collective basis states, even in this split basis. The Hamiltonian portion is given purely in terms of collective operators which are guaranteed to keep the state in the collective basis. The dissipative terms act solely on system A and system B individually and are permutation symmetric within the given subsystem. More explicitly, we have $\mathcal{D}^A_{\sigma^-}[|J_A, m_A\rangle\langle J_A, m'_A|]$ (and similarly for B), which is of the same form as Eq. (4.26) and thus takes collective states to collective states. Therefore, we have shown that the formalism developed in [41] applies to the split system collective basis as well.

Finally, we discuss what various entanglement quantities are formally in terms of the collective basis. Care must be taken with the placement of the multiplicity factor. To make sure it is in the correct place, simply perform the calculation while including the degeneracy label explicitly and then drop the label at the end. This should yield an expression with the multiplicity factor in the correct place. For example, consider the von Neumann entropy, $S_{\text{vN}} = -\text{Tr}(\rho \log \rho)$. Writing this in terms of the eigenvalues of the complete density matrix $\lambda^J_{m,i}$ with i the degeneracy label, we find

$$S_{\text{vN}} = -\sum_{J,m} \sum_{i=1} \lambda^J_{m,i} \log \lambda^J_{m,i} = -\sum_{J,m} d^J_N \lambda^J_m \log \lambda^J_m \,. \tag{4.37}$$

To obtain the final equality, we utilized the property of the collective states to set $\lambda^J_{m,i} = \lambda^J_m \;\forall\; i$. The quantities λ^J_m are the eigenvalues of the density matrix ρ^J in angular momentum sector J. From this simple procedure, we have identified the correct location for the multiplicity factor d^J_N. The structure shown here can be used for studying any non-linear function of the density matrix, i.e. the logarithmic negativity.

CHAPTER 5

CRITICAL PROPERTIES

In this chapter we utilize the formalism developed in the previous chapter to calculate a host of interesting features near the phase boundary of the DDIM. Namely, we investigate the effective temperature, which can be defined for nonequilibrium systems, as well as the critical exponents that characterize the phase transition. Furthermore, we find that the DDIM has two distinct universality classes. The details of these two universality classes will be discussed in Sec. **??**, but we briefly introduce them here. Along the entire phase boundary, except for a single point, the DDIM is in the same universality class as the classical Ising model with Glauber dynamics. The singular point, which we denote as the weakly-dissipative critical point, is at $\Delta = 2J, \Gamma \to 0$ and has the system in the same universality class as the infinite-range transverse-field Ising model at finite temperature. We characterize these classes and their exponents using a simple finite-size scaling analysis.

5.1 Correlation and Response Functions

The principle quantities of interest in a many-body system are correlation and response functions. Correlation functions characterize fluctuations in the system, and are signatures for many physical phenomena such as phase transitions and dynamics [4, 43]. Response functions tell us how a system responds to a small perturbation (as they are derived from linear response theory [43], and this response contains information about the excitation spectrum of the system as well as how it relaxes [4, 13, 14].

In the thermodynamic limit, where the quadratic action in Eq. (3.30) is exact, we can easily find the correlation and response functions by inverting the kernel. This inversion is more easily done in frequency space, where we find

$$\begin{aligned} C(\omega) = \frac{1}{N}\mathcal{F}_\omega\langle\{S_x(t), S_x(0)\}\rangle &= \langle m_c(\omega) m_c(-\omega)\rangle \\ &= \frac{-iP^K(\omega)}{P^R(\omega)P^A(\omega)}\,, \end{aligned} \tag{5.1a}$$

and the response function

$$\begin{aligned}\chi(\omega) &= \frac{1}{iN}\mathcal{F}_\omega\langle[S_x(t), S_x(0)]\rangle \\ &= \frac{1}{i}\langle m_q(\omega)m_c(-\omega) - m_c(\omega)m_q(-\omega)\rangle \\ &= \frac{1}{P^R(\omega)} - \frac{1}{P^A(\omega)}\,. \end{aligned} \tag{5.1b}$$

We have defined the Fourier transform operation, $\mathcal{F}_\omega(f(t)) = \int_t e^{i\omega t} f(t)$. The explicit forms of these functions can be obtained from Eqs. (3.32a) and (3.32b) as

$$C(\omega) = \frac{\Gamma(\Gamma^2 + 4(4\Delta^2 + \omega^2))}{2(\omega-\omega_1)(\omega-\omega_2)(\omega-\omega_1^*)(\omega-\omega_2^*)}\,, \tag{5.2a}$$

and

$$\chi(\omega) = 4\Delta\left(\frac{(\omega-\omega_1^*)(\omega-\omega_2^*) - (\omega-\omega_1)(\omega-\omega_2)}{(\omega-\omega_1)(\omega-\omega_2)(\omega-\omega_1^*)(\omega-\omega_2^*)}\right). \tag{5.2b}$$

The poles in these equations are given by

$$\omega_1 = -\frac{i}{2}(\Gamma - \Gamma_c)\,, \qquad \omega_2 = -\frac{i}{2}(\Gamma + \Gamma_c)\,, \tag{5.3}$$

where $\Gamma_c = 4\sqrt{(2J-\Delta)\Delta}$. We thus observe that ω_1 is the "soft mode" which vanishes at the phase transition, while we can identify ω_2 as the "fast mode" that remains finite. The soft mode is responsible for critical dynamics and signifies the critical slowdown as we approach the phase transition. The intuition behind this can be seen by writing the correlation function as $C(t) = c_1 e^{-i\omega_1|t|} + c_2 e^{-i\omega_2|t|}$ and considering the case where $\Gamma \to \Gamma_c$. At long times, we see that $C(t) \sim c_1 e^{-\omega_1 t}$ survives, while c_2 dies out because $\omega_2 \gg \omega_1$. We also see that the time-scale of the dynamics, $1/\omega_1$, diverges as we approach the phase boundary which is the reason for the nomenclature critical slowdown. Therefore, c_1 and ω_1 will determine the static and dynamical critical behaviour of the correlation function respectively. The limit $\Gamma_c \to 0$, where both poles become soft, gives rise to qualitatively different behavior as we shall discuss later.

We can easily Fourier transform Eqs. (5.2a) and (5.2b) back to the time domain by performing the contour integral over their simple poles. In the time domain, the correlation and response function are given by

$$C(t) = \frac{e^{-\Gamma|t|/2}}{\Gamma_c}\left(\frac{\Gamma\Gamma_c + 16(J-\Delta)\Delta}{\Gamma+\Gamma_c}e^{-\Gamma_c|t|/2} + \frac{\Gamma\Gamma_c - 16(J-\Delta)\Delta}{\Gamma-\Gamma_c}e^{\Gamma_c|t|/2}\right), \tag{5.4a}$$

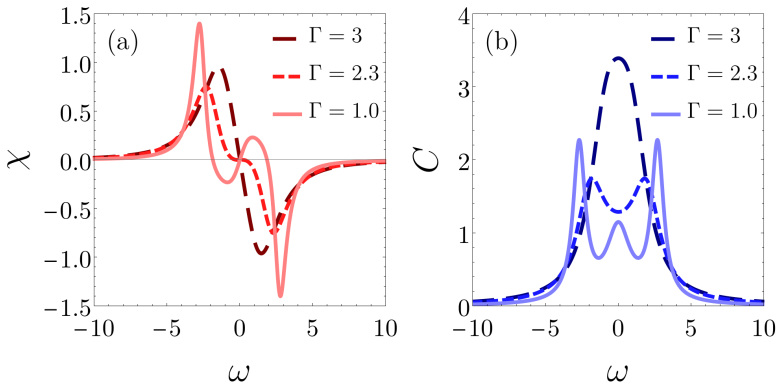

Figure 5.1 The response function (a) and correlation function (b) in the ordered phase ($J = 1, \Delta = 1$) for different values of Γ. (a) As we move away from the phase boundary, $\chi(\omega)$ at low frequencies plateaus before changing sign, indicating a gainy rather than lossy behavior. (b) The peak at $\omega = 0$, signifying the dominant soft mode near the phase boundary, splits into two as Γ is decreased. For sufficiently small Γ ($\lesssim 2.3$), another peak appears at $\omega = 0$.

and

$$\chi(t) = \mathrm{sgn}(t)\frac{4\Delta}{\Gamma_c}e^{-\Gamma|t|/2}\left(e^{-\Gamma_c|t|/2} - e^{\Gamma_c|t|/2}\right). \tag{5.4b}$$

We can identify two distinct regimes in the disordered phase. For $\Delta < 2J$, we see that Γ_c is real, and that both $C(t)$ and $\chi(t)$ are purely relaxational. On the other hand, Γ_c becomes imaginary for $\Delta > 2J$, hence complex-valued poles, and the dynamics becomes underdamped. In this regime, the overall decay rate is controlled by Γ, and the oscillation time scale is set by Γ_c. This behavior arises due to the competition between the interaction J and the transverse field Δ. For sufficiently large Δ, the transverse field is dominant and causes the large spin to precess about the z-axis; while on average the longitudinal spin components are zero, their temporal correlations expose the oscillations.

In the ordered phase, the correlation and response function can be evaluated numerically starting with the inverse response and Keldysh elements in Eqs. (3.34a) and (3.34b). In Fig. 5.2, we plot $\chi(\omega)$ and $C(\omega)$ within the ordered phase and for different values of Γ. As Γ is decreased, the low-frequency region of $\chi(\omega)$ changes sign, indicating that the system is no longer lossy and is rather "gainy" at low frequencies. This behavior is of course related to the driven nature of the system. Similarly, the correlation function shows a single peak at $\omega = 0$ for larger Γ close to the

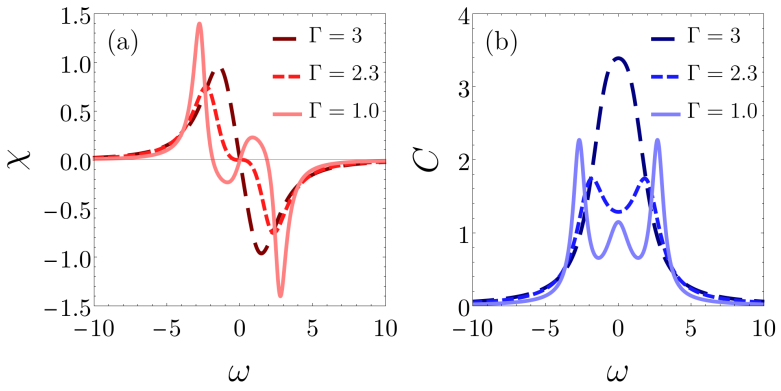

Figure 5.2 The response function (a) and correlation function (b) in the ordered phase ($J = 1, \Delta = 1$) for different values of Γ. (a) As we move away from the phase boundary, $\chi(\omega)$ at low frequencies plateaus before changing sign, indicating a gainy rather than lossy behavior. (b) The peak at $\omega = 0$, signifying the dominant soft mode near the phase boundary, splits into two as Γ is decreased. For sufficiently small Γ ($\lesssim 2.3$), another peak appears at $\omega = 0$.

phase boundary (within the ordered phase); this behavior can be attributed to the soft mode. As we move away from the phase boundary, this peak splits into two and eventually gives rise to a smaller peak at $\omega = 0$. Indeed, this appears at the same point where the low-frequency behavior of χ changes qualitatively. In Sec. 5.2, we show that this behavior can be interpreted as the emergence of a negative effective temperature.

5.2 Effective Thermalization Near Criticality

Driven-dissipative systems are inherently nonequilibrium, and therefore there is no intrinsic notion of temperature. However, a standard procedure is to define an *effective* temperature by imposing a fluctuation-dissipation relation (FDR)[13, 14, 33, 44–46],

$$P^K(\omega) = F(\omega)\left(P^R(\omega) - P^A(\omega)\right), \tag{5.5}$$

where $F(\omega)$ is a distribution function defined by this equation. In equilibrium, and at finite temperature, the distribution function only depends on temperature and takes the form $F(\omega) = \coth(\omega/2T)$. Specifically, the low-frequency limit of the distribution function yields the classical FDR with $F(\omega) = 2T/\omega$. While there is no intrinsic temperature in our driven-dissipative system, we can still impose the classical form of the FDR (to be justified later) to identify the effective

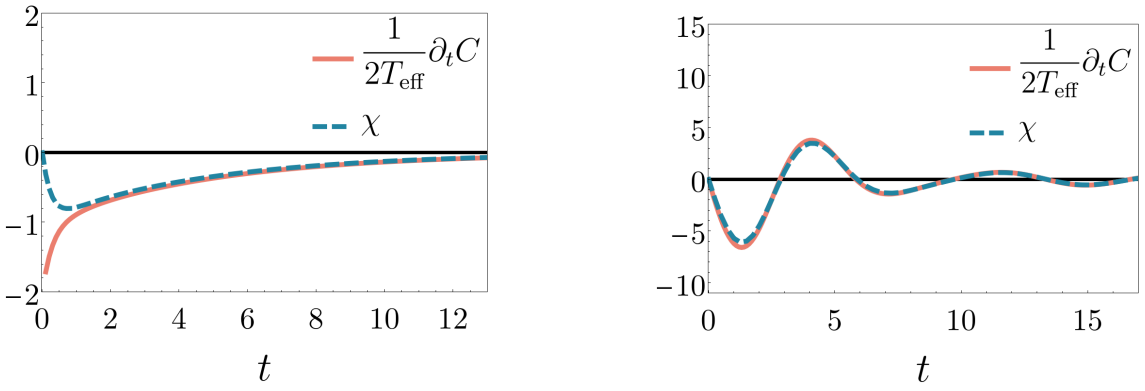

Figure 5.3 Numerical plot of the correlation and response functions with a system size of $N = 100$ obeying the classical FDR near the phase boundary. (Left) Generic critical point ($J = 1, \Delta = 1, \Gamma = 4$), where we see that the classical FDR $\chi(t) = \partial_t C(t)/2T_{\text{eff}}$ holds at long times ($t \gtrsim \Gamma^{-1}$) with $T_{\text{eff}} = J$. (Right) The weakly-dissipative critical point ($J = 1, \Delta = 2, \Gamma = 0.1$) where the classical FDR holds for exact numerics almost perfectly at all times with $T_{\text{eff}} = J$.

temperature; in the normal phase, we find

$$T_{\text{eff}} = \lim_{\omega\to 0} \frac{\omega}{2} \frac{P^K(\omega)}{P^R(\omega) - P^A(\omega)} = \frac{\Gamma^2 + 16\Delta^2}{32\Delta} . \tag{5.6}$$

The effective temperature diverges as $\Delta \to 0$ in harmony with the observation in Ref. [47] that, in the absence of a transverse field, the population (in the S_x basis) is that of a fully mixed state, hence infinite temperature. We must note however that an effective temperature defined at low frequencies is only sensible near a critical point where a slow mode dominates the dynamics. In contrast, various modes contribute to the effective temperature away from criticality, i.e., away from the phase boundary, which further complicates the interpretation of the low-frequency effective temperature.

Exactly at the phase transition, we find that the effective temperature is simply given by $T_{\text{eff}} = J$ everywhere along the phase boundary. Equation (5.6) can also be expressed in the time domain, $\chi(t) = \partial_t C(t)/2T_{\text{eff}}$, which provides another form of the classical FDR [48]. This relationship holds analytically for the correlation and response functions in Eqs. (5.4a) and (5.4b) with $T_{\text{eff}} = J$. We can further inspect the classical FDR at criticality using exact numerics: in Fig. 5.3(Left), we show that, with the exception of short times differences, this relation holds at criticality. We further inspect the behavior at the weakly dissipative critical point $\Gamma \to 0$ in Fig. 5.3(Right) and

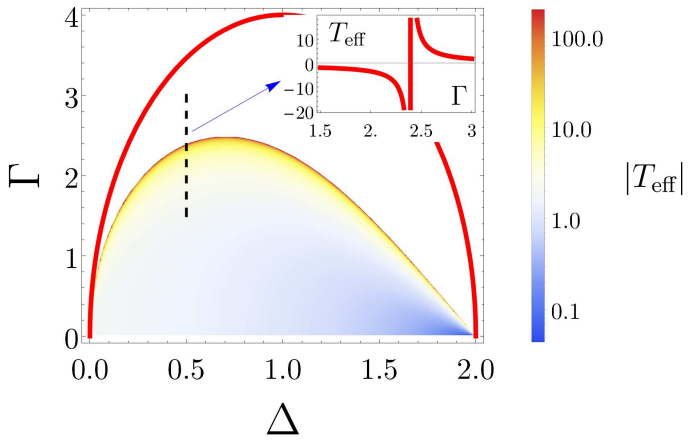

Figure 5.4 Density plot of $|T_{\text{eff}}|$ in the ordered phase as a function of Δ and Γ; we have set $J = 1$. The thick curve indicates the phase boundary and the highlighted region indicates the region with negative effective temperature. (Inset) The effective temperature in the ordered phase ($J = 1, \Delta = 0.5$) as a function of Γ, taken along the dashed line in the main figure. As Γ decreases, the effective temperature diverges and then flips sign.

find that the classical FDR holds remarkably well at all times. The agreement between T_{eff} in the time and frequency domains at the phase boundary further cements the applicability of the fluctuation-dissipation relation near phase transitions.

In the ordered phase, we can numerically evaluate the effective temperature by combining the expressions given in Eqs. (3.34a) and (3.34b) together with the definition of the effective temperature in Eq. (5.5). Interestingly, as Γ is lowered, the effective temperature diverges deep in the ordered phase and then flips sign; see the inset of Fig. 5.4. This behavior occurs due to the change in sign of the low-frequency behavior of $\chi(\omega)$ as was pointed out in Fig. 5.2(a). The curve corresponding to infinite temperature ends at the weakly dissipative critical point $\Gamma \to 0$ and $\Delta = 2J$. We can thus employ our field-theoretical toolbox to analytically investigate the origin of this behavior.

At a technical level, we want to characterize the fluctuations around the ordered field, m, within the ordered phase. To this end, we consider the action describing the fluctuations around the ordered field as

$$S = \int_{\omega} m_q P^R_{\text{ord}}(\omega) \delta m_c + \cdots \tag{5.7}$$

where $\delta m_c(t) = m_c(t) - m$ and $P^R_{\text{ord}}(\omega)$ is given exactly by Eq. (3.34a) (recall that $\langle m_q \rangle = 0$

always!) This quadratic description is found by first expanding Eq. (3.16) to the necessary order about $m_c = 0$, and then expanding that expression to second-order about $m_c = m$. To probe the effective temperature T_{eff}, we must expand $P^R_{\text{ord}}(\omega)$ at low frequencies as

$$P^R_{\text{ord}}(\omega) \sim -r + i\gamma_{\text{ord}}\omega + \cdots \tag{5.8}$$

Now, $\gamma_{\text{ord}} > 0$ indicates dissipation, while $\gamma_{\text{ord}} < 0$ implies gain as this coefficient characterizes friction in the low-frequency dynamics. Due to the definition of the low-frequency effective temperature in Eq. (5.6), there is no straightforward analogy with the equilibrium notion of population inversion. While the full expression for P^R in the ordered phase is not analytically tractable, we can utilize the diagrammatics developed in Sec. 3.3.4: the diagrams that contribute to P^R_{ord} in the ordered-phase can be found in Fig. 5.5. The explicit forms of the interaction coefficients, and an example calculation, can be found in Appendix 5.A. It turns out that to capture the negative temperature, we must include the sixth-order terms in the diagrammatic expansion. We find

$$P^R_{\text{ord}}(\omega) = P^R(\omega) + m^2 P^R_1(\omega) + m^4 P^R_2(\omega) + \cdots , \tag{5.9}$$

where m is given by Eq. (3.29), $P^R(\omega)$ by Eq. (3.32a), $P^R_1(\omega)$ is given by

$$\begin{aligned} iP^R_1(\omega) =& \overline{u}_{qccc}(-\omega, \omega, 0, 0) + \overline{u}_{qccc}(-\omega, 0, \omega, 0) \\ &+ \overline{u}_{qccc}(-\omega, 0, 0, \omega) , \end{aligned} \tag{5.10}$$

and $P^R_2(\omega)$ is given by

$$\begin{aligned} iP^R_2(\omega) =& \overline{u}_{qcccc}(-\omega, \omega, 0, 0, 0, 0) \\ &+ \overline{u}_{qcccc}(-\omega, 0, \omega, 0, 0, 0) + \overline{u}_{qcccc}(-\omega, 0, 0, \omega, 0, 0) \\ &+ \overline{u}_{qcccc}(-\omega, 0, 0, 0, \omega, 0) + \overline{u}_{qcccc}(-\omega, 0, 0, 0, 0, \omega) . \end{aligned} \tag{5.11}$$

Expanding Eq. (5.9) to first order in ω, we find the friction coefficient

$$\begin{aligned} \gamma_{\text{ord}} =& \frac{127J^2\Delta}{\Gamma(\Gamma^2 + 16\Delta^2)^4}\Big[26\Gamma^6 - 4096\Delta^4(\Delta - 2J)^2 + \\ & 16\Gamma^4\Delta(53\Delta - 84J) + 256\Gamma^2\Delta^2(68J^2 - 80J\Delta + 25\Delta^2)\Big] , \end{aligned} \tag{5.12}$$

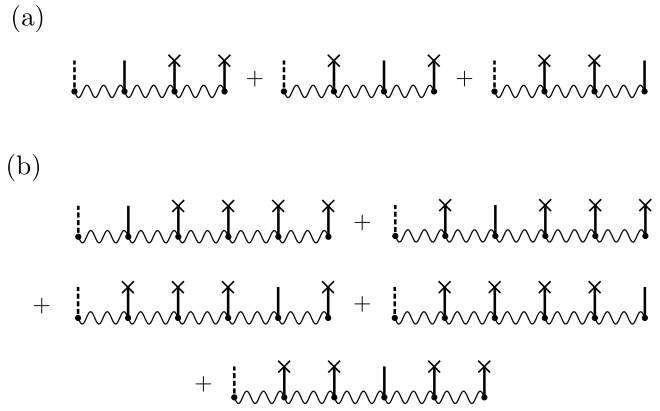

Figure 5.5 Diagrams contributing to (a) P_1^R and (b) P_2^R in calculating $\gamma_{\rm ord}$. A cross (x) at the end of a leg corresponds to evaluating the corresponding classical field at its saddle-point value.

which indeed captures the negative effective temperature in the ordered phase near the phase boundary at $\Delta = 2J$ and $\Gamma \to 0$; see Fig. 5.4. Indeed, we find that the infinite-temperature curve near the weakly dissipative critical point is given by the line $\Gamma = 2\sqrt{2}(2J - \Delta)$, in harmony with Fig. 5.4. We finally remark that, for $\Delta < 2J$, the effective temperature $T_{\rm eff} \to 0^-$ in the limit $\Gamma \to 0$.

Before closing this section, a remark about the effective temperature is in order. The latter temperature characterizes fluctuations and dissipation of the system at low frequencies. However, it does not imply that the steady state is a thermal state, i.e. $\rho \neq e^{-H/T_{\rm eff}}$. This can be seen by comparing the equilibrium phase diagram [28] versus the nonequilibrium phase diagram in Fig. 3.2. Specifically, the infinite-range Ising model in a transverse field undergoes a phase transition at a critical value of the transverse field that is $\Delta_c(T) < 2J$ at any finite temperature, a behavior that should be contrasted with our driven-dissipative model where at $\Delta = 0$ there is no phase transition.

5.3 Critical Behavior

Just like their equilibrium counterparts, nonequilibrium steady states may undergo phase transitions and exhibit critical phenomena. A characteristic feature of criticality is a diverging correlation length, where the length-scale of two-body correlations grows as the system approaches criticality [43]. The dynamical analog of this phenomena is called critical slowdown and is signaled by a diverging time scale in the dynamics of correlations [48] (as discussed in Sec. 5.1. While there

is no intrinsic length scale in an infinite-ranged model, we will identify the dynamical critical behavior of the model considered here and investigate the finite-size scaling with the system size N [31, 49] using standard scaling techniques. Interestingly, we shall see that two distinct dynamical critical behaviors emerge depending on the strength of dissipation.

It is well known that phase-transitions, in their exact sense, occur only in the thermodynamic limit [50]. However, signatures of the phase transition remain visible at finite system sizes. For example, suppose we have a correlation function $C(r, N)$ that is a function of the distance from the critical point as well as the system size. We know that in the limit $N \to \infty$, the correlation function should diverge as $r \to 0$, and at finite N the correlation function $C(r, N)$ remains finite. These two limits imply that the correlation function must *scale* in a way with N such that it diverges in the thermodynamic limit, i.e. $C(r = 0, N) \sim N^{\alpha}$ where α is the static scaling exponent. This exponent is a feature of the physics at the phase transition, and is one of the properties that defines the phase transition's universality class. A similar framework may be applied to the dynamics. As discussed previously, the dynamics of the correlation function experience critical slowdown, where the timescale of the dynamics diverges in the limit $r \to 0$. This occurs because the "gap", i.e. the distance of the Liouvillian's eigenvalue with the smallest real part from zero, closes at criticality. However, the gap remains finite for a finite system size N, therefore, critical slowdown is a feature of the thermodynamic limit. The timescale of the dynamics must then also scale with the system size, $t \sim N^{\zeta}$, where ζ is the dynamical exponent. The static exponent α and dynamical exponent ζ together characterize the universality class of the phase transition, and are our primary quantities of investigation in this section.

5.3.1 Criticality at Finite Γ

Before investigating the finite-size scaling, we first determine the scaling dimensions of the fields at the quadratic level of the action. A low-frequency expansion of Eq. (3.30) yields the quadratic action

$$S \sim \int_t m_q(-\gamma\partial_t - r)m_c + \frac{1}{2}Dm_q^2\,, \tag{5.13}$$

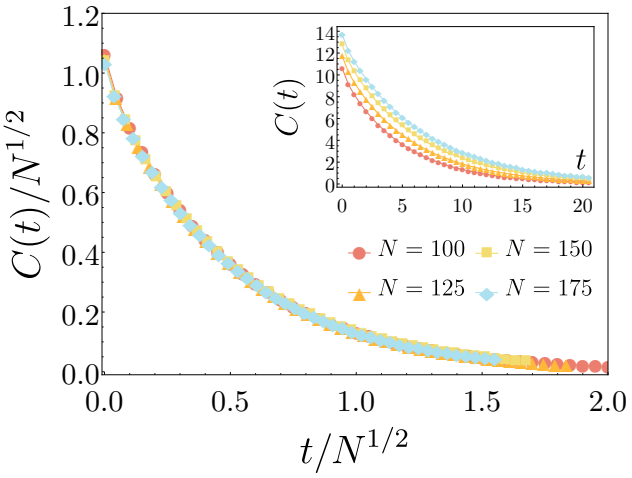

Figure 5.6 Exact numerics of the finite-size scaling behavior of the correlation function at a generic critical point ($J = 1, \Delta = 1, \Gamma = 4$). The critical dynamics is overdamped and is governed by a characteristic time scale that scales as $t \sim N^{1/2}$, typical of critical driven-dissipative systems.

with r the distance from the critical point, γ a damping parameter, and D the strength of the noise:

$$r = -P^R(\omega = 0) = \frac{2J[\Gamma^2 - 16\Delta(2J - \Delta)]}{\Gamma^2 + 16\Delta^2}, \tag{5.14a}$$

$$\gamma = -i\partial_\omega P^R(\omega)|_{\omega=0} = \frac{256J^2\Gamma\Delta}{(\Gamma^2 + 16\Delta^2)^2}, \tag{5.14b}$$

$$D = P^K(\omega = 0) = \frac{32iJ^2\Gamma}{\Gamma^2 + 16\Delta^2}. \tag{5.14c}$$

The m_q^2 term is referred to as "noise" because Eq. (5.13) may be mapped to a dynamical equation with a random noise term with strength D; see Sec. 5.4. To find the scaling dimensions of the fields, we demand that the action be scale invariant at the critical point ($r = 0$). One can see that the action is invariant upon rescaling [23]

$$t \to \lambda t, \quad m_c \to \sqrt{\lambda} m_c\,, \quad m_q \to \frac{1}{\sqrt{\lambda}} m_q\,, \tag{5.15}$$

with λ an arbitrary scaling parameter that can be chosen freely. These scaling relations determine the scaling dimensions of the fields to be $[m_c] = \frac{1}{2}$, $[m_q] = -\frac{1}{2}$; simply their dimensions with respect to time. These scaling dimensions in turn determine the scaling behavior of the correlation and response functions, and are consistent with Eqs. (5.4a) and (5.4b) in the limit $\Gamma \to \Gamma_c$; see also [51].

To determine the finite-size scaling behavior of the model, we must include finite-size corrections to the quadratic action in Eq. (5.13). To lowest order in $O(N^{-1})$, the finite-size corrections are given by the 4-legged diagrams derived in Sec. 3.3.4. Furthermore, it follows from the above scaling dimensions that the most relevant correction (in a renormalization-group sense) is the classical vertex which has a low-frequency limit of [14]

$$S_{\text{int}} = \frac{-u}{2N} \int_t m_c^3 m_q + \cdots , \tag{5.16}$$

with

$$u = 2i\overline{u}_{cccq}(\omega = 0) = \frac{2048 J^4 \Delta}{(\Gamma^2 + 16\Delta^2)^2} . \tag{5.17}$$

To see that this is true, perform the rescaling according to the prescription in Eq. (5.15) on the classical vertex and the quantum vertex. The classical vertex scales as $\lambda^2 \int_t m_c^3 m_q$ and the quantum vertex scales as $\sim \lambda^0 \int_t m_c m_q^3$. Ignoring the subtlety about the quantum vertex being marginally relevant (which is actually not a problem when we consider the scaling of N next), we see that the classical vertex grows with $\lambda \to \infty$.

We now demand that the full low-frequency expansion of the action, with the inclusion of the classical vertex and at a finite distance from the critical point ($r \neq 0$), remains scale invariant. This is achieved upon rescaling

$$\begin{gathered} t \to \lambda t, \quad m_c \to \sqrt{\lambda} m_c , \quad m_q \to \frac{1}{\sqrt{\lambda}} m_q, \\ r \to \frac{1}{\lambda} r , \quad N \to \lambda^2 N , \end{gathered} \tag{5.18}$$

where the first line, also given by Eq. (5.15), is included for completeness. Equipped with these scaling dimensions, the correlation function takes on the scaling form

$$C(t) = \langle m_c(t) m_c(0) \rangle = \lambda^{-1} \hat{C}(\lambda |t|, \lambda^{-1} r, \lambda^{-2} N^{-1}) , \tag{5.19}$$

with $\hat{C}$ a universal scaling function with scale invariant arguments. Setting $\lambda = r$, $t = 0$, and taking the thermodynamic limit $N \to \infty$, we obtain the "photon-flux" exponent $C \sim 1/r^{\nu}$ through the relation

$$C(0) = \frac{1}{r} \hat{C}(0, 1, 0) , \tag{5.20}$$

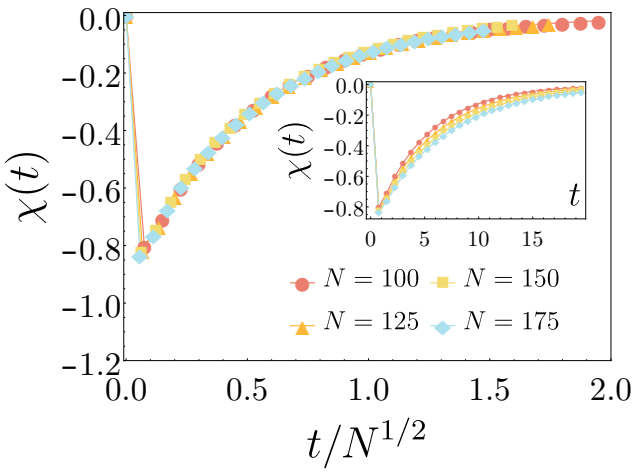

Figure 5.7 Finite-size scaling behavior of the response function at a generic critical point ($J = 1, \Delta = 1, \Gamma = 4$) from exact numerics. The amplitude of the response function does not scale with N, while the characteristic time scale of the dynamics scales as $t \sim N^{1/2}$, identifying the dynamical exponent $\zeta = 1/2$.

which establishes the exponent $\nu = 1$ [14]. Next we determine the finite-size scaling at criticality ($r = 0$). Here, we set $\lambda = N^{-1/2}$ in Eq. (5.19), which leads to the scaling form

$$C(t) = \sqrt{N}\hat{C}(t/\sqrt{N}, 0, 1)\,. \tag{5.21}$$

This equation identifies both static and dynamic finite-size critical exponents: the amplitude of correlations (i.e., fluctuations) scale as $C \sim N^{\alpha}$ with the exponent $\alpha = 1/2$, while a critical time scale emerges as $t \sim N^{\zeta}$ with the dynamical exponent $\zeta = 1/2$. A similar analysis yields the scaling form of the response function:

$$\chi(t) = \hat{\chi}(t/\sqrt{N}, 0, 1)\,. \tag{5.22}$$

We thus see that the amplitude of the response function does not scale with N. We confirm the (static as well as dynamic) scaling behavior of both the correlation and response functions in Figs. 5.6 and 5.7, respectively. Additionally, we see that the critical dynamics observed here is purely relaxational. In the next section, we show that a distinct dynamical critical behavior emerges at low dissipation.

5.3.2 Criticality at $\Gamma \to 0$

The effective classical behavior at a generic critical point is due to the competition between drive and dissipation. It is then interesting to consider the limit $\Gamma \to 0$ where dissipation is small compared to the energy scales in the system. Interestingly, the phase transition persists in this limit and occurs at $\Delta = 2J$ as $\Gamma \to 0$; see Fig. 5.11. One must be careful when considering this point as setting Γ to zero would make the problem unphysical since dissipation is required to find a unique nonequilibrium steady state. Rather, we shall consider the asymptotic behavior in the limit $\Gamma \to 0$ at the level of the low-frequency expansion of Eq. (3.30). The resulting action then becomes

$$\mathcal{S} \sim \int_t m_q(-a\partial_t^2 - \gamma\partial_t - r)m_c + \frac{1}{2}Dm_q^2\,, \tag{5.23}$$

where the parameters γ, r, and D are provided in Eq. (5.24) upon taking the appropriate limit:

$$r = \lim_{\Gamma\to 0} -P^R(\omega = 0) = \begin{cases} \frac{2J(\Delta-2J)}{\Delta} & \Delta > 2J \\ \frac{\Gamma^2}{32J} & \Delta = 2J \end{cases}, \tag{5.24a}$$

$$\gamma = \lim_{\Gamma\to 0} -i\partial_\omega P^R(\omega)|_{\omega=0} = \frac{J^2\Gamma}{256\Delta^3}, \tag{5.24b}$$

$$D = \lim_{\Gamma\to 0} P^K(\omega = 0) = \frac{i2J^2\Gamma}{\Delta^2}. \tag{5.24c}$$

The new parameter a is given by

$$a = \lim_{\Gamma\to 0} \partial_\omega^2 P^K(\omega)|_{\omega=0} = \frac{J^2}{\Delta^3}\,. \tag{5.25}$$

Indeed, the inertial term in the action (proportional to a) is required in the limit of vanishing dissipation, because the damping parameter $\gamma \sim \Gamma$ and the noise $D \sim \Gamma$ both vanish with Γ. To determine the new scaling dimensions of the fields, we once again seek a scaling transformation that keeps the action scale invariant, but this time we also should include the scaling of Γ itself. We find that the quadratic action at the critical point is invariant under

$$t \to \lambda t\,, \quad \Gamma \to \frac{1}{\lambda}\Gamma\,, \quad m_c \to \lambda m_c\,, \quad m_q \to m_q\,, \tag{5.26}$$

establishing the new scaling dimensions $[m_c] = 1$, $[m_q] = 0$. The new scaling dimensions alter the original scaling dimensions of the correlation and response functions, again in harmony with their behavior in the limit $\Gamma \to 0$; see also Ref. [51].

To obtain the finite-size scaling behavior, we once again include the classical vertex, which remains the most relevant interaction term. The full action (including the mass term) remain invariant if we impose the rescaling

$$r \to \frac{1}{\lambda^2} r, \quad N \to \lambda^4 N, \tag{5.27}$$

in addition to those in Eq. (5.26). From this, we find the scaling form for the correlation function as

$$C(t) = \frac{1}{\lambda^2} \hat{C}_0(\lambda |t|, \lambda^{-1}\Gamma, \lambda^{-2} r, \lambda^{-4} N^{-1}) \,, \tag{5.28}$$

where the subscript 0 denotes the scaling function near the weakly dissipative critical point. Also, notice the dependence of the nontrivial scaling of Γ in contrast with a generic critical point; cf. Eq. (5.19).

First, we consider the point $\Delta = 2J$ at finite yet small Γ. Setting $\lambda = \Gamma$ and $t = 0$ in the thermodynamic limit, we find

$$C(0) = \frac{1}{\Gamma^2} \hat{C}_0(0, 1, \text{const.}, 0) \propto \frac{1}{r} \,, \tag{5.29}$$

where the scaling behavior in the last step follows from the fact that $r \sim \Gamma^2$, rendering the same photon-flux exponent $\nu = 1$.

Next, we shall focus on finite-size scaling. To this end, we consider a weakly-dissipative critical point at finite yet small Γ; we shall choose $\Delta \lessapprox 2J$ to ensure criticality. Now, we set $\lambda^4 = N^{-1}$ together with $r = 0$ to find

$$C(t) = \sqrt{N} \hat{C}_0(|t| N^{-\frac{1}{4}}, \Gamma N^{\frac{1}{4}}, 0, 1) \,. \tag{5.30}$$

From this equation, we find that the weakly-dissipative limit does not affect the static scaling exponent, $\alpha = \frac{1}{2}$, but it *does* change the dynamical exponent to $\zeta = \frac{1}{4}$. We thus conclude that a weakly dissipative point changes the dynamical critical behavior. Repeating the above analysis for

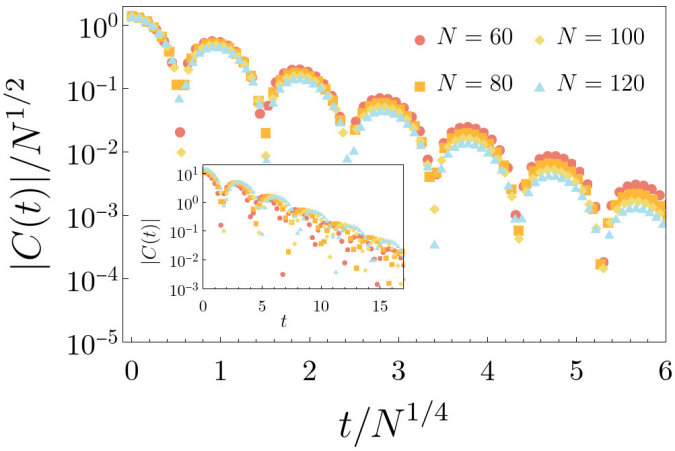

Figure 5.8 Finite-size scaling of the correlation function near the weakly dissipative critical point ($J = 1, \Delta = 2, \Gamma = 0.1$). The dynamics is underdamped in contrast with the purely relaxational behavior at a generic driven-dissipative phase transition, and exhibits the critical scaling $t \sim N^{1/4}$ to be contrasted with $t \sim N^{1/2}$ of relaxational dynamics; cf. Fig. 5.6.

the response function, we find the finite-size scaling form

$$\chi(t) = N^{\frac{1}{4}} \hat{\chi}_0(tN^{-\frac{1}{4}}, \Gamma N^{\frac{1}{4}}, 0, 1) \,. \tag{5.31}$$

In contrast with a generic critical point (Eq. (5.22)), the amplitude of the response function in the above equation grows with the system size as $\chi \sim N^{\frac{1}{4}}$. Figures 5.8 and 5.9 show the finite-size critical behavior of the correlation and response function, respectively, and confirm the prediction of the scaling analysis. In conclusion, while the static exponent α and the flux exponent ν remain the same everywhere on the phase boundary, the dynamical exponent ζ takes a different value in the weakly-dissipative limit.

What further distinguishes the weakly dissipative critical point is the fact that the dynamics is *underdamped* (see Figs. 5.8 and 5.9) in contrast with the typical relaxational/overdamped dynamics seen at a generic critical point, and generally in driven-dissipative systems. As Γ is further increased along the phase boundary, one should expect a crossover to overdamped critical dynamics. This is somewhat analogous to the quantum critical region and the crossover to thermal critical behavior [52]. In the context of the infinite-range model that we have considered in this work, the crossover behavior becomes manifest as a function of system size. Indeed, we can determine the crossover behavior from Eq. (5.30): for $\Gamma t \lesssim 1$ and $\Gamma \lesssim N^{-\frac{1}{4}}$, the critical dynamics is underdamped, while

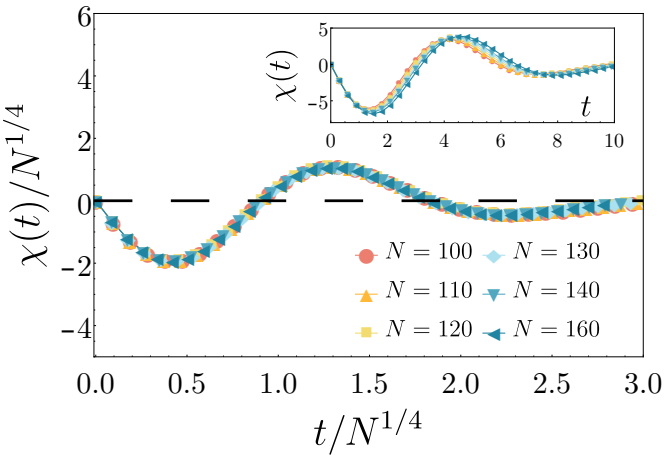

Figure 5.9 Finite-size scaling of the response function near the weakly dissipative critical point from exact numerics ($J = 1, \Delta = 2, \Gamma = 0.1$). The dynamics is distinguished from a generic critical point in that the dynamical critical exponent is different, $\zeta = 1/4$ and that it is underdamped; cf. Fig. 5.7.

for large times and/or large Γ the system experiences a dynamical crossover where we recover the usual relaxational behavior (while remaining on the phase boundary). To quantitatively investigate the crossover, we define the first zero of the correlation function, denoted by τ, as a measure of the oscillatory behavior of the underdamped dynamics. In Fig. 5.10, we plot τ as a function of Γ and for different system sizes. Indeed, we find that for sufficiently large values of Γ, this time scale diverges where the dynamics becomes overdamped. Furthermore, this figure shows that this time scales as $\tau \sim N^{\frac{1}{4}}\hat{\tau}(\Gamma N^{\frac{1}{4}})$ with $\hat{\tau}$ a universal scaling function, hence it confirms the scaling of the crossover value, $\Gamma_{\rm cr} \sim N^{-1/4}$.

One can gain some intuition for the underdamped critical behavior near the weakly-dissipative critical point from several different angles. First, the point $\Delta = 2J$ is exactly where Γ_c switches from real to imaginary, as a result of which Eq. (5.4a) shows underdamped dynamics even away from the phase boundary (when $\Delta > 2J$). Second, one can imagine that the underlying coherent dynamics generated by the first term in the Liouvillian in Eq. (3.5) could have a stronger effect in the limit $\Gamma \to 0$. Additionally, the infinite-range Ising model is integrable in the absence of dissipation; while dissipation generically spoils integrability, a property denoting systems with infinitely many conserved quantities, the dynamics is approximately integrable in the limit $\Gamma \to 0$, which could

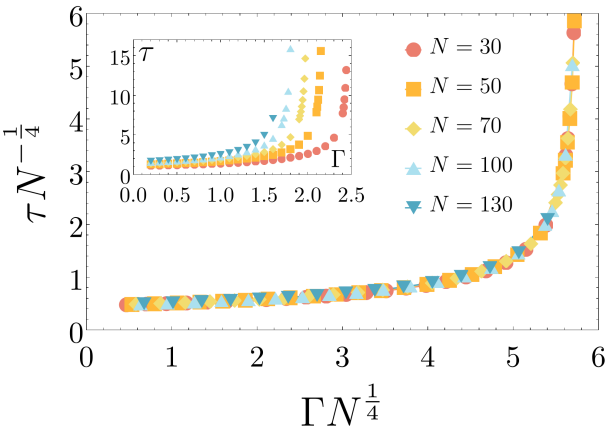

Figure 5.10 The first zero of the correlation function, τ, as a function of the dissipation rate Γ and at different system sizes ($J = 1$). Transverse field values Δ are chosen to lie along the right side of the phase boundary, $\Delta_c(\Gamma) = J + \sqrt{J^2 - \Gamma^2/16}$. Both τ and Γ are scaled with system size to make the scaling behavior manifest. The time scale τ diverges at sufficiently large Γ approximately when $\Gamma N^{1/4} \approx 6$. The inset shows the unscaled plots for comparison.

lead to nontrivial dynamics [53–56]. Nevertheless, in Sec. 5.5, we show that the underdamped dynamics survives to the first nontrivial order of integrability-breaking perturbations.

5.3.3 Comparison with Equilibrium

From the scaling dimensions and critical exponents, we can place each phase transition in its respective universality class. Remarkably, both finite-Γ and $\Gamma \to 0$ phase transitions are in equilibrium universality classes, albeit with a classical and quantum flavor, respectively. For a generic critical point at finite Γ, the scaling dimensions are $[m_c] = \frac{1}{2}$, $[m_q] = -\frac{1}{2}$ with the critical exponents $\alpha = 1/2$, $\zeta = 1/2$. These quantities place this phase transition in the same universality class as the classical infinite-ranged Ising model at finite temperature with Glauber-type dynamics (i.e. non-conserving dynamics) [57], which itself belongs to the "model A" class of Hohenberg & Halperin [58]. Despite the microscopic quantum dynamics, the combination of drive and dissipation render the critical behavior effectively classical and equilibrium-like. This appears to be the generic behavior in driven-dissipative phase transitions [13, 14, 59, 59–68]. However, there are exceptions such as classical yet truly nonequilibrium critical behavior [69], as well as the

emergence of quantum criticality in the limit of weak dissipation and drive [70, 71].

In the weakly-dissipative limit, we have found the scaling dimensions $[m_c] = 1$, $[m_q] = 0$, which are distinct from both classical ($[m_c] = \frac{1}{2}$, $[m_q] = -\frac{1}{2}$) and quantum ($[m_c] = \frac{1}{2}$, $[m_q] = \frac{1}{2}$) cases [14, 33]. These scaling dimensions lead to the new set of critical exponents $\alpha = 1/2$, $\zeta = 1/4$, as opposed to the quantum critical exponents $\alpha = 1/3$, $\zeta = 1/3$ [33]. The former exponents place this phase transition in the same universality class as the finite-temperature transverse-field infinite-range Ising model, i.e. the Hamiltonian in Eq. (3.4). Therefore, while the phase transition is equilibrium-like, it resembles the quantum Ising model at finite temperature rather than the classical stochastic Ising model. For comparison, see Fig. 5.B.1 in Appendix 5.B. Various exponents and the comparison against classical and quantum equilibrium settings can be found in Table 5.1.

The comparison between the driven-dissipative and equilibrium behaviors can be taken one step further due to the existence of a dynamical crossover in both cases. As shown previously, the weakly-dissipative point is an unstable fixed point with respect to dissipation, where upon renormalization the critical dynamics undergoes a crossover from underdamped to overdamped dynamics; see Fig. 5.11(a). This crossover can be understood as Γ scaling inversely to time upon rescaling at the weakly-dissipative critical point, which then sets a crossover-time that scales as $\sim N^{1/4}$. The equilibrium analog of a dynamical crossover occurs at finite temperature. Upon renormalization, the (perfectly oscillatory) coherent quantum critical dynamics undergoes a crossover to underdamped dynamics, as shown in Fig. 5.11(b). Similarly to our driven-dissipative system, the temperature T scales inversely as that of time; one can see this from the equilibrium fluctuation-dissipation relation $C = i \coth(\omega/2T)\chi$ where ω and T scale in the same way [14, 48]. A similar line of reasoning indicates a crossover-time $\sim N^{1/3}$. In short, the dynamical crossover of the driven-dissipative Ising model is distinguished from its equilibrium analog not only by the critical exponents but also by the nature of the crossover (underdamped-to-overdamped vs coherent-to-underdamped crossover, respectively).

Despite both universality classes being equilibrium-like, there are still signatures of the microscopic nonequilibrium nature of the model. As we will discuss in Ch. **??**, the FDR between

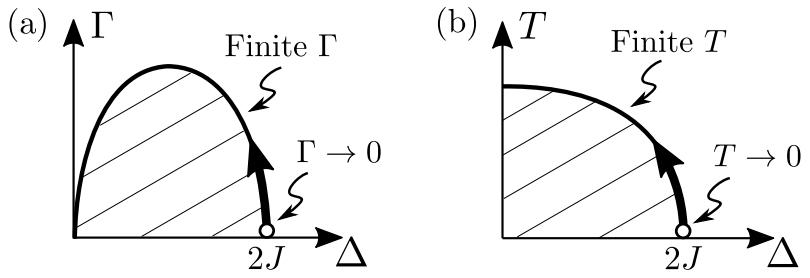

Figure 5.11 Schematic phase diagrams of the infinite-range (a) driven-dissipative Ising model (DDIM), and (b) equilibrium Ising model in a transverse field. The shaded regions denote the ordered phase. The weakly dissipative critical point of the DDIM, $\Gamma \to 0$ in (a), exhibits underdamped dynamics in contrast with the relaxational dynamics at a generic critical point. Analogously, the equilibrium model in (b) exhibits distinct (quantum and thermal) dynamics at zero and finite temperature. Both $\Gamma \to 0$ and $T \to 0$ define unstable fixed points but with respect to dissipation and thermal fluctuations, respectively. The weakly dissipative dynamics in (a) exhibits identical critical scaling to a finite-temperature critical point in (b)

correlation and response functions for S_x and S_y are modified from their equilibrium form, something that is only possible in nonequilibrium. The modified form of the FDR is indicative of the breaking of detailed balance (i.e. time reversal symmetry).

5.4 Langevin Description

An alternative, and established, way of understanding the critical behavior of a driven-dissipative system is through the lens of the Langevin equation, a stochastic differential equation used to describe noisy systems [5]. Near a critical point, where we have shown the classical vertex is the most relevant finite-size correction, we can map the low-frequency limit of the Keldysh action to a Langevin equation [4, 13, 14]. Putting together the quadratic action from Eq. (3.30) with the interaction in Eq. (5.16), the action reads

$$S \sim \int_t \Big[-(\gamma\partial_t + r)m_c(t) - \frac{u}{2N} m_c^3(t) + \frac{1}{2} D m_q(t) \Big] m_q(t)\,, \tag{5.32}$$

with the action parameters given by Eqs. (5.17), (5.24) and (5.25). The first step in mapping to the Langevin equation is a Hubbard-Stratonovich transformation of the quantum field m_q to introduce

	Driven-Diss.		Class.	Quantum	
	$\Gamma > 0$	$\Gamma \to 0$	$T > 0$	$T > 0$	$T \to 0$
$t \sim N^{\zeta}$	$\frac{1}{2}$	$\frac{1}{4}$	$\frac{1}{2}$	$\frac{1}{4}$	$\frac{1}{3}$
$C \sim N^{\alpha}$	$\frac{1}{2}$	$\frac{1}{2}$	$\frac{1}{2}$	$\frac{1}{2}$	$\frac{1}{3}$

Table 5.1 Driven-dissipative vs. equilibrium classical/ quantum Ising models. A generic (finite-Γ) critical point exhibits the same critical behavior as the classical stochastic Ising model, while the weakly dissipative ($\Gamma \to 0$) critical point can be identified with the quantum Ising model at finite temperature.

a noise field $f(t)$ as

$$S = \int_t \Big[-(\gamma\partial_t + r)m_c(t) - \frac{u}{2N}m_c^3(t) + \sqrt{2}f(t)\Big]m_q(t) - \int_t \frac{1}{D}f(t)^2 \,. \tag{5.33}$$

Now, integrating over m_q yields a delta function whose argument is the Langevin equation ($m = m_c/\sqrt{2}$):

$$\gamma\partial_t m(t) = -rm(t) - \frac{1}{N}um^3(t) + f(t) \,. \tag{5.34}$$

The term $f(t)$ characterizes a white noise with a Gaussian distribution, mean $\langle f(t)\rangle = 0$, and variance $\langle f(t)f(t')\rangle = -i\frac{1}{2}D\delta(t-t') = 2\gamma T_{\text{eff}}\delta(t-t')$. It is now clear that Eq. (5.32) near criticality is equivalent to an overdamped Langevin equation, with an effective temperature T_{eff} and in an effective potential given by

$$\mathcal{H} = \frac{1}{2}rm^2 + \frac{1}{4N}um^4 \,. \tag{5.35}$$

Indeed, Eq. (5.34) reproduces the overdamped critical dynamics discussed in Sec.5.3.1. The stochastic Langevin equation can be turned to a Fokker-Planck equation that describes the evolution of the probability distribution [4, 48]; with the effective equilibrium dynamics, the steady-state probability distribution of m takes the form

$$P_{\text{eq}}(m) \sim e^{-\mathcal{H}/T_{\text{eff}}} \,. \tag{5.36}$$

The nature of the dynamics changes in the limit $\Gamma \to 0$. In this case, dissipation is vanishingly small, $\gamma \sim \Gamma \to 0$, therefore we should also include the term proportional to ω^2 in the low-frequency

expansion of $P^R(\omega)$. Following a similar procedure in this limit, we arrive at the Langevin equation

$$a\partial_t^2 m(t) + \gamma \partial_t m(t) = -rm(t) - \frac{u}{N} m^3(t) + f(t)\,, \tag{5.37}$$

with the parameters taken from Eq. (5.24) in the same limit. Incidentally, we have identified underdamped dynamics and persistent oscillations in Sec. 5.3.2. Now, we can see that these oscillations are due to the inertial term that can be of the same order as dissipation (since $\gamma \to 0$). Again, one can identify the corresponding Fokker-Planck equation, also known as the Kramers-Chandrasekhar equation, whose steady-state solution is just the Maxwell-Boltzmann distribution [72]:

$$P(m, \dot{m}) \sim e^{-(\mathcal{H} + \frac{1}{2} a \dot{m}^2)/T_{\text{eff}}}\,. \tag{5.38}$$

This distribution only differs from Eq. (5.36) in the multiplicative Gaussian distribution of $\dot{m}$. The probability distribution of m in Eq. (5.38) is identical to that of Eq. (5.36) upon integrating out $\dot{m}$. In other words, the static properties are identical irrespective of dissipation. In contrast, the critical dynamics is markedly different as we have seen in the previous subsections.

Before closing this section, We emphasize that the Langevin equations derived here are only valid near the phase boundary and outside the heated region, since they are based on the dynamics of the slow mode.

5.5 Beyond the Infinite-Range Model

The infinite-range Ising model is rather special as the dynamics of the order parameter is exactly determined by mean field, although fluctuations at, or close to, criticality require a separate treatment as discussed in previous sections. In this section, we utilize the diagrammatical technology developed in this work to investigate the effects of non-mean-field perturbations, and specifically short-range interactions, on the dynamics. Most importantly, we show that the underdamped dynamical critical behavior in the limit $\Gamma \to 0$ persists even in the presence of the short-range interactions.

To investigate the role of integrability at the weakly-dissipative critical point, we add a nearest-neighbour interaction to the Hamiltonian in Eq. (3.4):

$$H_{\mathrm{NN}} = H - \lambda \sum_i \sigma_i^x \sigma_{i+1}^x. \tag{5.39}$$

We shall consider the perturbative limit $\lambda \ll J, \Delta$ and assume periodic boundary conditions. The short-range interaction alters the mean-field structure of the infinite-range Ising model, breaks its integrability [73], and could modify the phase boundary. A standard way to study such perturbations is to view them as spin-wave fluctuations, which have been investigated in other nonequilibrium settings such as quantum quenches [34, 73, 74]. While our model is distinct due to its driven-dissipative dynamics, we can still resort to a similar picture in terms of spin waves

$$\tilde{\sigma}_k^\alpha = \sum_{j=1}^{N} e^{-ikj} \sigma_j^\alpha \,,$$

where $k = 2\pi n/N$ with $n \in \{0, 1, \cdots, N-1\}$. We shall identify the collective spin as the $k = 0$ mode; without short-range interactions, there is no coupling between this and other modes with $k \neq 0$, however, the short-range interaction couples them and thus spoils the mean-field nature of the model. Naively, one might expect that spin waves act as an effective bath for the "large spin" corresponding to the $k = 0$ mode, which would lead to an effective dissipation (even in the limit $\Gamma \to 0$). However, we will show using the diagrammatic techniques that this is not the case, and therefore the underdamped critical dynamics at the weakly dissipative critical point is robust against short-range interactions.

5.5.1 Short-Range Perturbation via Field Theory

The quantum-to-classical mapping process is not altered much by the inclusion of short-range interactions. The steps leading to the Hubbard-Stratonovich transformation in Eq. (3.13) are identical, except now we must also perform a multi-dimensional Hubbard-Stratonovich transformation on the short-range interaction terms in the vectorized Liouvillian. The short-range Ising perturbation is diagonalized in the σ^x basis, same as before. The Hubbard-Stratonovich transformation reads

$$\pm \frac{i}{2} \lambda \delta t (\boldsymbol{\sigma}^{(u/l)})^T \mathbf{D}^{-1} \boldsymbol{\sigma}^{(u/l)} \to \mp \frac{i}{2\lambda \delta t} (\boldsymbol{m}^{(u/l)})^T \mathbf{D}\, \boldsymbol{m}^{(u/l)} \pm i\, (\boldsymbol{m}^{(u/l)})^T \boldsymbol{\sigma}^{(u/l)} \,, \tag{5.40}$$

where $\boldsymbol{\sigma} = (\sigma_1, ..., \sigma_N)$ represents the spins, while $\boldsymbol{m}^{(u/l)} = (m_1^{(u/l)}, ..., m_N^{(u/l)})$ denotes the scalar fields on the upper/lower branches of the vectorized space, respectively. The kernel $\mathbf{D}^{-1}$, representing the nearest-neighbour interaction, is given by

$$\mathbf{D}^{-1} = \begin{pmatrix} 0 & 1 & & & 1 \\ 1 & \ddots & \ddots & & \\ & \ddots & \ddots & \ddots & \\ & & \ddots & \ddots & 1 \\ 1 & & & 1 & 0 \end{pmatrix}, \tag{5.41}$$

with 1 next to the diagonal (note the periodic boundary conditions) and 0 everywhere else. This kernel is invertible for odd N or even N not divisible by 4; for simplicity, we take N to be odd. After tracing out the spins, redefining the local fields $\boldsymbol{m}^{(u/l)}/(2\lambda\delta t) \to \boldsymbol{m}^{(u/l)}$, rotating to the Keldysh basis $\boldsymbol{m}_{c/q} = (\boldsymbol{m}^{(u)} \pm \boldsymbol{m}^{(l)})/\sqrt{2}$, and taking the continuum limit, we find the exact Keldysh action including the short-range interaction:

$$S = -2JN \int_t m_c m_q - 2\lambda \int_t \boldsymbol{m}^T \widetilde{\mathbf{P}}\, \boldsymbol{m} - i \sum_i \ln \mathrm{Tr} \left(\mathcal{T} e^{\int_t \mathbb{T} + \mathbb{T}'_i} \right) . \tag{5.42}$$

Here, $\boldsymbol{m}$ denotes a column vector with $\boldsymbol{m}_c$ stacked on top of $\boldsymbol{m}_q$. The kernel for the local fields is given by

$$\widetilde{\mathbf{P}} = \begin{pmatrix} \mathbf{0} & \mathbf{D} \\ \mathbf{D} & \mathbf{0} \end{pmatrix}. \tag{5.43}$$

Furthermore, the short-range interaction leads to an additional matrix added to the matrix $\mathbb{T}$ in the exponential:

$$\mathbb{T}'_i = i2\sqrt{2}\lambda\, \mathrm{diag}(m_{i,q}, m_{i,c}, -m_{i,c}, -m_{i,q}) . \tag{5.44}$$

Ideally, we must integrate out the local fields to obtain an effective action in terms of only the original collective field m. In order to switch to a picture in terms of spin waves, we introduce the Fourier transform of the local fields as

$$m_j = \frac{1}{N} \sum_k e^{ikj} m_k , \tag{5.45}$$

where $k = 2\pi n/N$ with $n \in \{0, 1, ..., N-1\}$. The action too can be recast in the Fourier space. In this basis, the matrix $\mathbf{D} = \mathrm{diag}\{D_k\}$ takes a diagonal form with the matrix elements (recalling that

N is odd)

$$D_k = \sum_{j=0}^{N-1} e^{-ikj} D_j = \frac{1}{2} \sec k \,, \tag{5.46}$$

where $j = l - m$ with l and m the row and column labels of the matrix $\mathbf{D}$, respectively; here, we have used the translational invariance due to periodic boundary condition.

Finally, we remark that $m_{k=0}$ too represents the collective field m that is originally introduced through the Hubbard-Stratonovich transformation of the infinite-rang Ising interaction. Indeed, it can be shown by introducing source fields that m and $m_{k=0}$ are redundant. Therefore, to simplify the subsequent treatment, we introduce the new fields $\overline{m} = \sqrt{N}m + \frac{\lambda}{J\sqrt{N}} m_0$, $\widetilde{m} = \sqrt{N}m - \frac{1}{\sqrt{N}} m_0$, where $\overline{m}$ serves as the new order parameter, while $\widetilde{m}$ is entirely decoupled from all other fields and appears quadratically, and can be simply integrated out. Absorbing a factor of $\sqrt{\lambda/JN}$ into m_k, we find the total action

$$S = \frac{-2J^2}{J+\lambda} \int_t \overline{m}_c(t)\overline{m}_q(t) - i \sum_j \ln \mathrm{Tr} \left(\mathcal{T} e^{\int_t \mathbb{T} + \mathbb{T}'_j} \right) - 2J \sum_{k \neq 0} \begin{pmatrix} m_{-k,c} \\ m_{-k,q} \end{pmatrix}^T \begin{pmatrix} 0 & D_k \\ D_k & 0 \end{pmatrix} \begin{pmatrix} m_{k,c} \\ m_{k,q} \end{pmatrix} , \tag{5.47}$$

where the matrices in the log-trace are given by

$$\mathbb{T} = \mathbb{T}_0 + i2\sqrt{2} \frac{J}{\sqrt{N}} \mathrm{diag}(\overline{m}_q, \overline{m}_c, -\overline{m}_c, -\overline{m}_q) \,, \tag{5.48}$$

with $\mathbb{T}_0$ defined in Eq. (3.25), and

$$\mathbb{T}'_j = i\sqrt{\frac{8J\lambda}{N}} \sum_{k \neq 0} e^{ikj} \, \mathrm{diag}(m_{q,k}, m_{c,k}, -m_{c,k}, -m_{q,k}) \,. \tag{5.49}$$

Notice that $m_{k=0}$ does not appear in the action, and the collective field is completely characterized through $\overline{m}_{c/q}(t)$.

5.5.2 Quadratic Action

We now follow a similar procedure as before and expand Eq. (5.47) to quadratic order in both $\overline{m}$ and m_k:

$$S = \frac{1}{2} \int_{t,t'} \begin{pmatrix} \overline{m}_c \\ \overline{m}_q \end{pmatrix}_t^T \begin{pmatrix} 0 & P^A \\ P^R & P^K \end{pmatrix}_{t-t'} \begin{pmatrix} \overline{m}_c \\ \overline{m}_q \end{pmatrix}_{t'} + \frac{1}{2} \sum_{k \neq 0} \int_{t,t'} \begin{pmatrix} m_{-k,c} \\ m_{-k,q} \end{pmatrix}_t^T \begin{pmatrix} 0 & P^A_k \\ P^R_k & P^K_k \end{pmatrix}_{t-t'} \begin{pmatrix} m_{k,c} \\ m_{k,q} \end{pmatrix}_{t'} . \tag{5.50}$$

The quadratic action takes the Keldysh structure with the elements (recalling that $P^R(t) = P^A(-t)$)

$$\begin{aligned} P^R(t) &= \frac{-2J^2}{J+\lambda}\delta(t) + \Theta(t)8J^2 e^{-\frac{\Gamma}{2}|t|}\sin(2\Delta t), \\ P^K(t) &= i8J^2 e^{-\frac{\Gamma}{2}|t|}\cos(2\Delta t), \end{aligned} \tag{5.51}$$

and

$$\begin{aligned} P_k^R(t) &= -4JD_k\delta(t) + \Theta(t)8J\lambda e^{-\frac{\Gamma}{2}|t|}\sin(2\Delta t), \\ P_k^K(t) &= i8J\lambda e^{-\frac{\Gamma}{2}|t|}\cos(2\Delta t). \end{aligned} \tag{5.52}$$

One can immediately see that the collective field $\overline{m}$ is decoupled from spin waves m_k at the level of Eq. (5.50). This is because any (bi)linear coupling between $\overline{m}$ and m_k is forbidden by momentum conservation. To investigate the effect of spin waves, we need to go to higher-order terms that characterize the interaction between these fields. As we shall see, the nonlinear coupling will dramatically change the effect of spin waves on the collective mode: while linear coupling of the two fields will mimic a thermal bath (of spin waves) at finite temperature [75], the nonlinear coupling will have no such effect. For another setting where nonlinear coupling changes the nature of dissipation, see Ref. [76].

Next, we take advantage of the perturbative nature of spin waves and calculate their contribution to the self-energy whose low-frequency behavior determines how spin waves impact the dynamics of the order parameter $\overline{m}$. To this end, we first list the free Green's functions describing spin waves in the time domain:

$$G_k^R(t) = -\frac{1}{4JD_k}\delta(t) - \frac{2\lambda\Delta}{JD_k^2\Delta_k}\Theta(t)e^{-\Gamma t/2}\sin\left(\frac{\Delta_k t}{2}\right), \tag{5.53}$$

and

$$G_k^K(t) = \frac{-i\lambda e^{-\Gamma|t|/2}}{4JD_k^2\Delta_k(\Gamma^2+\Delta_k^2)}\left[\Delta_k(2\Gamma^2+\Delta_k^2+16\Delta^2)\cos\frac{\Delta_k t}{2} - \Gamma(\Delta_k^2-16\Delta^2)\sin\frac{\Delta_k|t|}{2}\right], \tag{5.54}$$

where $\Delta_k = 4\sqrt{\Delta(\Delta-\lambda/D_k)}$. It is also useful to cast the Green's functions in frequency space:

$$G_k^R(\omega) = \frac{1}{P_k^R(\omega)} = \frac{-1}{4JD_k}\frac{(\omega+\omega^+)(\omega+\omega^-)}{(\omega-\omega_a)(\omega-\omega_b)}, \tag{5.55}$$

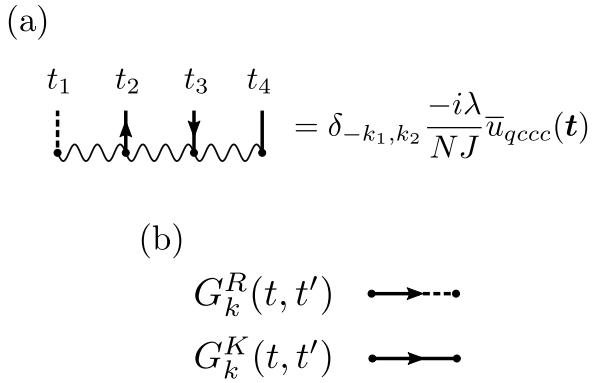

Figure 5.12 (a) A representative diagram involving spin waves, $m_{k,c/q}$. An additional prefactor of $\sqrt{\lambda/J}$ arises for each appearance of spin wave compared to that of the collective field; cf. Fig. **??**. The Kronecker delta enforces momentum conservation. (b) Contracted arrowed legs represent spin-wave Green's functions.

and

$$G^K_k(\omega) = -P^K_k(\omega)|G^R_{k,0}(\omega)|^2 = \frac{-i\lambda\Gamma}{4JD_k^2} \frac{(\omega+\omega^+)(\omega+\omega^{+*}) + (\omega+\omega^-)(\omega+\omega^{-*})}{(\omega-\omega_a)(\omega-\omega_b)(\omega-\omega_a^*)(\omega-\omega_b^*)}\,, \tag{5.56}$$

with $\omega^{+/-} = i\Gamma/2 \pm 2\Delta$ and $\omega_{a/b} = (-i\Gamma \pm \Delta_k)/2$.

Finally, we identify the low-frequency effective temperature of spin waves:

$$T_{\text{eff},k} = \lim_{\omega\to 0} \frac{\omega}{2} \frac{G^K_k(\omega)}{G^R_k(\omega) - G^A_k(\omega)} = \frac{\Gamma^2 + 16\Delta^2}{32\Delta}\,. \tag{5.57}$$

Interestingly, this effective temperature is k-independent and is in fact equal to the effective temperature of the collective mode; cf. Eq. (5.6). The equivalence of the effective temperature is perhaps unsurprising given that at this quadratic level the system is not interacting, so the effective temperature is simply that of a single-particle and would be equal for all modes.

5.5.3 Self-Energy

In this section, we compute the correction to the self-energy due to spin waves and investigate their effect on the phase diagram and the dynamics, particularly at the weakly dissipative point. Our starting point is the Keldysh form of the familiar Dyson equation [4],

$$\boldsymbol{\mathcal{G}}^{-1} = \mathbf{G}^{-1} - \boldsymbol{\Sigma}\,, \tag{5.58}$$

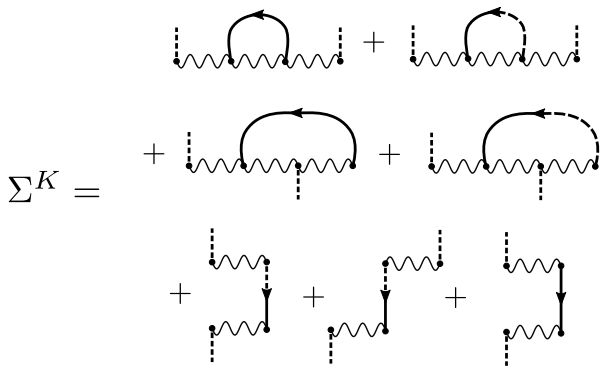

Figure 5.13 Diagrams contributing to the Keldysh component of the self-energy, Σ^K, to the order $\sim \lambda^2$.

where $\boldsymbol{\mathcal{G}}$ is the exact Green's function for the collective field, and $\mathbf{G}^{-1}$ is given by the kernel in the first term in Eq. (5.50). The self-energy $\boldsymbol{\Sigma}$ has the typical Keldysh structure and takes the form

$$\boldsymbol{\Sigma} = \begin{pmatrix} 0 & \Sigma^A \\ \Sigma^R & \Sigma^K \end{pmatrix} . \tag{5.59}$$

The low-frequency expansion of the retarded and Keldysh elements of the self-energy will renormalize the parameters describing the dynamics of the collective field as $\Sigma^R(\omega) \sim -\delta r + i\delta\gamma\omega$ and $\Sigma^K(\omega = 0) = \delta D$. At any generic critical point, the spin waves will simply provide a correction $\delta\gamma$ and δD to the otherwise finite values of dissipation and fluctuations, respectively. However, the weakly-dissipative critical point where $\Gamma \to 0$ is particularly susceptible to the coupling to the spin waves, as they could very well generate dissipation (even when $\Gamma \to 0$).

To calculate the self-energy, we utilize the diagrammatic representation developed in Sec. 3.3.4; we also include lines with an arrow to denote spin waves with a nonzero momentum in addition to those without an arrow which refer to the collective field. The connected diagrams inside the logarithm in Eq. (3.37) are modified accordingly: we include an additional prefactor of $\sqrt{\lambda/J}$ for each appearance of the m_k fields, and keep track of momentum indices. The diagrams resultant from expanding the logarithm in Eq. (3.41) should be summed over all momenta, with an overall Kronecker delta enforcing momentum conservation. An example of the classical vertex for the spin waves can be found in Fig. 5.12.

The lowest nontrivial correction to the self-energy arises at the order $O(\lambda^2)$ due to a combination

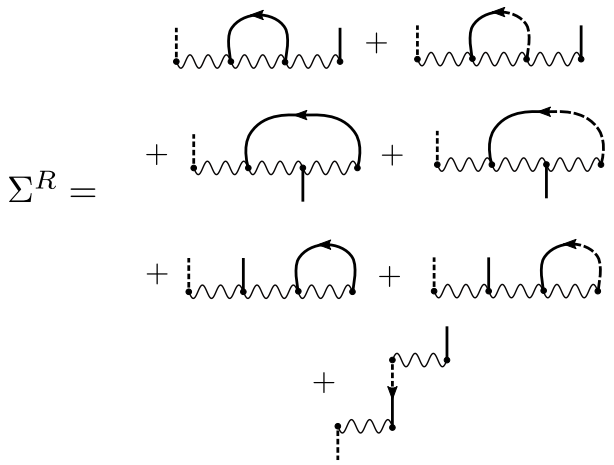

Figure 5.14 Diagrams contributing to the retarded component of the self-energy, Σ^R, to the order $\sim \lambda^2$.

of momentum conservation and the fact that $\mathbf{D}^{-1}$ is traceless. The one-loop diagrams contributing to Σ^K to the order $O(\lambda^2)$ are depicted in Fig. 5.13, while those contributing to Σ^R are given in Fig. 5.14. All other diagrams are either higher order in λ or are suppressed as $O(1/N)$. Note that only diagrams with two external quantum legs contribute to Σ^K, while those with one external quantum and another classical leg contribute to Σ^R, in harmony with the Keldysh structure of the action at the quadratic level. As an example calculation, the self-energy contribution to Σ^K due to the $\overline{u}_{qccq}$ one-loop diagram is given by

$$\Sigma^K_{(qccq)}(\omega) = \frac{-\lambda}{JN} \sum_{k\neq 0} \int_{\omega'} \left[\overline{u}_{qccq}(-\omega, \omega', -\omega', \omega) + \overline{u}_{qccq}(\omega, \omega', -\omega', -\omega)\right] G^K_{k,0}(\omega') \,. \tag{5.60}$$

The overall minus sign follows from a factor of $-i$ from the perturbative expansion of the path integral multiplied by another factor of $-i$ from the connected four-legged diagrams in Eq. (3.41). The above expression must be symmetrized with respect to the external frequency due to the same symmetry of the Keldysh component P^K. The interaction coefficient in frequency space is given by

$$\overline{u}_{qccq}(\boldsymbol{\omega}) = \frac{i256\Delta^2 J^4}{\omega_1 + \omega_2 - i\Gamma} f(\omega_1, \omega_4) \,, \tag{5.61}$$

where $f(x, y) = 1/[(x - \omega^+)(x - \omega^-)(y - \omega^{+*})(y - \omega^{-*})]$. Setting $\omega_1 = \omega_4 = 0$ and expanding to

lowest non-zero order in λ, we find the correction

$$\Sigma^K_{(qccq)}(0) = \frac{-i49152J^2\Delta^2\Gamma\lambda^2}{(\Gamma^2+16\Delta^2)^2(9\Gamma^2+16\Delta^2)}\,, \tag{5.62}$$

where we have used the fact that $\sum_{k\neq 0} 1/D_k^2 = 2N-1/2$ and neglected terms of $O(1/N)$. Repeating this calculation for all of the diagrams in Fig. 5.13, we find that the Keldysh component of the self-energy at low frequencies is given by

$$\Sigma^K(0) = \delta D = \frac{i16384J^2\Delta^2\Gamma}{(\Gamma^2+16\Delta^2)^3}\lambda^2\,. \tag{5.63}$$

Similarly, the retarded component of the self-energy is determined by considering the diagrams in Fig. 5.14. Performing the calculations, we find

$$\Sigma^R(\omega) \sim +\delta r + \delta\gamma i\omega = \frac{1536\lambda^2J^2\Delta}{(\Gamma^2+16\Delta^2)^2} + \frac{8192\lambda^2J^2\Delta\Gamma}{(\Gamma^2+16\Delta^2)^3}i\omega\,. \tag{5.64}$$

The above equations produce the first nontrivial correction to the self-energy due to the coupling to spin waves. At a generic critical point, these corrections remain finite and simply act as shifts to the noise and dissipation, as expected. Interestingly, we find from Eqs. (5.63) and (5.64) that $\delta\gamma$ and δD vanish in the limit $\Gamma \to 0$. In other words, while spin waves renormalize the low-frequency parameters, they do not qualitatively change the nature of the dynamics even in the limit $\Gamma \to 0$. We thus conclude that the underdamped critical dynamics at the weakly-dissipative point is robust against generic perturbations in Eq. (3.4) exemplified by short-range interactions, at least to the lowest nontrivial order ($\sim \lambda^2$).

Finally, we can inspect the effect of spin waves on the phase boundary of the model. These effects can be seen by setting the renormalized mass $r_{\text{ren}} \equiv r + \delta r$ to zero, where r is the bare mass defined in Eq. (5.24):

$$[\Gamma^2 + 16\Delta(\Delta - 2\overline{J})](\overline{J}-\lambda)^2 + \frac{768\overline{J}^3\Delta}{(\Gamma^2+16\Delta^2)}\lambda^2 = 0\,, \tag{5.65}$$

where we have defined $\overline{J} = J + \lambda$ and dropped terms of $O(\lambda^3)$ or higher. We have redefined J to include the contribution of the short-range interaction to the collective mode, and to solely separate out the effect of spin waves. In Fig. 5.15, one can see that ordered region shrinks due to

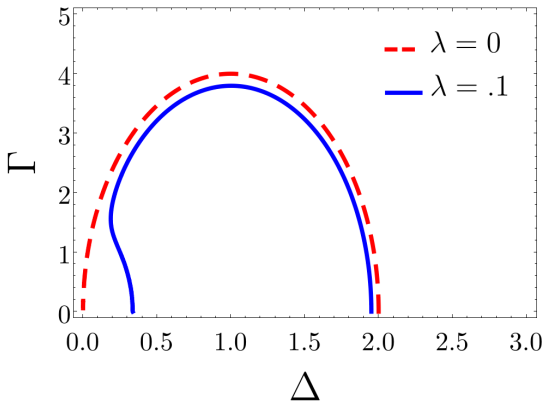

Figure 5.15 Phase boundary in the presence and absence of short-range interactions; here, $J = 1$ and an exaggerated value of $\lambda = .1$ is chosen for better visualization. The feature around $\Delta \sim \lambda$ could be an artifact of our perturbation scheme, which requires $\lambda \ll \Delta$.

the coupling to spin waves. This is expected as spin waves introduce more fluctuations and thus disfavor ordering. Finally, we remark that Eq. (5.65) should not be trusted near $\Delta \to 0$ since it was implicitly assumed that $\Delta \gg \lambda$ in our perturbative calculation (to expand Δ_k in powers of λ); however, it is possible that short-range interactions dramatically alter the phase boundary near the origin, in a fashion that could be related to the predicted first-order phase transition in the DDIM in d dimensions [59, 66].

APPENDIX

5.A Interaction coefficients

There are many relevant interaction coefficients necessary to compute the diagrams in Sec. 3.3.4. They are defined by Eq. (3.38) in the time domain and in Eq. (3.40) in the frequency domain. Here, we list the relevant interaction coefficients for the four-legged one-loop diagrams in Figs. 5.13 and 5.14 in the frequency domain:

$$\overline{u}_{qccc}(\boldsymbol{\omega}) = \frac{-128\Delta J^4(\Gamma/2 - i\omega_4)}{\omega_1 + \omega_2 - i\Gamma} f(\omega_1, \omega_4)\,, \tag{5.66}$$

$$\overline{u}_{qcqq}(\boldsymbol{\omega}) = \frac{i128\Delta J^4(\Gamma/2 - i\omega_4)}{(\omega_1 + \omega_2 - i\epsilon)(\omega_1 + \omega_2 - i\Gamma)} f(\omega_1, \omega_4)\,, \tag{5.67}$$

$$\overline{u}_{qcqc}(\boldsymbol{\omega}) = \frac{256\Delta^2 J^4\Gamma}{(\omega_1 + \omega_2 - i\epsilon)(\omega_1 + \omega_2 - i\Gamma)} f(\omega_1, \omega_4)\,, \tag{5.68}$$

$$\overline{u}_{qccq}(\boldsymbol{\omega}) = \frac{i256\Delta^2\lambda J^3}{\omega_1 + \omega_2 - i\Gamma} f(\omega_1, \omega_4)\,, \tag{5.69}$$

$$\overline{u}_{qc}(\omega_1, \omega_2)\overline{u}_{qc}(\omega_3, \omega_4) = -256\Delta^2 J^4 2\pi\delta(\omega_1 + \omega_2) f(\omega_1, \omega_4)\,. \tag{5.70}$$

$$\overline{u}_{qq}(\omega_1, \omega_2)\overline{u}_{qc}(\omega_3, \omega_4) = -i128\Delta J^4(i\omega_1 + \Gamma/2) 2\pi\delta(\omega_1 + \omega_2) f(\omega_1, \omega_4)\,. \tag{5.71}$$

Recall that in the definition of the diagrammatics, we introduce an infinitesimal regularization ϵ that we take to zero at the end of the calculation. This is necessary due to the pole at $\omega = 0$ from the steady state eigenvalue of Eq. (3.25). When calculating the interaction coefficients for terms containing spin wave fields m_k, we simply multiply by these coefficients by $\sqrt{\lambda/J}$ for each power of the spin wave field, see Fig. 5.12 for an example.

We also list here the interaction coefficient for the six-legged classical vertex used to calculate the damping parameter in the ordered phase in Sec. 5.2,

$$\begin{aligned}\overline{u}_{qccccc}(\boldsymbol{\omega}) = {} & \frac{-256J^6\Delta(\Gamma + 2i(\omega_1 + \omega_2 + \omega_3)(\Gamma - 2i\omega_6)}{(\omega_1 + \omega_2 + \omega_3 - \omega^+)(\omega_1 + \omega_2 + \omega_3 - \omega^-)} \\ & \times \frac{f(\omega_1, \omega_6)}{(\omega_1 + \omega_2 - i\Gamma)(\omega_5 + \omega_6 + i\Gamma)}\,,\end{aligned} \tag{5.72}$$

where $\boldsymbol{\omega} = (\omega_1, ..., \omega_n)$ (for an n-legged diagram), $f(x, y) = 1/[(x-\omega^+)(x-\omega^-)(y-\omega^{+*})(y-\omega^{-*})]$, and $\omega^{+/-} = i\Gamma/2 \pm 2\Delta$. For self-energy calculations, it is useful to recall that $\sum_{k\neq 0} 1/D_k = -1/2$ and $\sum_{k\neq 0} 1/D_k^2 = 2N - 1/2$, where D_k is defined in Eq. (5.46).

5.B Equilibrium Quantum Ising Model

In this section, we report the dynamics of the equilibrium infinite-range Ising model at finite temperature (in the absence of dissipation). Specifically, we demonstrate via exact numerical simulation that the thermal critical point of this model belongs to the same (static and dynamic) universality class as the driven-dissipative Ising model in the weakly dissipative regime. We start with the same Hamiltonian

$$H = -\frac{J}{N} S_x^2 + \Delta S_z \,. \tag{5.73}$$

This Hamiltonian features a thermal phase transition to an ordered phase where the Ising Z_2 symmetry is broken at the critical temperature [28]

$$T_c = \frac{2\Delta}{\ln\left(\frac{1+\Delta/2J}{1-\Delta/2J}\right)} \,. \tag{5.74}$$

The Hamiltonian conserves the total spin (i.e., $[H, \vec{S}] = 0$) which thus defines a good quantum number. In the angular-momentum basis defined by $|S, m\rangle$, the Hamiltonian becomes block diagonal with each block corresponding to a total spin S. However, each sector is highly degenerate with a multiplicity of $D(S)$. The multiplicity is given by $D(N/2) = 1, D(N/2-1) = N-1, D(N/2-2) = N(N-3)/2$, and

$$D(N/2 - p) = \frac{N(N-1)...(N-p+2)}{p!}(N - 2p + 1) \,, \tag{5.75}$$

for $3 \leq p \leq N/2$ [28]. The thermal state is then given by

$$\rho(\beta) = e^{-\beta H} = \bigoplus_{S=0}^{N/2} \left(\bigoplus_{i=1}^{D(S)} e^{-\beta H_S} \right), \tag{5.76}$$

which is to be understood as the direct sum over each unique spin sector with the corresponding

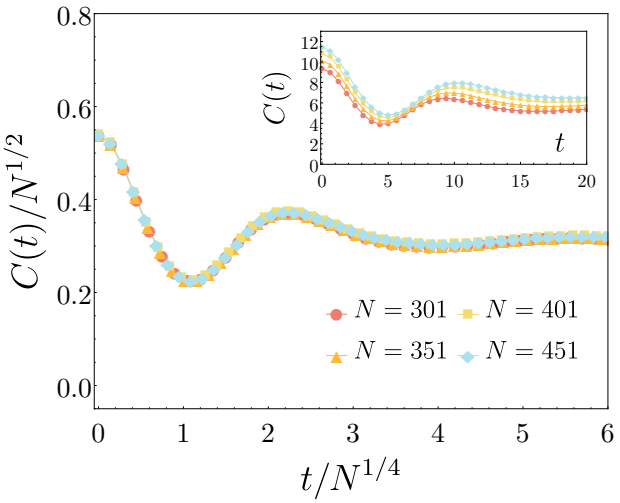

Figure 5.B.1 Finite-size scaling behavior of the infinite-range Ising model at a thermal critical point ($J = 1, \Delta = 1, T = 1.82048$). At this critical point, fluctuations scale as $N^{1/2}$, while the critical dynamics is underdamped and is governed by a characteristic time scale $t \sim N^{1/4}$. These exponents are identical to those of the driven-dissipative Ising model in the weakly dissipative regime (see Fig. 3 of the main text).

multiplicity $D(S)$. We then numerically calculate the correlation function

$$\begin{aligned} C(t) &= \frac{1}{N}\langle\{S_x(t), S_x(0)\}\rangle = \frac{2}{N}\mathrm{Re}\langle S_x(t)S_x(0)\rangle \\ &= \frac{2}{N}\mathrm{ReTr}\left(e^{-iHt}S_x e^{iHt}S_x\rho(\beta)\right). \end{aligned} \tag{5.77}$$

A plot of the correlation function and its finite-size scaling behavior can be found in Fig. 5.B.1. There, we see that the dynamical exponent, defined via $t \sim N^{\zeta}$, is given by $\zeta = 1/4$ and that the dynamics is underdamped just like at the weakly-dissipative critical point of the driven-dissipative Ising model discussed in Sec. 5.3.2.

5.C Classical (Stochastic) Ising Model

For completeness, here we introduce the classical stochastic Ising model [57]. The infinite-range (classical) Ising Hamiltonian is given by

$$\mathcal{H} = -\frac{J}{N}S^2, \tag{5.78}$$

where $S = \sum_i^N s_i$ with the Ising spin variable $s_i = \pm 1$. While the Hamiltonian (being a c number and commuting with all observables) does not impose any intrinsic dynamics, a stochastic, Glauber-type

dynamics can be imposed via the (classical) master equation

$$\begin{aligned}\frac{d}{dt}P(\{s\};t)&\\ &= -\sum_{i=1}^{N} W(s_i \to -s_i, t)P(s_1, ..., s_i, ..., s_N; t)\\ &+ \sum_{i=1}^{N} W(-s_i \to s_i, t)P(s_1, ..., -s_i, ..., s_N; t)\,.\end{aligned} \tag{5.79}$$

Here, $P(\{s\};t)$ denotes the probability that the system is in a spin configuration $\{s\}$ at time t, and $W(s_i \to -s_i, t)$ represents the transition probability rate of a spin flip at site i and at time t. Under equilibrium conditions, the probability and transition rates satisfy detailed balance [50],

$$\frac{W(s_i \to -s_i)}{W(-s_i \to s_i)} = \frac{P(s_1, ..., -s_i, ..., s_N)}{P(s_1, ..., s_i, ..., s_N)}\,, \tag{5.80}$$

with the transition rate being of the Glauber type (characterizing a non-conserved order parameter),

$$W(s_i \to -s_i) = \frac{1}{2\tau_0}[1 - s_i \tanh(\beta E)]\,. \tag{5.81}$$

Here, τ_0 defines the characteristic time scale of Glauber dynamics, and $E = -(2J/N)\sum_i^N s_j$. From here, one can simulate the relaxation of the system from a near-equilibrium state using Monte Carlo methods combined with the transition rate given above. Monte-Carlo simulations of the this model at criticality are consistent with a critical dynamical scaling where $t \sim N^{1/2}$ [57].

CHAPTER 6

MODIFIED TIME-REVERSAL SYMMETRY AT CRITICALITY

nonequilibrium systems are host to exciting physics because the general guiding principles of equilibrium statistical mechanics are not directly applicable in this new domain. One such general feature is the principle of detailed balance in equilibrium [77]. Extensions of this principle to the quantum domain have been studied extensively for both closed and open systems [78–81]. In all such settings, detailed balance is directly tied to time-reversal symmetry (TRS) under reversing the direction of time (in two-time correlators, e.g.). A second defining characteristic of equilibrium systems is the fluctuation-dissipation relations (FDRs) relating the dynamical response of the system to their inherent fluctuations. Importantly, these two principles are not independent: a proper formulation of the TRS leads to the FDRs [82].

The paradigm of driven-dissipative systems we are considering in this work constitutes a generic nonequilibrium setting. The competition between drive and dissipation leads the system towards a nonequilibrium steady state far from thermal equilibrium. Due to the nonequilibrium dissipative dynamics, both TRS and FDR are generally broken in these steady states [83]; the guiding principles of equilibrium physics are thus absent in their driven-dissipative counterparts.

Nonetheless, it has become increasingly clear that the critical properties of a large class of many-body driven-dissipative systems (yet not all [69, 84–87]) are described by an effective equilibrium behavior near their respective phase transitions [13, 14, 60–68, 88, 89]. We have shown in Ch. 5 that the DDIM appears to fall in this category as well.

In this chapter we will show that both FDR and TRS are broken even macroscopically at or near criticality. This is shown by inspecting different observables that overlap with the order parameter and crucially encompass both even and odd operators under time-reversal transformation. We show that these observables satisfy emergent FDR-like relations but with effective temperatures that are opposite in sign; we dub such relations FDR*. Moreover, while TRS is broken macroscopically, we show that a modified form of the time-reversal symmetry of two-time correlators, dubbed TRS*,

emerges at or near criticality where correlation and response functions exhibit definite, but possibly opposite, parities under time-reversal transformation. This is in sharp contrast with equilibrium where correlation and response functions exhibit the same parity.

We showcase our results using the DDIM, as it provides the minimal driven-dissipative model with an Ising type phase transition. We also consider a short-range quadratic model of driven-dissipative bosons with the Ising symmetry. These models provide an ideal testbed for the general questions about the fate of the FDR and TRS in driven-dissipative systems, the role of the time-reversal symmetry (breaking), and the emergence of modified fluctuation-dissipation relations.

6.1 Fluctuation-Dissipation Relations

Characteristic information about a given quantum system and a set of observables O_i can be obtained from the two-point functions

$$C_{O_iO_j}(t) = \langle\{O_i(t), O_j\}\rangle, \quad \chi_{O_iO_j}(t) = -i\Theta(t)\langle[O_i(t), O_j]\rangle, \tag{6.1}$$

which define the correlation function and the causal response function, respectively; the former captures fluctuations (e.g., at equal times), while the latter describes the response of the system to a perturbation at an earlier time. While we have defined the correlation and response functions earlier in this text, we redefine them here in a more general fashion for the purposes of this chapter. The function $\Theta(t)$ is the Heaviside step function, used to enforce causality. The fluctuation-dissipation theorem, a pillar of statistical mechanics, relates these two quantities in equilibrium. We write the fluctuation-dissipation relation (FDR) as [48]

$$\text{FDR}: \qquad \chi_{O_iO_j}(t) = \frac{1}{2T}\Theta(t)\partial_t C_{O_iO_j}, \tag{6.2}$$

valid for classical systems (with the respective classical definitions of $C(t)$ and χ(t) [43]), as well as quantum systems at finite temperature and long times [48]. An alternative representation of the FDR in the frequency domain is

$$\chi''_{O_iO_j}(\omega) = \frac{\omega}{4T}C_{O_iO_j}(\omega)\,, \tag{6.3}$$

where $\chi''_{O_iO_j}(t) \equiv \frac{1}{2}\langle[O_i(t), O_j]\rangle$, and the Fourier transform has been defined as $f(\omega) = \int_t e^{i\omega t} f(t)$ for a function f. Furthermore, if the system satisfies *microreversiblity*, or (quantum) detailed balance, two-time correlators exhibit a time-reversal symmetry [79, 80]. Assuming that the operator O_i has a definite parity ϵ_i under time-reversal (in the absence of magnetic fields), the correlation and response functions then satisfy [90]

$$C_{O_iO_j}(t) = \epsilon_i\epsilon_j C_{O_jO_i}(t)\,, \tag{6.4a}$$

$$\chi_{O_iO_j}(t) = \epsilon_i\epsilon_j \chi_{O_jO_i}(t)\,. \tag{6.4b}$$

In this work, we shall refer to such relations as TRS of two-time correlators, or just TRS. Notice that these set of equations are also consistent with the FDR in Eq. (6.2), and are valid in the frequency domain as well. The above equations form the origin of the Onsager reciprocity relations [91].

FDR and TRS are both broken in driven-dissipative systems as they give rise to a nonequilibrium steady states at long times. Extensive effort has gone into identifying the steady states of many-body driven-dissipative systems as well as their phase transitions. A large body of work, however, has shown that a variety of driven-dissipative many-body systems exhibit critical behavior that is *effectively* equilibrium [13, 14, 60–68, 88, 89, 92]. Specifically, an effective temperature T_{eff} emerges that governs the critical properties (e.g., critical exponents) near their phase transitions at long times/wavelengths. An effective TRS may be then expected to emerge as well given that TRS and FDR are intimately tied [82].

We consider driven-dissipative systems whose Hamiltonian—in the rotating frame—is itself time-reversal symmetric: $THT^{-1} = H$ with T the antiunitary operator associated with the time-reversal transformation; here, $T = K$ is simply complex conjugation. This is clearly satisfied by Eq. (3.4), and is also satisfied by the bosonic lattice model we will consider here. Dissipative coupling to the environment, however, explicitly breaks TRS and exposes the nonequilibrium nature of the system. Additionally, for both models the dynamics under the Liouvillian $\mathcal{L}$ comes with an Ising $\mathbb{Z}_2$ symmetry that defines the order parameter at the phase transition. nonequilibrium systems with the $\mathbb{Z}_2$ symmetry are generally expected to fall under the familiar Ising universality class at their phase transitions. Previous work on driven-dissipative Ising-type systems has reported an emergent

FDR governing the order-parameter dynamics for some T_{eff} [14, 44, 89, 92–94], and the DDIM is no exception (see Ch. 5).

Notwithstanding the evidence for emergent equilibrium near criticality, here we show that FDR and TRS are both macroscopically broken in quadratic driven-dissipative Ising-type systems. This becomes manifest by considering other observables that overlap with the order parameter, i.e., observables that share the same $\mathbb{Z}_2$ symmetry. In the Ising model, for example, beside S_x typically signifying the order parameter, we will also consider S_y (with the transverse field along the z direction). This expanded set of observables exhibits critical scaling, but they do not obey an effective equilibrium FDR. Interestingly, however, we show that a modified form of the FDR emerges at long times,

$$\text{FDR}^* : \qquad \chi_{O_i O_j^*}(t) \simeq \frac{1}{2T_{\text{eff}}}\Theta(t)\partial_t C_{O_i O_j}, \tag{6.5}$$

where the $\simeq$ sign means we have neglected noncritical corrections here and throughout the rest of this chapter; we dub this modified relation FDR*. Here, we have assumed that the O_i's are Hermitian operators [1] which have the same Ising symmetry as the order parameter; we have also defined $O_j^* = TO_jT^{-1}$ (recall that $T = K$). In the example of the Ising spin model, $S_x^* = S_x$ while $S_y^* = -S_y$. We emphasize that FDR* is only applicable for this subset of observables, and not for all observables as is the case in Eq. (6.2). In the frequency domain, FDR* takes the form

$$\text{Im}\chi_{O_i O_j^*}(\omega) \simeq \frac{\omega}{4T_{\text{eff}}} C_{O_i O_j}(\omega)\,, \tag{6.6}$$

which does not reduce to Eq. (6.3), in particular when the two operators have opposite parities. The FDR* is radically different from its equilibrium counterpart, and has important consequences. To see this, let us again assume that the operator O_i has a definite parity ϵ_i under time-reversal transformation. In this case, the FDR can be written as

$$\chi_{O_i O_j}(t) \simeq \frac{\epsilon_j}{2T_{\text{eff}}}\Theta(t)\partial_t C_{O_i O_j}. \tag{6.7}$$

This means that an emergent FDR is satisfied with $\chi_{O_i O_j} = (1/2T_{ij})\partial_t C_{O_i O_j}$ but with different temperatures for different observables, $T_{ij} = \epsilon_j T_{\text{eff}}$, same in magnitude but possibly with opposite

[1] Unlike the standard FDR, the FDR* is sensitive to the operators being Hermitian or not; see Section 6.6.2.

signs depending on the observables. For example, if O_1 is even under time-reversal ($\epsilon_1 = 1$) and O_2 is odd ($\epsilon_2 = -1$), we find $T_{11} = -T_{12} = T_{21} = -T_{22} = T_{\text{eff}}$.

We further show that an unusual form of TRS holds at or near criticality:

$$C_{O_iO_j}(t) \simeq C_{O_jO_i}(t), \tag{6.8a}$$

$$\chi_{O_iO_j}(t) \simeq \epsilon_i\epsilon_j\chi_{O_jO_i}(t). \tag{6.8b}$$

In parallel with FDR*, the above relations will be referred to as TRS*. Notice that the above equations are consistent with the FDR* in Eq. (6.7). Interestingly, the correlation and response functions transform differently under time-reversal transformation, in sharp contrast with equilibrium; cf. Eq. (6.4). While violating TRS, these functions still have a definite parity under time-reversal transformation. Moreover, combining Eqs. (6.7) and (6.8), we further show that the Onsager reciprocity relation finds a modified form with the opposite parity. This is surprising in light of the broken TRS, but is a direct consequence of the emergent TRS*.

We will derive these results in the following sections using the Keldysh field-theory we have developed in the previous chapters, and we connect the slow mode discussed in Sec. 5.1 to the emergence of $TRS*$. We show that the FDR* and TRS* are a consequence of the non-Hermitian form of the dynamics generator, due to the TRS of the Hamiltonian, $THT^{-1} = H$, combined with the Ising $\mathbb{Z}_2$ symmetry of the Liouvillian $\mathcal{L}$.

6.2 Time-Reversal in the DDIM

In this section, we briefly go over the implications of time-reversal symmetry in the DDIM. The LMG Hamiltonian given by Eq. (3.4), as well as the DDIM Liouvillian, has been discussed extensively in Ch. 3. We repeat it here for the sake of the reader

$$H = -\frac{J}{N}S_x^2 + \Delta S_z\,. \tag{6.9}$$

In general, the form of the time-reversal operator depends on the form of the Hamiltonian, but it is always anti-unitary. Here, the time-reversal operator $T = K$ is simply complex conjugation. The Hamiltonian in Eq. (3.4) is time-reversal symmetric because it is real, which can be seen by

writing out all of the Pauli matrices in the basis of σ^z. Time-reversal transformation (i.e., acting with the anti-unitary operator T together with sending $t \to -t$) leaves the von Neumann equation $\partial_t \rho = -i[H, \rho]$ invariant. In the ground state, this symmetry enforces $\langle S_y \rangle = 0$ as $TS_yT^{-1} = -S_y$; this is true even in the ordered phase where $\langle S_y \rangle = 0$ while $\langle S_x \rangle \neq 0$, see Eq. (3.8). Furthermore, correlators such as $\langle \{S_x, S_y\} \rangle$ that are odd under time-reversal must be zero.

These symmetry considerations can be extended to thermal states under unitary dynamics as they satisfy the KMS condition and exhibit an equilibrium symmetry that involves time-reversal [95, 96]. Two time-correlators then satisfy the symmetry relations in Eq. (6.8). However, the driven-dissipative model in Eq. (3.5) breaks such symmetries. This is because Eq. (3.5) is derived in the rotating frame of the drive, hence breaking detailed balance. The resulting steady state is then *not* a thermal state, and TRS of two-time correlators no longer holds [97]. Specifically, this allows for nonzero expectation values of odd observables such as $\langle S_y \rangle$ (in the ordered phase) and correlators such as $\langle \{S_x, S_y\} \rangle$. In fact, as we will see in the following sections, the fact that S_y can now spontaneously order is deeply connected to the existence of $TRS*$.

6.3 Correlation and Response Functions For S_x and S_y

We will now utilize the field theory that we established in Ch. 3 to calculate the necessary observables to showcase the modified TRS and FDR. To obtain the correlation and response functions for S_y and the cross-correlations with S_x, we introduce source fields $\alpha^{(u/l)}$ and $\beta^{(u/l)}$ to $\mathbb{L}$, the vectorized form of Eq. (3.5), which couple to S_x and S_y respectively:

$$\mathbb{L}'(t) = \mathbb{L} + i\alpha^{(u)}(t)\frac{S_x}{\sqrt{N}} \otimes I - i\alpha^{(l)}(t) I \otimes \frac{S_x}{\sqrt{N}} + i\beta^{(u)}(t)\frac{S_y}{\sqrt{N}} \otimes I + i\beta^{(l)}(t) I \otimes \frac{S_y}{\sqrt{N}}, \qquad (6.10)$$

and perform the nonequilibrium quantum-to-classical mapping as usual. The absence of a minus sign on the last term stems from the vectorization transformation in the mapping. Introducing the sources does not affect the quadratic term in m in Eq. (3.16), but changes the $\mathbb{T}$ matrix to the new

matrix $\mathbb{T}' = \mathbb{T} + \mathbb{T}_\alpha + \mathbb{T}_\beta$ where

$$\mathbb{T}_\alpha = i\sqrt{\frac{2}{N}}\begin{pmatrix} \alpha_q & 0 & 0 & 0 \\ 0 & \alpha_c & 0 & 0 \\ 0 & 0 & -\alpha_c & 0 \\ 0 & 0 & 0 & -\alpha_q \end{pmatrix}, \tag{6.11}$$

and

$$\mathbb{T}_\beta = \frac{1}{\sqrt{2N}}\begin{pmatrix} 0 & -\beta_c + \beta_q & -\beta_c - \beta_q & 0 \\ \beta_c - \beta_q & 0 & 0 & -\beta_c - \beta_q \\ -\beta_c - \beta_q & 0 & 0 & -\beta_c + \beta_q \\ 0 & -\beta_c - \beta_q & \beta_c - \beta_q & 0 \end{pmatrix}. \tag{6.12}$$

We have performed the Keldysh rotation $\alpha_{c/q} = (\alpha^{(u)} \pm \alpha^{(l)})/\sqrt{2}$, $\beta_{c/q} = (\beta^{(u)} \pm \beta^{(l)})/\sqrt{2}$ for convenience. Next, we expand the action to quadratic order in both $m_{c/q}$ and the source fields around $m_{c/q} = \alpha_{c/q} = \beta_{c/q} = 0$,

$$S = \frac{1}{2}\int_{t,t'} \begin{pmatrix} m_c \\ m_q \\ \alpha_c \\ \alpha_q \\ \beta_c \\ \beta_q \end{pmatrix}_t^T \begin{pmatrix} \mathbf{P} & 0 & 0 \\ 4J\mathbf{P}_{\alpha\alpha} & \mathbf{P}_{\alpha\alpha} & 0 \\ 4J\mathbf{P}_{\beta\alpha} & 2\mathbf{P}_{\beta\alpha} & \mathbf{P}_{\beta\beta} \end{pmatrix}_{t-t'} \begin{pmatrix} m_c \\ m_q \\ \alpha_c \\ \alpha_q \\ \beta_c \\ \beta_q \end{pmatrix}_{t'}, \tag{6.13}$$

where the kernel becomes a lower triangular block matrix. The block matrices take the usual Keldysh structure

$$\mathbf{P} = \begin{pmatrix} 0 & P^A \\ P^R & P^K \end{pmatrix}, \qquad \mathbf{P}_{\alpha\alpha} = \frac{1}{4J^2}\left[\mathbf{P} + \begin{pmatrix} 0 & 2J\delta(t) \\ 2J\delta(t) & 0 \end{pmatrix}\right],$$
$$\mathbf{P}_{\beta\alpha} = \begin{pmatrix} 0 & P^A_{\beta\alpha} \\ P^R_{\beta\alpha} & P^K_{\beta\alpha} \end{pmatrix}, \qquad \mathbf{P}_{\beta\beta} = \mathbf{P}_{\alpha\alpha},$$

and the matrix elements for each block matrix are

$$P^R(t) = P^A(-t) = -2J\delta(t) + \Theta(t)8J^2 e^{-\frac{\Gamma}{2}t}\sin(2\Delta t), \tag{6.14a}$$

$$P^K(t) = i8J^2 e^{-\frac{\Gamma}{2}|t|}\cos(2\Delta t), \tag{6.14b}$$

$$P^R_{\beta\alpha}(t) = -P^A_{\beta\alpha}(-t) = -\Theta(t)2e^{-\frac{\Gamma}{2}|t|}\cos(2\Delta t), \tag{6.14c}$$

$$P^K_{\beta\alpha}(t) = -i2e^{-\frac{\Gamma}{2}|t|}\sin(2\Delta t), \tag{6.14d}$$

Equation (6.13) is exact in the thermodynamic limit, as higher-order terms in the expansion are at least of the order $O(1/N)$ for the same reasons discussed in Ch. 3.

After Fourier transformation, defined as $m(t) = \int_\omega e^{-i\omega t} m(\omega)$ with the integration measure $\int_\omega = \int_{-\infty}^{\infty} d\omega/2\pi$, we integrate out the $m_{c/q}$ fields to obtain the generating functional $W[\alpha_{c/q}, \beta_{c/q}] = -i \ln Z$ as

$$W = -\frac{1}{2} \int_\omega \begin{pmatrix} \alpha_q \\ \beta_q \\ \alpha_c \\ \beta_c \end{pmatrix}^\dagger_\omega \begin{pmatrix} \mathbf{G}^K & \mathbf{G}^R \\ \mathbf{G}^A & 0 \end{pmatrix}_\omega \begin{pmatrix} \alpha_q \\ \beta_q \\ \alpha_c \\ \beta_c \end{pmatrix}_\omega . \tag{6.15}$$

The Green's function block matrices are given by

$$\mathbf{G}^K = \begin{pmatrix} G^K_{xx} & G^K_{xy} \\ G^K_{yx} & G^K_{yy} \end{pmatrix}, \qquad \mathbf{G}^R = \begin{pmatrix} G^R_{xx} & G^R_{xy} \\ G^R_{yx} & G^R_{yy} \end{pmatrix}, \tag{6.16}$$

and satisfy $\mathbf{G}^K(\omega) = -[\mathbf{G}^K]^\dagger(\omega)$ and $\mathbf{G}^R(\omega) = [\mathbf{G}^A]^\dagger(\omega)$. In terms of the original observables S_x, S_y, the Green's functions become $G^K_{jj'}(\omega) = -i\mathcal{F}_\omega \langle\{S_j(t), S_{j'}(0)\}\rangle/N$ and $G^R_{jj'}(\omega) = -i\mathcal{F}_\omega \Theta(t)\langle[S_j(t), S_{j'}(0)]\rangle/N$, with $\mathcal{F}_\omega(f(t)) = \int_{-\infty}^{\infty} dt e^{i\omega t} f(t)$. The elements of Eq. (6.16) are given by

$$G^K_{xx}(\omega) = \frac{-i\Gamma[\Gamma^2 + 4(4\Delta^2 + \omega^2)]}{2(\omega - \omega_1)(\omega - \omega_2)(\omega - \omega_1^*)(\omega - \omega_2^*)}, \tag{6.17a}$$

$$G^K_{xy}(\omega) = \frac{4\Gamma(iJ\Gamma + 2J\omega - 2\Delta\omega)}{(\omega - \omega_1)(\omega - \omega_2)(\omega - \omega_1^*)(\omega - \omega_2^*)}, \tag{6.17b}$$

$$G^K_{yy}(\omega) = \frac{-i\Gamma[\Gamma^2 + 16(2J - \Delta)^2 + 4\omega^2]}{2(\omega - \omega_1)(\omega - \omega_2)(\omega - \omega_1^*)(\omega - \omega_2^*)}, \tag{6.17c}$$

$$G^R_{xx}(\omega) = \frac{4\Delta}{(\omega - \omega_1)(\omega - \omega_2)}, \tag{6.17d}$$

$$G^R_{xy}(\omega) = \frac{\Gamma - 2i\omega}{(\omega - \omega_1)(\omega - \omega_2)}, \tag{6.17e}$$

$$G^R_{yx}(\omega) = \frac{-\Gamma + 2i\omega}{(\omega - \omega_1)(\omega - \omega_2)}, \tag{6.17f}$$

$$G^R_{yy}(\omega) = \frac{-4(2J - \Delta)}{(\omega - \omega_1)(\omega - \omega_2)}, \tag{6.17g}$$

where $\omega_{1/2} = -\frac{i}{2}(\Gamma \mp \Gamma_c)$, $\Gamma_c = 4\sqrt{\Delta(2J - \Delta)}$. The quantities G^R_{xx} and G^K_{xx} should be familiar, as they were calculated in Sec. 5.1, but we list them here for completeness. The correlation and response functions contain S_y are new and require the sources to be calculated as the m field is not directly related to S_y.

6.4 Nonequilibrium Signatures

In this section, we discuss the macroscopic, critical behavior of the DDIM. It is generally believed that such Ising models find an emergent equilibrium behavior near their phase transition. This is often argued by considering a single observable such as the order parameter and showing that it satisfies an effective FDR [14, 44, 89, 93, 94], or by inspecting the critical exponents and determining that the phase transition falls under an equilibrium universality class as we have showed is the case for the DDIM in Ch. 5. In contrast, we consider different observables and show that the associated FDR and TRS are both violated even macroscopically. Beyond the violation of FDR and TRS, we show that a modified form of these relations emerge, dubbed as the FDR* and TRS*, which govern the critical behavior of this system. In the following subsections, we derive the effective temperatures for different set of observables, discuss the breaking and emergence of (modified) TRS, and finally discuss our results in the limit of vanishing dissipation.

6.4.1 Effective temperature

At thermal equilibrium and at low frequencies, the FDR in frequency space can be written as

$$G^R_{ij}(\omega) - G^A_{ij}(\omega) = \frac{\omega}{2T} G^K_{ij}(\omega)\,. \tag{6.18}$$

We focus on the low-frequency limit as we will investigate the system at or near criticality where the dynamics is governed by a soft mode. To compare against the FDR in the time domain, we identify $C_{O_iO_j}(t) \equiv iG^K_{ij}(t)$ and $\chi_{O_iO_j}(t) \equiv G^R_{ij}(t)$.[2] The above equation follows from another version of the FDR given by [48]

$$-i\chi''_{O_iO_j}(t) = \frac{1}{4T}\partial_t C_{O_iO_j}(t)\,, \tag{6.19}$$

where $\chi''_{O_iO_j}(t) \equiv \frac{1}{2}\langle[O_i(t), O_j]\rangle = \frac{1}{2i}\big(G^R_{ij}(t) - G^A_{ij}(t)\big)$; the retarded and advanced Green functions are defined directly from the operators as $G^{R/A}_{ij}(t) \equiv \mp i\Theta(\pm t)\langle[O_i(t), O_j]\rangle$. While Eq. (6.2) is restricted to $t > 0$, the above equation is valid at all t, making it more suitable for the transition to

[2] We are including a normalization factor $1/N$ in the definition of correlation and response functions for convenience.

Fourier space, i.e., Eq. (6.18). Of course, the two (causal and non-causal) versions of the FDR are equivalent in equilibrium.

Equation (6.18) has been extensively used to identify an effective temperature even for nonequilibrium systems [44, 93, 98]. In the nonequilibrium setting of our model, however, we would immediately run into a problem for $i \neq j$ when the corresponding operators have different parities under time-reversal transformation (e.g., T_{eff} becomes infinite or complex valued). To see why, let us anticipate that the TRS* relations reported in Eq. (6.8) indeed hold, a fact that we will later justify near criticality and at long times. It is then easy to see that

$$C_{O_iO_j}(t) = C_{O_jO_i}(-t) \simeq C_{O_iO_j}(-t)\,, \tag{6.20}$$

while

$$\chi''_{O_iO_j}(t) = -\chi''_{O_jO_i}(-t) \simeq -\epsilon_i\epsilon_j\chi_{O_iO_j}(-t)\,. \tag{6.21}$$

Now for two distinct operators O_i and O_j where $\epsilon_i = -\epsilon_j$, we find that both $C_{O_iO_j}(t)$ and $\chi_{O_iO_j}(t)$ are even in time (for a fixed set of operators). However, this is not compatible with Eq. (6.19) as it requires $C_{O_iO_j}(t)$ and $\chi_{O_iO_j}(t)$ to have opposite parities. Postulating an effective FDR in this case, valid for all t, forces us to include a sign function, $\text{sgn}(t)$. That is, we should substitute

$$\chi''_{O_iO_j}(t) = \big(G^R_{ij}(t) - G^A_{ij}(t)\big)/2i \to \text{sgn}(t)\chi''_{O_iO_j}(t) = \big(G^R_{ij}(t) + G^A_{ij}(t)\big)/2i\,, \tag{6.22}$$

on the left hand side of Eq. (6.19) when $\epsilon_i = -\epsilon_j$. Notice that the extended FDR is consistent with the causal FDR in Eq. (6.2) when $t > 0$, but is now conveniently valid at all times. This extension is informed by the anticipated form of the TRS* which we will justify later. The fluctuation-dissipation relation is now conveniently cast in frequency space: for arbitrary operators O_i and O_j (with i and j being the same or distinct), the updated FDR takes the form

$$G^R_{ij}(\omega) - \epsilon_i\epsilon_j G^A_{ij}(\omega) = \frac{\omega}{2T_{ij}(\omega)} G^K_{ij}(\omega)\,, \tag{6.23}$$

where we have now allowed for a frequency- and operator-dependent effective temperature $T_{ij}(\omega)$. It is now clear that, while for $\epsilon_i = \epsilon_j$ the above equation recovers the structure of the FDR (cf.

Eq. (6.18)), a different combination, $G^R_{ij}(\omega) + G^A_{ij}(\omega)$, appears on the left hand side when $\epsilon_i = -\epsilon_j$. The above equation can be brought into a more compact version again by anticipating the TRS* in Eq. (6.8b) to write $\epsilon_i \epsilon_j G^A_{ij}(\omega) \simeq G^A_{ji}(\omega)$. Utilizing the relation $G^A_{ji}(\omega) = G^R_{ij}(\omega)^*$, we are finally in a position to write an equation for the effective temperature in the low-frequency limit:

$$T_{ij} = \lim_{\omega\to 0} \frac{\omega}{2} \frac{G^K_{ij}}{G^R_{ij}(\omega) - G^A_{ji}(\omega)} = \lim_{\omega\to 0} \frac{\omega}{4} \frac{-iG^K_{ij}}{\mathrm{Im}\, G^R_{ij}(\omega)} \,. \tag{6.24}$$

We have taken the low-frequency limit appropriate near criticality. Again we stress that the above equation is consistent with the standard form of the effective FDR for $i = j$, and it correctly incorporates the TRS* for $i \neq j$ with opposite parities.

A shorter, but perhaps less physically motivated, route to the above equation is to start directly from the causal form of the FDR in Eq. (6.2). The Fourier transform of this equation is given by [90]

$$\chi_{O_i O_j}(\omega) = \frac{1}{2T} \left[\mathrm{P} \int \frac{d\omega'}{2\pi} \frac{\omega'}{\omega - \omega'} C_{O_i O_j}(\omega') - \frac{i\omega}{2} C_{O_i O_j}(\omega) \right] , \tag{6.25}$$

where P stands for the principal part. Here too, we shall assume the TRS* in Eq. (6.8a): with $C_{O_i O_j}(t) \simeq C_{O_j O_i}(t) = C_{O_i O_j}(-t)$ regardless of the operators' parities, the correlation function $C_{ij}(t)$ is even in time, hence its Fourier transform, $C_{O_i O_j}(\omega)$, is purely real. Taking the imaginary part of the above equation then yields

$$\mathrm{Im}\, \chi_{O_i O_j}(\omega) = -\frac{\omega}{4T} C_{O_i O_j}(\omega) \tag{6.26}$$

where T has to be identified with the effective temperature $T_{ij}(\omega)$. Therefore, we arrive at the same definition of the effective temperature in Eq. (6.24).

Using Eq. (6.24), we can now identify the effective temperature in the driven-dissipative Ising model (defining $i, j \in \{x, y\}$)

$$T_{xx} = \frac{\Gamma^2 + 16\Delta^2}{32\Delta} \,, \tag{6.27a}$$

$$T_{yy} = \frac{\Gamma^2 + 16(\Delta - 2J)^2}{32(\Delta - 2J)} \,, \tag{6.27b}$$

$$T_{xy} = -T_{yx} = \frac{-2J\Gamma^2}{\Gamma^2 + 16\Delta(2J - \Delta)} \,. \tag{6.27c}$$

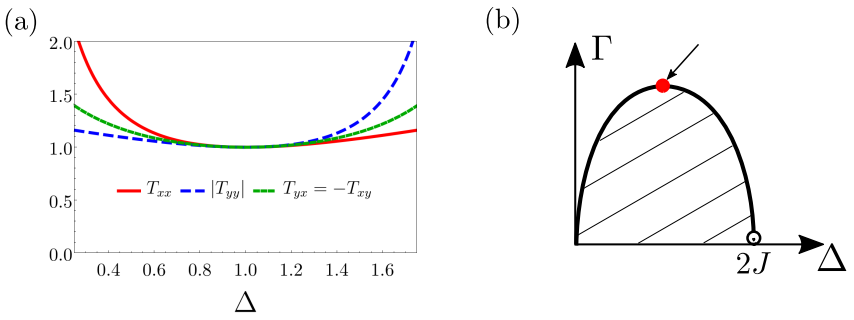

Figure 6.4.1 (a) Effective temperatures T_{xx}, T_{xy}, T_{yx} and T_{yy} as a function of Δ at or away from the phase boundary; we choose the parameters $J = 1, \Gamma = 4$ with the point $\Delta = 1$ representing the critical point at the tip of the phase boundary (see the red dot in panel (b)). The effective temperatures become equal up to a sign at the critical point. The same pattern emerges on any point along the phase boundary and away from $\Gamma = 0$. (b) The phase diagram of the DDIM. The shaded region is the ordered phase where $\langle S_{x,y} \rangle \neq 0$.

These expressions are calculated everywhere in the normal phase and generally take different values (see also [93]), underscoring the nonequilibrium nature of the model at the microscopic level. We note that the effective temperatures reported above have a physical significance only near the phase transition where the slow mode governs the dynamics. This is because we have neglected noncritical contributions in the derivation of Eq. (6.23) by invoking TRS*. Equations (6.27a) and (6.27b) display non-analytic behaviour, though in different regions of the phase diagram. T_{xx} diverges when $\Delta \to 0$, in agreement with Ref. [47] that reports an infinite temperature in the σ^x basis. In contrast, T_{yy} diverges when $\Delta = 2J$ for any finite value of Γ. This divergence coincides with the change in the dynamical behaviour from overdamped to underdamped dynamics as pointed out in [98]. Finally, $T_{xy} = -T_{yx}$ are everywhere finite but opposite for the opposite order of the observables; this is tied to the TRS* as we will discuss later.

The definition of the low-frequency effective temperature is particularly motivated near the phase boundary where there exists a soft mode that characterizes the low-frequency dynamics [98]. Interestingly, at (or near) the phase transition, we find

$$T_{xx} = -T_{xy} = T_{yx} = -T_{yy} = J. \tag{6.28}$$

Remarkably, these effective temperatures find the same magnitude, but possibly with different signs.

While focusing on a single observable (say S_x) and its dynamics, one might be led to conclude that the system is in effective equilibrium. However, a different observable (say S_y) exhibits the opposite effective temperature. Notice that all correlation functions (involving S_x and/or S_y) are divergent at the phase transition, i.e., they are all sensitive to the soft mode; we will make this more precise in Section 6.5 where we develop an effective field theory. This suggests that although the critical behavior is governed by a single (soft) mode at the transition, the system is genuinely nonequilibrium even *macroscopically*.

To support these analytical results, we have numerically simulated [94] the FDR in the time domain (cf. Eq. (6.2)) and at a representative critical point on the phase boundary for a finite, yet large, system with $N = 100$ spins. Correlation and response functions at criticality and at a finite system size require an analysis beyond the quadratic treatment presented here and thus serves as a nontrivial check of our results. Also, working in the time domain and restricting to $t > 0$, we circumvent the issues that arise in the frequency domain; see the discussion in the beginning of this subsection. Indeed, we find an excellent agreement in Fig. 6.4.2 between the analytical results (in frequency space) and the numerical results (in the time domain) with the exception of short time differences; the discrepancy at short times is a consequence of the fact that the (observable-dependent) effective temperature is defined in the zero-frequency limit of Eq. (6.23), therefore characterizing the long-time dynamics. In fact, the agreement is remarkably good even at relatively short times $Jt \gtrsim 1$. Finally, we remark that the difference at short times is not due to finite-size effects, and exists even in the limit $N \to \infty$.

6.4.2 TRS breaking

Broken TRS allows for nonzero correlators such as $\langle\{S_x, S_y\}\rangle$ that are otherwise odd under the time-reversal transformation. Indeed, we find that this correlator is nonzero and is even critical.

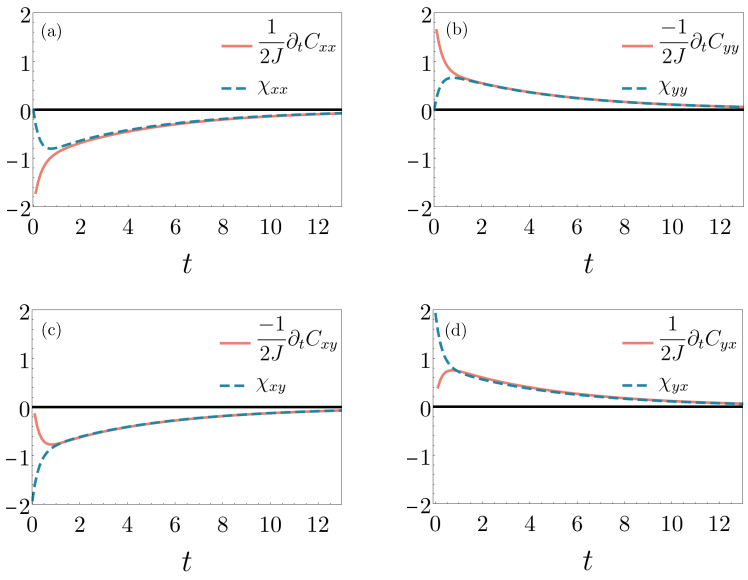

Figure 6.4.2 Numerical plots of correlation and response functions at a representative critical point with $J = 1, \Delta = 1, \Gamma = 4$ and the system size $N = 100$. A modified fluctuation-dissipation relation, $\chi_{O_i O_j}(t) = \Theta(t) C_{O_i O_j}(t)/2T_{ij}$, emerges at long times. The effective temperatures take the same value up to a sign: $T_{xx} = -T_{xy} = T_{yx} = -T_{yy} = J$.

More precisely, we find from Eq. (6.17b) that

$$C_{xy}(t) \equiv iG^K_{xy}(t) = \frac{4}{\Gamma_c}\left[\frac{-J\Gamma + \mathrm{sgn}(t)(J-\Delta)(\Gamma-\Gamma_c)}{\Gamma-\Gamma_c} e^{-\frac{\Gamma-\Gamma_c}{2}|t|} - \frac{-J\Gamma + \mathrm{sgn}(t)(J-\Delta)(\Gamma+\Gamma_c)}{\Gamma+\Gamma_c} e^{-\frac{\Gamma+\Gamma_c}{2}|t|}\right]. \tag{6.29}$$

(For ease of notation, we have replaced $C_{S_i S_j}$ by C_{ij}; similarly for χ_{ij}.) Specifically, at equal times, we have $C_{xy}(t=0) = -8J\Gamma/(\Gamma^2 - \Gamma_c^2)$. Indeed, the equal-time cross correlation diverges as $\sim 1/(\Gamma - \Gamma_c)$ upon approaching the critical point $\Gamma \to \Gamma_c$. This is a stark manifestation of broken TRS at a macroscopic level. We also note that both $C_{xx}, C_{yy} \sim 1/(\Gamma - \Gamma_c)$ diverge in a similar fashion. Again, this is because S_x and S_y share the same soft mode, as will be shown in Section 6.5.

The macroscopic breaking of TRS alters the Onsager symmetry relations in an exotic fashion that is distinct for the correlation and response functions. Indeed, the analytical expression in Eq. (6.29) shows that, near criticality and at sufficiently long times,

$$C_{xy}(t) \simeq -\frac{4J\Gamma}{\Gamma_c(\Gamma-\Gamma_c)} e^{-\frac{\Gamma-\Gamma_c}{2}|t|}, \tag{6.30}$$

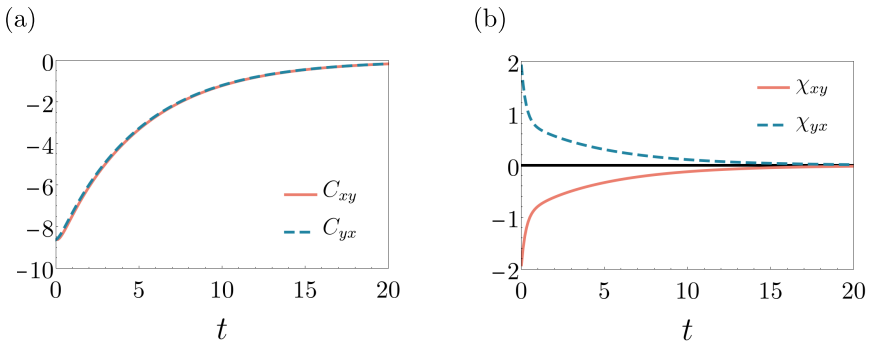

Figure 6.4.3 Cross-correlation and -response functions at criticality ($J = 1, \Delta = 1, \Gamma = 4, N = 100$). A modified form of TRS emerges at criticality where correlation (panel a) and response (panel b) functions exhibit opposite parities under time-reversal transformation.

hence, $C_{xy}(t) \simeq C_{xy}(-t)$, or equivalently, $C_{xy}(t) \simeq C_{yx}(t)$ up to noncritical corrections; far from criticality, the correlation functions do not generally satisfy this symmetry relation. Furthermore, the analytical expressions for the response functions in Eqs. (6.17e) and (6.17f) show that $\chi_{xy}(t) = -\chi_{yx}(t)$. Interestingly, the cross-correlation and -response functions exhibit opposite parities. These analytical considerations are further supported by the numerical simulation shown in Fig. 6.4.3 at criticality confirming

$$C_{xy}(t) \simeq C_{yx}(t)\,, \tag{6.31a}$$

$$\chi_{xy}(t) \simeq -\chi_{yx}(t)\,, \tag{6.31b}$$

consistent with the TRS* in Eq. (6.8). Despite the broken TRS, the correlation and response functions retain definite, though distinct, parities under time-reversal.

6.4.3 Weakly-dissipative limit

In this section, we briefly consider the weakly-dissipative critical point at at $\Delta \to 2J$ and $\Gamma \to 0$; see Fig. 6.4.1(b). It was shown in Sec. 6.4.3 that this limit leads to a different critical dynamics than a generic critical point at finite Γ [94, 98]. Here, we are interested in the TRS breaking and its possible emergence in the limit of vanishing dissipation. Interestingly, we find that the fate of the TRS depends on the way that this critical point is approached, and that this distinction only exists

in the thermodynamic limit where the system is gapless at the phase boundary. We shall consider two different scenarios below.

In the first scenario, let us set $\Delta = 2J$ and take the limit $\Gamma \to 0$. Fourier transforming Eq. (6.17c) to the time domain gives

$$C_{yy}(t) = \lim_{\Delta \to 2J} iG^K_{yy}(t) = 2e^{-\frac{1}{2}\Gamma|t|} . \tag{6.32}$$

We thus see that the S_y correlator is finite at the weakly-dissipative critical point, indicating that S_y has become "gapped". This appears to suggest a return to the equilibrium scenario where S_y plays no role in critical behaviour. However, the cross-correlation given by Eq. (6.29) remains nonzero and even *critical* at the weakly-dissipative point: $C_{xy}(t = 0) \sim 1/\Gamma$. Therefore, even in the limit of vanishing dissipation, TRS is macroscopically broken.

In the second scenario, we consider $\Delta > 2J$ and first take the limit $\Gamma \to 0$. In this case, we have $\Gamma_c = i\sqrt{\Delta(\Delta - 2J)} \equiv i\omega_c$, which then leads to

$$\lim_{\Gamma \to 0} C_{xy}(t) = \frac{-4(\Delta - J)}{\omega_c} \sin\left(\frac{\omega_c t}{2}\right) . \tag{6.33}$$

This expression goes to zero at $t = 0$ for any value of Δ including the weakly dissipative critical point as $\Delta \to 2J^+$, recovering the equilibrium result.

The different behavior in the two scenarios lies in the fact that the system has a finite dissipative gap when we send $\Gamma \to 0$ before sending $\Delta \to 2J$ but not *vice versa*. It has been shown that the steady state of a system with a finite dissipative gap becomes purely a function of the Hamiltonian in the limit of vanishing dissipation, i.e., $\rho_{\text{ss}} = f(H)$ [56]; see also [53]. In this case, the steady state for our model can be written as a function of the Hamiltonian in Eq. (3.4), and thus respects TRS. A system of finite size would fall under this category as well because the system will always be gapped for $N < \infty$, irrespective of the order of limits taken w.r.t. Δ and Γ. The argument about weakly-dissipative states commuting with H in gapped systems, however, fails in a *gapless* system corresponding to the first order of limits, where we sent $\Delta \to 2J$ before taking the weakly-dissipative limit. Indeed, we find that in this case the TRS is macroscopically broken even in the limit of vanishing dissipation.

One can also determine the behavior of the effective temperature at the weakly-dissipative critical point. However, since the operator S_y is gapped, the definition of the low-frequency effective temperature doesn't seem appropriate. In fact, one finds that the effective temperatures involving this operator take different values (and even diverge) depending on the order of limits. Therefore, we will avoid discussing the effective temperature in this limit

6.5 Effective Field Theory

In this section, we develop a simple, generic field-theory analysis that elucidates the origin of the effective temperatures and their signs as well as FDR* and TRS*. We first need to construct an action that maps the spin operators S_x and S_y to the fields $x(t)$ and $y(t)$, respectively. This is achieved by starting from the generating functional W in Eq. (6.15) and constructing a quadratic action in terms of x and y fields that exactly reproduces the correlations of the corresponding operators. This is simply done via a Hubbard-Stratonovich transformation on $\exp(iW[\alpha_{c/q}, \beta_{c/q}])$ as

$$e^{iW} = \int \mathcal{D}[x_{c/q}, y_{c/q}] e^{i\mathcal{S}_{\text{eff}}[x_{c/q}, y_{c/q}] + i\int_\omega j^T(-\omega)v(\omega)}, \tag{6.34}$$

where we have absorbed an unimportant normalization factor into the measure, and we have defined the source field vector $j = (\alpha_q, \beta_q, \alpha_c, \beta_c)^T$ and the Hubbard-Stratonovich field vector $v = (x_c, y_c, x_q, y_q)^T$. The resulting action is given by

$$S_{\text{eff}} = \frac{1}{2}\int_\omega v^\dagger(\omega) \begin{pmatrix} \mathbf{0} & \mathbf{D}^A \\ \mathbf{D}^R & \mathbf{D}^K \end{pmatrix}_\omega v(\omega), \tag{6.35}$$

where we have written the kernel in terms of 2×2 block matrices:

$$\mathbf{D}^R(\omega) = [\mathbf{D}^A]^T(-\omega) = \begin{pmatrix} 2J - \Delta & \frac{1}{4}(\Gamma - 2i\omega) \\ \frac{1}{4}(-\Gamma + 2i\omega) & -\Delta \end{pmatrix}, \quad \mathbf{D}^K(\omega) = i\frac{\Gamma}{2}\begin{pmatrix} 1 & 0 \\ 0 & 1 \end{pmatrix}. \tag{6.36}$$

The kernel in Eq. (6.35) is simply the inverse of the Greens function, i.e. the kernel in Eq. (6.15). By inspecting the form of $\mathbf{D}^R$, we can identify the soft mode. At the critical point ($\Gamma \to \Gamma_c \equiv 4\sqrt{\Delta(2J - \Delta)}$), this matrix takes the form

$$\mathbf{D}^R_{\text{cr}}(\omega = 0) = \begin{pmatrix} 2J - \Delta & \sqrt{\Delta(2J - \Delta)} \\ -\sqrt{\Delta(2J - \Delta)} & -\Delta \end{pmatrix}. \tag{6.37}$$

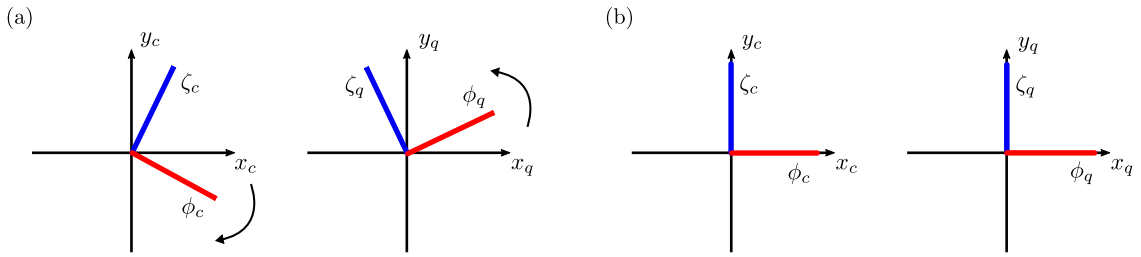

Figure 6.5.1 Schematic representation of the massless and massive fields ϕ and ζ in terms of the x and y fields that represent S_x and S_y. (a) The gapped/gapless fields are shown at a generic critical point. The classical and quantum fields are rotated with respect to the x-y axes, but in opposite directions, a fact that leads to the opposite signs of the effective temperatures. (b) At the weakly-dissipative critical point, $\Delta = 2J$, $\Gamma \to 0$, the gapless and gapped fields align with the x and y axes, respectively, similar to thermal equilibrium.

A convenient decomposition of $\mathbf{D}^R_{\rm cr}(\omega = 0)$ is given by $\mathbf{D}^R_{\rm cr}(\omega = 0) = \mathbf{U}\mathbf{\Lambda}\mathbf{U}$ where

$$\mathbf{U} = \frac{1}{\sqrt{2J\Delta}} \begin{pmatrix} \Delta & -\frac{1}{4}\Gamma_c \\ \frac{1}{4}\Gamma_c & \Delta \end{pmatrix}, \quad \mathbf{\Lambda} = \begin{pmatrix} 0 & 0 \\ 0 & -2J \end{pmatrix}, \tag{6.38}$$

valid for $0 < \Delta < 2J$; the regime $\Delta > 2J$ needs to be dealt with separately. The matrix $\mathbf{U}$ is orthogonal, i.e., $\mathbf{U}\mathbf{U}^T = \mathbf{I}$. Notice that this decomposition can be viewed as a singular-value decomposition, $\mathbf{D}^R_{\rm cr}(\omega = 0) = \mathbf{U}\mathbf{\Lambda}\mathbf{V}^T$, where $\mathbf{V} = \mathbf{U}^T$ with both $\mathbf{U}$ and $\mathbf{V}$ being orthogonal matrices. In this sense, the left and right singular vectors (corresponding to quantum and classical field respectively) are rotated with respect to the original vectors in Eq. (6.35) in opposite directions; see Fig. 6.5.1(a). As we shall see, this is the reason behind the new FDR* and TRS*.

This decomposition allows us to introduce new fields ϕ and ζ which are given by the original fields x and y upon rotation by $\mathbf{U}$,

$$\begin{pmatrix} \phi_c \\ \zeta_c \end{pmatrix} = \mathbf{U} \begin{pmatrix} x_c \\ y_c \end{pmatrix} = \frac{1}{\sqrt{2J\Delta}} \begin{pmatrix} \Delta x_c - \frac{1}{4}\Gamma_c\, y_c \\ \frac{1}{4}\Gamma_c\, x_c + \Delta y_c \end{pmatrix}, \tag{6.39a}$$

$$\begin{pmatrix} \phi_q \\ \zeta_q \end{pmatrix} = \mathbf{U}^T \begin{pmatrix} x_q \\ y_q \end{pmatrix} = \frac{1}{\sqrt{2J\Delta}} \begin{pmatrix} \Delta x_q + \frac{1}{4}\Gamma_c\, y_q \\ -\frac{1}{4}\Gamma_c\, x_q + \Delta y_q \end{pmatrix}. \tag{6.39b}$$

We note that the diagonal elements of $\mathbf{\Lambda}$ define the masses of the fields ϕ and ζ on the phase boundary. Therefore, we can identify ϕ as the soft mode and ζ as the gapped field. In addition, the Keldysh element of the kernel remains unchanged, $\mathbf{U}^T\mathbf{D}^K\mathbf{U} = \mathbf{D}^K$.

6.5.1 FDR* and TRS*

The field-theory representation makes the origin of the results shown in Section 6.4 clear. The correlation and response functions can now be expressed in terms of ϕ and ζ. At the phase boundary, the low-frequency effective temperature is captured purely by the soft mode ϕ because ζ is gapped and does not affect the low-frequency behavior of the model. In other words, the dominant contribution to the effective temperature follows from the correlation and response functions involving ϕ, while those involving ζ as well as the cross-correlations produce noncritical corrections which can be neglected. We have, up to these corrections,

$$T_{xx} \simeq T_\phi, \tag{6.40a}$$

$$T_{xy} \simeq \frac{U_{12}}{U_{21}} T_\phi = -T_\phi, \tag{6.40b}$$

$$T_{yx} \simeq T_\phi, \tag{6.40c}$$

$$T_{yy} \simeq \frac{U_{12}}{U_{21}} T_\phi = -T_\phi, \tag{6.40d}$$

where

$$T_\phi \equiv \lim_{\omega \to 0} \frac{\omega}{2} \frac{\langle \phi_c(\omega)\phi_c(-\omega)\rangle}{\langle \phi_c(\omega)\phi_q(-\omega)\rangle - \langle \phi_q(\omega)\phi_c(-\omega)\rangle}, \tag{6.40e}$$

can be viewed as the effective temperature of the soft mode. This interesting result is purely a consequence of the non-Hermitian structure of Eq. (6.37).

Technically, one can see that the same pattern of effective temperatures emerges whenever the inverse retarded Green's function $\mathbf{D}_0 \equiv \mathbf{D}^R_{\rm cr}(\omega = 0)$ obeys the relation

$$\tau^z \mathbf{D}_0 \, \tau^z = \mathbf{D}_0^T \,, \quad \text{with} \quad \tau^z = \begin{pmatrix} 1 & 0 \\ 0 & -1 \end{pmatrix}, \tag{6.41}$$

which simply states that the off-diagonal part of the matrix $\mathbf{D}_0$ is antisymmetric. Note that $\mathbf{D}_0$ is real, but non-Hermitian.

The fact that the kernel $\mathbf{D}_0$ satisfies the above property can be argued solely on the grounds that the Hamiltonian itself is time-reversal symmetric. To show this, let us assume the contrary, namely that the off-diagonal part of the matrix $\mathbf{D}_0$ has a symmetric component. This would give rise to a coupling $\sim x_c y_q + x_q y_c$ where the fields' time dependence is implicit. Rewriting the classical

and quantum fields in terms of the fields on the upper and lower branches of the Keldysh contour (see Ch. 2.3), such coupling becomes $\sim x^{(u)}y^{(u)} - x^{(l)}y^{(l)}$. This term takes the structure of a Hamiltonian contribution to the action ($H^{(u)} - H^{(l)}$); however, the Hamiltonian does not couple x and y since it is time-reversal invariant. We should then conclude that the off-diagonal part of $\mathbf{D}_0$ is antisymmetric and cannot originate from the Hamiltonian dynamics. In equilibrium, the off-diagonal terms are simply zero (at $\omega = 0$); however, in a driven-dissipative system, dissipation naturally gives rise to nonzero (though antisymmetric) off-diagonal matrix elements.

The role of the $\mathbb{Z}_2$ symmetry in this analysis is to guarantee that there is only one soft mode described by a single real field, in contrast with other symmetries (such as $U(1)$ symmetry) which would require more (or complex) fields to describe the critical behavior. In addition, an explicit $\mathbb{Z}_2$ symmetry forbids a linear term in the action whose existence could alter our results.

We remark that a generalized version of the FDR,

$$\mathbf{G}^K(\omega) = \mathbf{G}^R(\omega)\mathbf{F}(\omega) - \mathbf{F}(\omega)\mathbf{G}^A(\omega)\,,$$

is also utilized in the literature [13, 14] to determine the distribution function matrix $\mathbf{F}(\omega)$. While in thermal equilibrium $\mathbf{F}(\omega) = \coth(\omega/2T)\mathbf{I}$ is proportional to the identity, the distribution function is allowed to become a nontrivial matrix in driven-dissipative systems, as shown in the context of the open Dicke model (possessing the same symmetries as those considered here). For the cavity mode, it was shown that this matrix finds two eigenvalues, $\pm\lambda(\omega)$, whose low-frequency behaviour is given by $\lambda(\omega) \sim 2T_{\text{eff}}/\omega$ [14]. The positive eigenvalue was then identified as the effective temperature. In contrast, our analysis clarifies the interpretation of the negative effective temperature in the form of the FDR* in Eq. (6.5) and its origin due to time-reversal symmetry breaking.

Next, we derive the TRS* relations for the correlation and response functions in Eq. (6.8), namely $C_{xy}(t) \simeq C_{yx}(t)$ while $\chi_{xy}(t) \simeq -\chi_{yx}(t)$ up to noncritical corrections. As with the effective temperatures, the key is to keep only the critical contributions from $\phi_{c/q}$. Recall that $\zeta_{c/q}$ are gapped, hence leading to noncritical corrections at or near the phase transition. The symmetry of

the correlation function follows in a simple fashion as

$$C_{xy}(t) = 2\langle x_c(t)y_c(0)\rangle \simeq 2U_{11}U_{12}\langle \phi_c(t)\phi_c(0)\rangle \simeq 2\langle y_c(t)x_c(0)\rangle = C_{yx}(t). \tag{6.42}$$

For the response function, we have

$$\begin{aligned} \chi_{xy}(t) &= \langle x_c(t)y_q(0)\rangle \simeq U_{11}U_{21}\langle \phi_c(t)\phi_q(0)\rangle\,, \\ \chi_{yx}(t) &= \langle y_c(t)x_q(0)\rangle \simeq U_{12}U_{11}\langle \phi_c(t)\phi_q(0)\rangle\,. \end{aligned} \tag{6.43}$$

Again using the fact that $U_{12} = -U_{21}$, one can see that $\chi_{xy}(t) \simeq -\chi_{yx}(t)$.

Finally, we remark that the field y becomes gapped at the weakly dissipative point as one can see from Eq. (6.39) (see also Fig. 6.5.1(b)), which leads to the noncritical $\langle S_y^2\rangle$ fluctuations. One thus recovers the equilibrium behavior, although, care should be taken with the $\Gamma \to 0$ limit due to the order of limits discussed in Section 6.4.3.

6.5.2 Onsager reciprocity relations

In this section, we derive the modified form of the Onsager reciprocity relations. As a starting point, consider the saddle-point solution of Eq. (6.35): $\mathbf{D}^R(i\partial_t)\cdot\mathbf{x}(t) = 0$ where we have replaced $\omega \to i\partial_t$ and defined $\mathbf{x} = (x, y)$; we have dropped the subscript c for convenience. By rearranging the time derivatives, we find the equation

$$\frac{\mathrm{d}}{\mathrm{d}t}\mathbf{x}(t) = -\mathbf{M}\cdot\mathbf{x}(t)\,, \qquad \text{with} \quad \mathbf{M} = \begin{pmatrix} \Gamma/2 & 2\Delta \\ 4J - 2\Delta & \Gamma/2 \end{pmatrix}. \tag{6.44}$$

This equation describes the average dynamics of $\mathbf{x}(t)$ (i.e., $\langle S_{x,y}\rangle$) near the steady state and governs its decay to zero.

Adopting a slightly more general notation, the dynamics near the steady state can be written as

$$\frac{\mathrm{d}}{\mathrm{d}t}\langle x_i\rangle_t = -\sum M_{ik}\langle x_k\rangle_t, \tag{6.45}$$

where $\{x_i\}$ denote a set of macroscopic variables, and $\langle\cdot\rangle_t$ represents the statistical (and, the quantum) average at time t; we later specialize to the variable $\mathbf{x}$ by setting $x_1 \equiv x$ and $x_2 \equiv y$. Now defining $L_{ij} = \sum_k M_{ik}\langle x_k x_j\rangle$, Onsager reciprocity relations in equilibrium take the form

$$L_{ij} = \epsilon_i\epsilon_j L_{ji}\,, \tag{6.46}$$

where ϵ_i denotes the parity of the corresponding field under time-reversal transofrmation. These relations are a direct consequence of the equilibrium FDR—in the form of Onsager's regression hypothesis—together with the TRS. The Onsager reciprocity relations are of great importance for their fundamental significance as well as practical applications. We shall refer the interested reader to Ref. [90] for the proof of the reciprocity relations in a classical setting.

In the nonequilibrium context of our model with both FDR and TRS broken, the Onsager reciprocity relations do not generally hold; however, given the modified form of the FDR* and TRS* in Eqs. (6.7) and (6.8), one may expect a modified form of the Onsager relations perhaps with a different parity than the one expected in equilibrium. Here, we show that this is indeed the case. To this end, we first note that the Onsager's regression hypothesis is modified in a straightforward fashion as

$$\langle x_i \rangle_t = \epsilon_j \frac{\lambda}{k_B T} \langle x_i(t) x_j(0) \rangle, \tag{6.47}$$

assuming that a "magnetic" field λ has been applied along the j direction before it is turned off at time $t = 0$. The only difference from the standard Onsager regression hypothesis is the prefactor ϵ_j appearing out in front, a factor that simply carries over from Eq. (6.7). Combining with Eq. (6.45), we have

$$\frac{\mathrm{d}}{\mathrm{d}t} \langle x_i(t) x_j(0) \rangle = -\sum M_{ik} \langle x_k(t) x_j(0) \rangle. \tag{6.48}$$

Notice that the factors of ϵ_j cancel out on both sides. Finally, using the TRS* of the correlation function, $C_{ij}(t) = C_{ji}(t)$ regardless of the corresponding parities, and setting $t = 0$, we find[3]

$$L_{ij} \simeq L_{ji} \,. \tag{6.49}$$

Notice the absence of the TRS parity factors $\epsilon_i \epsilon_j$; cf. the equilibrium Onsager reciprocity relation in Eq. (6.46).

To verify that this relation holds in our nonequilibrium setting, it is important to distinguish the contribution of the soft mode, responsible for the critical behavior, from the gapped mode.

[3]Since the modified FDR doesn't hold at short times, setting $t = 0$ might seem problematic. However, the error incurred in the process only amounts to a noncritical correction.

Therefore, we shall consider the dynamics at a coarse-grained level where the gapped mode is "integrated out". To this end, let's write

$$\mathbf{M} = m\boldsymbol{\phi}^R\boldsymbol{\phi}^L + M\boldsymbol{\zeta}^R\boldsymbol{\zeta}^L, \tag{6.50}$$

where we have used a dyadic notation. Here, $\boldsymbol{\phi}^{R/L}$ and $\boldsymbol{\zeta}^{R/L}$ define the right/left eigenvectors of the matrix $\mathbf{M}$. These vectors are biorthonormall, that is, $\boldsymbol{\phi}^L\cdot\boldsymbol{\phi}^R = \boldsymbol{\zeta}^L\cdot\boldsymbol{\zeta}^R = 1$ while $\boldsymbol{\phi}^L\cdot\boldsymbol{\zeta}^R = \boldsymbol{\zeta}^L\cdot\boldsymbol{\phi}^R = 0$. Furthermore, m and M represent the two eigenvalues of the matrix $\mathbf{M}$: the eigenvalue m vanishes at the critical point defining the soft mode, while M remains finite (at the order of J) and defines the gapped mode. The notation for the soft and gapped modes mirror our conventions for the effective field theory. In fact, the above diagonalization is a similar decomposition to that of the previous section but in a different basis (notice that $\mathbf{M}$ is "rotated" with respect to $\mathbf{D}^R$). While we do not need the explicit form of the eigenvalues and the (right and left) eigenvectors, here we provide them for completeness:

$$\begin{aligned}
\boldsymbol{\phi}^R &= \left(-\sqrt{\frac{\Delta}{2J-\Delta}}\,,1\right), \quad \boldsymbol{\phi}^L = \frac{1}{2}\left(-\sqrt{\frac{2J-\Delta}{\Delta}}\,,1\right), \quad m = \Gamma - 4\sqrt{(2J-\Delta)\Delta}\,,\\
\boldsymbol{\zeta}^R &= \left(\sqrt{\frac{\Delta}{2J-\Delta}}\,,1\right), \quad \boldsymbol{\zeta}^L = \frac{1}{2}\left(\sqrt{\frac{2J-\Delta}{\Delta}}\,,1\right), \quad M = \Gamma + 4\sqrt{(2J-\Delta)\Delta}\,.
\end{aligned} \tag{6.51}$$

Now, the coarse-grained dynamics at sufficiently long times is governed solely by the soft mode, while the gapped field quickly decays to zero ($\boldsymbol{\zeta}^L\cdot\mathbf{x} = 0$). Therefore, the slow dynamics is given by

$$\frac{\mathrm{d}}{\mathrm{d}t}\mathbf{x} = -\overline{\mathbf{M}}\cdot\mathbf{x}\,, \tag{6.52}$$

where we have defined $\overline{\mathbf{M}} = m\boldsymbol{\phi}^R\boldsymbol{\phi}^L$ keeping only the critical component. We are finally in a position to study the relation between L_{xy} and L_{yx} explicitly defined by

$$\begin{aligned}
L_{xy} &= \overline{M}_{xx}\langle xy\rangle + \overline{M}_{xy}\langle yy\rangle\,,\\
L_{yx} &= \overline{M}_{yx}\langle xx\rangle + \overline{M}_{yy}\langle yx\rangle\,.
\end{aligned} \tag{6.53}$$

Now notice that the fluctuations $\langle x_i x_j\rangle \sim \boldsymbol{\phi}^R_i\boldsymbol{\phi}^R_j\langle\phi^2\rangle$ where $\langle\phi^2\rangle$ represents the critical fluctuations (to be identified with $\langle\phi_c^2\rangle$ in the previous section); this simply means that the dominant contribution

to fluctuations is given by the overlap of dynamical variables with the critical field. Additionally, using the biorthogonality $\boldsymbol{\zeta}^L \cdot \boldsymbol{\phi}^R = 0$, we have $\left(\zeta_1^L, \zeta_2^L\right) \propto \left(-\phi_2^R, \phi_1^R\right)$. We can then write

$$L_{xy} - L_{yx} \propto \boldsymbol{\zeta}^L \cdot \overline{\mathbf{M}} \cdot \boldsymbol{\phi}^R = 0\,, \tag{6.54}$$

where the last equality follows from $\boldsymbol{\zeta}^L \cdot \overline{\mathbf{M}} \propto \boldsymbol{\zeta}^L \cdot \boldsymbol{\phi}^R = 0$.[4] We thus arrive at the relation $L_{yx} \simeq L_{xy}$ in harmony with our modified version of the Onsager reciprocity relation. This should be contrasted with the reciprocity relation in equilibrium: $L_{xy} = -L_{yx}$ with x (y) even (odd) under time-reversal transformation.

6.6 Driven-Dissipative Coupled Bosons

In this section, we go beyond the infinite-range model discussed so far and consider a quadratic model of driven-dissipative bosons. The model being quadratic can be solved exactly using any number of techniques. For a coherent presentation, we will adopt a simple (Keldysh) field-theoretical analysis. Our main point is however that the conclusions of this in this chapter apply to a wider range of models. To be specific, consider a bosonic model on a cubic lattice in d dimensions with the Hamiltonian

$$H = -\frac{J}{2d} \sum_{\langle \mathbf{ij} \rangle} (a_{\mathbf{i}} + a_{\mathbf{i}}^\dagger)(a_{\mathbf{j}} + a_{\mathbf{j}}^\dagger) + 2\Delta \sum_{\mathbf{i}} a_{\mathbf{i}}^\dagger a_{\mathbf{i}}\,, \tag{6.55}$$

and subject to the dissipation

$$L_{\mathbf{i}} = \sqrt{\Gamma}\, a_{\mathbf{i}}\,. \tag{6.56}$$

The coefficients in the Hamiltonian are chosen for later convenience. Notice that the Hamiltonian is time-reversal symmetric. This follows from either writing the operator a in terms of two quadratures that are even and odd under time-reversal (see below), or directly by noting that $TaT^{-1} = a$ and similarly for $a^\dagger$ (site index suppressed) although T is antiunitary ($TiT^{-1} = -i$) [99]. The above bosonic Hamiltonian is therefore real and time-reversal symmetric. In addition, the Liouvillian governing the dynamics is $\mathbb{Z}_2$ symmetric under the transformation $a \to -a$, similar

[4] While one might be tempted to conclude that $\overline{\mathbf{M}} \propto m \to 0$ at the critical point, the product $m\langle\phi^2\rangle$ remains finite due to the diverging fluctuations and thus L_{xy} assumes a nonzero value at the critical point.

to the driven-dissipative Ising model considered in Eq. (3.5). This symmetry is broken at the phase transition where $\langle a \rangle$ becomes nonzero in the ordered phase. As discussed in Sec. **??**, the $\mathbb{Z}_2$ symmetry provides a minimal setting where the time-reversal symmetry breaking or emergence can be investigated near criticality.

The Keldysh action for this model can be constructed in a straightforward fashion using a coherent-state representation mapping operators to c-valued fields as $a_{\mathbf{i}} \to a_{\mathbf{i}}(t)$ and $a_{\mathbf{i}}^\dagger \to a_{\mathbf{i}}^*(t)$. A path integral formalism can be straightforwardly constructed in terms of these bosonic fields on a closed contour using the techniques developed in Sec. 2.3. The mapping to the path integral produces the Keldysh action [89]

$$S_K = S_H + S_D \,, \tag{6.57}$$

where $S_{H,D}$ represent the coherent and dissipative terms, respectively. The coherent term in the action is given by

$$S_H = \sum_{\sigma=+,-} \sigma \int_t \Big[\sum_{\mathbf{i}} a_{\mathbf{i}\sigma}^* i\partial_t a_{\mathbf{i}\sigma} - H[a_{\mathbf{i}\sigma}, a_{\mathbf{i}\sigma}^*] \Big] \,, \tag{6.58}$$

with $\sigma = \pm$ representing the forward (upper) and backward (lower) branches of the contour. We use the plus and minus signs here for the Keldysh contour branches for notational compactness. The last term represents the (normal-ordered) Hamiltonian in the coherent-state representation. The relative sign of the forward and backward branches has its origin in the commutator $[H, \rho]$. The dissipative term in the action takes the form

$$S_D = -i\Gamma \sum_{\mathbf{i}} \int_t \Big[a_{\mathbf{i}+} a_{\mathbf{i}-}^* - \frac{1}{2} \left(a_{\mathbf{i}+}^* a_{\mathbf{i}+} + a_{\mathbf{i}-}^* a_{\mathbf{i}-} \right) \Big] \,. \tag{6.59}$$

Upon a Keldysh rotation $a_{cl/q} \equiv (a_+ \pm a_-)/\sqrt{2}$ (site index $\mathbf{i}$ being implicit), the Keldysh action is then written in terms of classical and quantum fields. Here, it is more convenient to cast the bosonic field in terms of its real and imaginary parts (the two quadratures) as $a_{\mathbf{i}}(t) = (\Phi_{\mathbf{i}}(t) - i\Pi_{\mathbf{i}}(t))/2$ where the factor of $1/2$ is chosen for later convenience. The corresponding operators can be viewed as position and the conjugate momentum. These Hermitian operators obey the same symmetry relations as S_x and S_y in the DDIM, where Φ is even under TRS while Π is odd. The anti-unitary

nature of the time-reversal transformation makes the bosonic fields real and invariant under TRS. The Lagrangian L_K defined via the Keldysh action $S_K = \int dt L_K$ then takes the form [89]

$$L_K = \sum_{\mathbf{i}} \frac{1}{2}\Phi_{\mathbf{i}q}\partial_t\Pi_{\mathbf{i}c} - \frac{1}{2}\Pi_{\mathbf{i}q}\partial_t\Phi_{\mathbf{i}c} - \Delta(\Phi_{\mathbf{i}c}\Phi_{\mathbf{i}q} + \Pi_{\mathbf{i}c}\Pi_{\mathbf{i}q}) + \frac{\Gamma}{4}(\Phi_{\mathbf{i}q}\Pi_{\mathbf{i}c} - \Phi_{\mathbf{i}c}\Pi_{\mathbf{i}q} + i\Phi_{\mathbf{i}q}^2 + i\Pi_{\mathbf{i}q}^2) + \sum_{\langle \mathbf{ij}\rangle} \frac{J}{2d}(\Phi_{\mathbf{i}c}\Phi_{\mathbf{j}q} + \Phi_{\mathbf{i}q}\Phi_{\mathbf{j}c}), \tag{6.60}$$

in terms of classical and quantum fields $\Phi_{\mathbf{i}c/q}$ and $\Pi_{\mathbf{i}c/q}$. In momentum space, the Keldysh action takes almost an identical form to Eq. (6.35) with the substitution $v \to (\Phi_c, \Pi_c, \Phi_q, \Pi_q)$ where the frequency and momentum $(\omega, \mathbf{k})$ are implicit and $J \to J_{\mathbf{k}} = \frac{J}{d}(\cos k_1 + \cdots + \cos k_d)$. This implies that this model too exhibits a phase transition at the same set of parameters. While a nonlinear term is needed to regulate things on the ordered side, we shall only consider the critical behavior.

6.6.1 Green's functions

Since Eq. (6.60) is identical to Eq. (6.35) upon the above substitutions, we can immediately write the correlation and response functions of Φ and Π. They are simply given by Eq. (6.17) once J is substituted by $J_{\mathbf{k}}$. Using the definitions of the bosonic variables in terms of the real fields, we can easily determine the form of the bosonic Green's functions:

$$\mathbf{G}^K = \begin{pmatrix} G^K_{aa^\dagger} & G^K_{aa} \\ G^K_{a^\dagger a^\dagger} & G^K_{a^\dagger a} \end{pmatrix}, \quad \mathbf{G}^R = \begin{pmatrix} G^R_{aa^\dagger} & G^R_{aa} \\ G^R_{a^\dagger a^\dagger} & G^R_{a^\dagger a} \end{pmatrix}, \tag{6.61}$$

where

$$G^K_{aa^\dagger}(\omega,\mathbf{k}) = \left[G^K_{a^\dagger a}(-\omega,\mathbf{k})\right] = \frac{-i\Gamma\left(3\Gamma^2+4(32J_{\mathbf{k}}^2+12\Delta^2+8\Delta\omega+3\omega^2-8J_{\mathbf{k}}(4\Delta+\omega))\right)}{8(\omega-\omega_1)(\omega-\omega_2)(\omega-\omega_1^*)(\omega-\omega_2^*)}\,, \tag{6.62a}$$

$$G^K_{aa}(\omega,\mathbf{k}) = -\left[G^K_{a^\dagger a^\dagger}(\omega,\mathbf{k})\right]^* = \frac{i\Gamma\left(128J_{\mathbf{k}}^2+\Gamma^2-16iJ_{\mathbf{k}}(\Gamma-8i\Delta)+4(4\Delta^2+\omega^2)\right)}{8(\omega-\omega_1)(\omega-\omega_2)(\omega-\omega_1^*)(\omega-\omega_2^*)}\,, \tag{6.62b}$$

$$G^R_{aa^\dagger}(\omega,\mathbf{k}) = \left[G^R_{a^\dagger a}(-\omega,\mathbf{k})\right]^* = \frac{-4J_{\mathbf{k}}+4\Delta+2\omega+i\Gamma}{2(\omega-\omega_1)(\omega-\omega_2)}\,, \tag{6.62c}$$

$$G^R_{aa}(\omega,\mathbf{k}) = \left[G^R_{a^\dagger a^\dagger}(\omega,\mathbf{k})\right]^* = \frac{-2(J_{\mathbf{k}}-\Delta)}{(\omega-\omega_1)(\omega-\omega_2)}\,, \tag{6.62d}$$

and $\mathbf{G}^R(\omega,\mathbf{k}) = [\mathbf{G}^A(\omega,\mathbf{k})]^\dagger$, $\mathbf{G}^K(\omega,\mathbf{k}) = -[\mathbf{G}^K(\omega,\mathbf{k})]^\dagger$. In a slight abuse of notation, we have defined the modes $\omega_{1/2} = -i(\Gamma \mp \Gamma_c(J_{\mathbf{k}}))/2$ (introduced earlier in Section 5.1) and defined the function $\Gamma_c(J) \equiv 4\sqrt{\Delta(2J-\Delta)}$.

For comparison with the FDR in the time-domain, we quote the long-wavelength ($\mathbf{k} \to 0$) limit of the correlation and response functions at criticality:

$$G^K_{aa^\dagger}(t,\mathbf{k}) = G^K_{a^\dagger a}(-t,\mathbf{k}) \sim \frac{-i4dJ}{\Delta\mathbf{k}^2}e^{-A\mathbf{k}^2|t|}\,, \tag{6.63a}$$

$$G^K_{aa}(t,\mathbf{k}) = -\left[G^K_{a^\dagger a^\dagger}(t,\mathbf{k})\right]^* \sim \frac{4d}{\mathbf{k}^2}\left[\frac{-i(J+\Delta)}{\Delta}+\frac{4(2J-\Delta)}{\Gamma_c}\right]e^{-A\mathbf{k}^2|t|}\,, \tag{6.63b}$$

$$G^R_{aa^\dagger}(t,\mathbf{k}) = \left[G^R_{a^\dagger a}(t,\mathbf{k})\right]^* \sim \Theta(t)\left(\frac{8(J-\Delta)}{\Gamma_c}-2i\right)e^{-A\mathbf{k}^2t}\,, \tag{6.63c}$$

$$G^R_{aa}(t,\mathbf{k}) = \left[G^R_{a^\dagger a^\dagger}(t,\mathbf{k})\right]^* \sim \Theta(t)\frac{-8J}{\Gamma_c}e^{-A\mathbf{k}^2t}\,, \tag{6.63d}$$

where we have defined $A = -J\Gamma_c/4d(2J-\Delta)$ and $\Gamma_c = \Gamma_c(J)$. The expressions above are obtained by first setting $\Gamma = \Gamma_c$ and then taking the limit $\mathbf{k} \to 0$ while keeping $\mathbf{k}^2 t = \text{const}$. These expressions are valid all along the phase boundary except at the weakly-dissipative critical point since we have assumed $\mathbf{k}^2 \ll 2J-\Delta$ in our derivation.

6.6.2 FDR* for non-Hermitian operators

The Green's functions of Φ and Π of the short-range model considered here are identical to those of the DDIM once we substitute $J \to J_{\mathbf{k}}$. Therefore, the low-frequency effective temperatures of

this model in the long-wavelength limit $\mathbf{k} \to 0$ are *identical* to those of the DDIM in Eq. (6.27). In other words, at criticality and at long wavelengths and frequencies this short-ranged model obeys the FDR*. The latter can be extended to the bosonic operators $a_{\mathbf{k}}$ and $a_{\mathbf{k}}^\dagger$ too. Taking the linear combination of the FDR* for the two quadratures, we find

$$\chi_{a_{\mathbf{k}}^\dagger a_{\mathbf{k}}} \simeq \frac{1}{2T_{\text{eff}}}\Theta(t)\partial_t C_{a_{-\mathbf{k}}^\dagger a_{\mathbf{k}}^\dagger}, \qquad \chi_{a_{\mathbf{k}} a_{-\mathbf{k}}} \simeq \frac{1}{2T_{\text{eff}}}\Theta(t)\partial_t C_{a_{\mathbf{k}} a_{\mathbf{k}}^\dagger}. \tag{6.64}$$

These relations can be explicitly verified by plugging in Eq. (6.63) with the effective temperature identified as $T_{\text{eff}} = J$. Interestingly, the set of operators on the two sides of these FDR-like equations are different, namely the first operator (appearing at the earlier time) transforms into its adjoint between the two sides of these equations.

The above equation suggests a more general form of the FDR* also applicable to non-Hermitian operators,

$$\chi_{O_i O_j^T}(t) \simeq \frac{1}{2T_{\text{eff}}}\Theta(t)\partial_t C_{O_i O_j}, \tag{6.65}$$

where the O_i's are not necessarily Hermitian. The transpose T arises due to the combined action of taking the adjoint as well as conjugation due to the time-reversal transformation. This equation reduces to the FDR* for Hermitian operator in Eq. (6.5), while reproducing Eq. (6.64) for non-Hermitian (but real) bosonic operators.

6.6.3 Weakly-dissipative limit

Finally, we investigate the bosonic Green's functions at the weakly-dissipative point; this parallels our discussion of the weakly-dissipative DDIM in Section 6.4.3. Again we must be careful in taking the order of limits. We shall first Fourier transform Eq. (6.62) to the time domain, send $\Delta \to 2J$, and then take the long-wavelength limit $\mathbf{k} \to 0$ in which case we have $J_{\mathbf{k}} \sim J(1 - \mathbf{k}^2/2d)$ and $\Gamma_c(J_{\mathbf{k}}) \sim i4\sqrt{2}J|\mathbf{k}|/d$. Finally, we take the weakly-dissipative limit $\Gamma \to 0$ and report only the

critical contribution at long wavelengths:

$$G^K_{\alpha\beta}(t,\mathbf{k}) \sim -i\frac{2d^2}{\mathbf{k}^2}\cos\left(\frac{2\sqrt{2}J}{d}|\mathbf{k}|t\right), \tag{6.66a}$$

$$G^R_{\alpha\beta}(t,\mathbf{k}) \sim -\Theta(t)\frac{2\sqrt{2}d}{|\mathbf{k}|}\sin\left(\frac{2\sqrt{2}J}{d}|\mathbf{k}|t\right), \tag{6.66b}$$

for $\alpha,\beta \in \{a, a^\dagger\}$. Note that the dynamical exponent (z) is now different as the scaling variable is $|\mathbf{k}|t$ compared to $\mathbf{k}^2 t$ in Eq. (6.63), i.e., we find ballistic ($z = 1$) rather than diffusive dynamics ($z = 2$). Fluctuations diverge in the same fashion, $G^K_{\alpha\beta} \sim 1/\mathbf{k}^2$, regardless of the dissipation, while the dynamical behavior undergoes a crossover; for a similar behavior of the DDIM, see Ref. [94]. As we kept $\mathbf{k}$ finite while taking $\Gamma \to 0$, the system remains gapped. Therefore, the density matrix commutes with the Hamiltonian, in parallel with our discussion in Section 6.4.3. The TRS is then restored and the correlation and response functions satisfy the equilibrium FDR as one can directly see from Eq. (6.66). If we instead take $\mathbf{k} \to 0$ before sending $\Gamma \to 0$, we find that the cross-correlation $G^K_{\Phi\Pi}(t = 0, \mathbf{k} = 0) \sim 1/\Gamma$ diverges even at the weakly-dissipative critical point, while this quantity remains zero in equilibrium as it is odd under the time-reversal transformation.

CHAPTER 7

INFORMATION AND ENTANGLEMENT

Quantum entanglement is a defining signature of quantum mechanics, characterized by a nontrivial superposition of multi-particle states, and has been a subject of intense research for the past decades [100]. Additionally, it has been shown to be useful as a resource for quantum computation [101–103] and metrology [104, 105]. However, quantum entanglement is delicate as it will be spoiled by any interaction with the environment, i.e. dissipation. The common solution is to further isolate the system and to cool it down to lower temperatures in the hope of minimizing dissipation and thermal fluctuations. An alternative avenue is, turning a foe to a friend, to use dissipation to our advantage in order to create states that have rich entanglement behavior [106–110]. We follow the second path and apply this framework to the DDIM.

In this chapter, we investigate the entanglement features of the DDIM using analytical and numerical techniques. Despite the presence of spontaneous emission, we show that the nonequilibrium steady state of this model hosts interesting entanglement features, especially near the $\mathbb{Z}_2$ symmetry breaking Ising phase transition. Specifically, we calculate three separate quantities relevant to quantum information, namely the logarithmic negativity $E_{\mathcal{N}}$, and the quantum Fisher information F, and the spin squeezing parameter ξ. The logarithmic negativity is an entanglement monotone [111] that is easily computable for many-body mixed states, and the quantum Fisher information, a quantity typically used in metrology to quantify a bound on measurement precision, can also characterize entanglement in a many-body spin state [112–116]. The spin squeezing parameter ξ measures how squeezed the state is with respect to the spin operators and is connected to the concurrence [117–119], meaning it is also an entanglement witness. We also calculate the von Neumann entropy and mutual information, which capture both classical and quantum correlations in a mixed state and provide a useful point of comparison for true entanglement measuring quantities.

To obtain exact expressions of the entanglement measures, we utilize covariance matrix tech-

niques [110, 120–125] to take advantage of the Gaussian nature of fluctuations in the nonequilibrium steady state. These methods allow us access to the aforementioned quantities in the thermodynamic limit. We find that the von Neumann entropy is finite in the normal phase except at the phase boundary where it diverges logarithmically with the system size. It then transitions to volume law behaviour in the ordered phase. This transition to volume law is distinct from the area-to-volume law transition in measurement-induced phase transitions [126, 127], and is due to the infinite-range interactions in the system. The logarithmic negativity is finite everywhere in the phase diagram and peaks at the phase boundary where it takes the value $E_{\mathcal{N}} = 1/2$. For the quantum Fisher information densities $f_\alpha = F(S_\alpha)/N$ of the collective spin operators S_α, with $\alpha \in \{x, y, z\}$ and $F(S_\alpha)$ the corresponding quantum Fisher information, we find that they are all bounded from above by $f_\alpha \leq 2$ everywhere in the normal phase. This bound is uniquely saturated at the critical point, where the direction of the spin operator that yields the optimal density f_{opt} is dictated by the direction of the gapless mode that characterizes the critical properties of the phase transition [128]. In addition, a density greater than unity indicates that the state is at least 2-particle entangled. The mode orthogonal to the gapless mode, i.e. the gapped mode, corresponds to the direction that is most squeezed, and this mode achieves a squeezing value of exactly $\xi = 1/2$ at the phase boundary, with ξ the squeezing parameter. In line with the other entanglement quantities, the squeezing parameter reaches its minimum at the phase boundary.

7.1 Covariance Matrix Method

The DDIM cannot be solely characterized by the mean-field solution in Eq. (3.7), as there are quantum and statistical fluctuations on top of the expectation values of observables that are neglected by a mean-field analysis. However, we can completely characterize fluctuations via two-point correlations. We have shown in Ch. 3 that the Liouvillian in Eq. (3.5) may be mapped exactly to a classical action, consisting of a pair of real Hubbard-Stratonovich fields m_c, m_q [94], whose exact form is given by Eq. (3.16). This action may be expanded in powers of the fields, and is shown to be exactly quadratic with higher order corrections of $O(1/N)$; see Eq. (3.30).

Furthermore, the fields m_c and m_q are directly related to fluctuations of S_x, as discussed in Sec. 3.3.1. Fluctuations of the operators S_y and S_z can be determined by introducing source fields to the path integral, and this too can be shown to be quadratic in the thermodynamic limit, see Appendix 7.A. We can therefore take the DDIM to be exactly quadratic in the thermodynamic limit. This result directly implies that the steady state of the model is a Gaussian state, as it is completely characterized by two-point correlation functions.

A Gaussian state can be fully parameterized by a displacement vector $\mathbf{d}$ plus a covariance matrix σ,

$$d_i = \mathrm{Tr}(\rho r_i)\,, \tag{7.1}$$

$$\sigma_{ij} = \mathrm{Tr}(\rho\{\Delta r_i, \Delta r_j\})\,, \tag{7.2}$$

where ρ is the steady state density matrix, $\mathbf{r} = (x_1, x_2, ..., p_1, p_2, ...)^T$ is the vector of position and momentum operators, and $\Delta\mathbf{r} = \mathbf{r} - \mathbf{d}$. The curly brackets denote the anti-commutator. We will calculate each entanglement measure using the covariance matrix and its symplectic eigenvalues [120–125]. The symplectic eigenvalues are defined as the eigenvalues of $i\Omega\sigma$, where

$$\Omega = \begin{pmatrix} 0 & I \\ -I & 0 \end{pmatrix}, \tag{7.3}$$

with I the identity matrix, encodes the canonical commutation relations of the position and momenta operators

$$[r_i, r_j] = i\Omega_{ij}\,. \tag{7.4}$$

The eigenvalues always come in pairs $\pm\nu_i$ and are bounded from below by 1. In the following subsections, we discuss how the covariance matrix formalism applies to the driven-dissipative Ising model in the normal and ordered phases.

7.1.1 Normal Phase

A key observation is that in the normal phase, the total spin is polarized in the negative z-direction with negligible fluctuations. This means that we can readily make the approximation $[S_x, S_y] =$

$2iS_z \rightarrow [S_x, S_y] = -2iN$, and then rescale the spin operators, $x = S_x/\sqrt{2N}, p = -S_y/\sqrt{2N}$, such that we retrieve the canonical commutation relations $[x, p] = i$. This identification gives a single pair of position and conjugate momentum operators, meaning we simply have a single mode covariance matrix with $\mathbf{r} = (x, p)$.

The correlation functions for the steady state of Eq. (**??**) in the normal phase have been computed in a previous work [128]. They were derived using an exact mapping to a Keldysh path integral. However, we omit the technical details as they are outside the scope of this paper; we only require the correlation functions here. The exact analytical expressions for the correlation functions of x and p are

$$\sigma_{11} = 1 + \frac{16J\Delta}{\Gamma^2 - \Gamma_c^2}, \tag{7.5}$$

$$\sigma_{12} = \sigma_{21} = \frac{4J\Gamma}{\Gamma^2 - \Gamma_c^2}, \tag{7.6}$$

$$\sigma_{22} = 1 + \frac{16J(2J - \Delta)}{\Gamma^2 - \Gamma_c^2}. \tag{7.7}$$

Desired quantities can be calculated using the covariance matrix representation of the density matrix. On the other hand, the logarithmic negativity and mutual information require that that we split the system in two and have correlation functions between the two halves. In this case, our covariance matrix, now denoted as σ^{AB} for two subsystems A and B, becomes a 4×4 matrix as

$$\sigma^{AB} = \begin{pmatrix} X & K \\ K & P \end{pmatrix}, \tag{7.8}$$

with the block matrices

$$X = I + \frac{8J\Delta}{\Gamma^2 - \Gamma_c^2} \begin{pmatrix} 1 & 1 \\ 1 & 1 \end{pmatrix}, \tag{7.9}$$

$$P = I + \frac{8J(2J - \Delta)}{\Gamma^2 - \Gamma_c^2} \begin{pmatrix} 1 & 1 \\ 1 & 1 \end{pmatrix}, \tag{7.10}$$

$$K = \frac{2J\Gamma}{\Gamma^2 - \Gamma_c^2} \begin{pmatrix} 1 & 1 \\ 1 & 1 \end{pmatrix}. \tag{7.11}$$

For a derivation of these quantities, see Appendix A. We emphasize that these exact expressions are only valid in the normal phase.

7.1.2 Ordered Phase

The covariance matrix techniques discussed in the previous subsection apply only to systems that can be described by bosonic modes. In the normal phase, the DDIM satisfies this condition as the total spin is fully polarized in the z-direction, and excitations of the spin can be seen as excitations of a bosonic mode (akin to a Holstein-Primakoff transformation) [14, 28]. However, this picture no longer applies in the ordered phase. While we can always rotate our spin variables such that the spin is pointing along the z-direction, there is a technical problem: generically, there will be non-negligible fluctuations along all spin directions, implying that the Holstein-Primakoff picture is no longer valid. In contrast, in the normal phase $\langle S_z^2 \rangle / N \sim 0$, allowing us to make the replacement $S_z \sim -N$ in the commutation relation that defines the quadratures of the bosonic mode. In light of this discussion, we utilize quantum trajectory simulations, introduced in Sec. 4.2, to numerically calculate the desired entanglement measures in the ordered phase.

7.2 Entropy and Information Measures

The von Neumann entropy,

$$S_{\mathrm{vN}}(\rho) = -\mathrm{Tr}(\rho \log \rho)\,, \tag{7.12}$$

the quantum equivalent of the Shannon entropy, is a useful measure of correlations in a quantum system. However, it is not generally a good indicator of "quantum correlation", i.e. entanglement, in the system. It can predict nontrivial behaviour, especially at criticality, and is useful for comparison with other quantities. In this section, we analytically calculate the von Neumann entropy S_{vN} both in the normal and ordered phases, and use exact numerical solutions to supplement our findings at the critical point as well as the ordered phase. We then supplement these results by calculating the mutual information.

The von Neumann entropy in the normal phase can be calculated purely in terms of the symplectic eigenvalues of the covariance matrix, as the mean-field contribution to the entropy is zero because the mean-field state is pure in the normal phase. In general, it has been previously

shown that S_{vN} for a Gaussian state can be expressed as [122]

$$S_{\text{vN}}(\rho) = \frac{\nu+1}{2}\log\left(\frac{\nu+1}{2}\right) - \frac{\nu-1}{2}\log\left(\frac{\nu-1}{2}\right), \tag{7.13}$$

where ν is the symplectic eigenvalue of σ. Equipped with the covariance matrix, given by Eq. (7.5), we find

$$\nu = \sqrt{1 + \frac{16J^2}{\Gamma^2 - \Gamma_c^2}}\,. \tag{7.14}$$

This eigenvalue satisfies $\nu \geq 1$ in the normal phase $\Gamma > \Gamma_c$. In addition, setting $J = 0$ we find $\nu = 1$, which means the state is pure [122]. Indeed, if there is no interaction then the steady state is a pure state with all spins pointing down. Plugging this into Eq. (7.13), we find the von Neumann entropy everywhere in the normal phase. From the form of the symplectic eigenvalue, we can see that the von Neumann entropy diverges at $\Gamma = \Gamma_c$, signifying the onset of criticality. This is expected as fluctuations also diverge at the critical point [98]. This phase transition was shown to be in the same university class as the finite-temperature transverse-field Ising model [98], where the transtion is dominated by classical thermal fluctuations. Thus, we expect S_{vN} to diverge as it captures classical correlations as well. In addition, near the critical point, the von Neumann entropy diverges as $S_{\text{vN}} \sim -\frac{1}{2}\log\gamma$, where $\gamma = \Gamma - \Gamma_c$. Taking advantage of the finite-size scaling analysis previously performed in [94, 98], we have the scaling behavior $\gamma \sim 1/\sqrt{N}$ at the critical point, which tells us that

$$S_{\text{vN}} \sim \frac{1}{4}\log N\,. \tag{7.15}$$

The coefficient of the logarithm is $1/4$, distinct from the zero-temperature equilibrium value of $1/6$ [129] and the volume law at finite-temperature. The mutual information, however, is the same ($\sim \frac{1}{4}\log N$) as that of the Ising model at finite temperature [130]. This simply follows from the split-system covariance matrix in Eq. (7.8).

To complement the von Neumann entropy, we can also calculate the purity of the state $\mu = \text{Tr}(\rho^2)$. In terms of the covariance matrix, the purity is given by

$$\mu = \frac{1}{\sqrt{\text{Det}\,\sigma}}\,. \tag{7.16}$$

Conveniently, the symplectic eigenvalue of a single-mode covariance matrix is directly related to the determinant of the matrix, $\mathrm{Det}\,\sigma = \nu^2$, meaning that

$$\mu = \frac{1}{\nu}\,. \tag{7.17}$$

From this expression, it is clear that the purity contribution from the part of the density matrix describing Gaussian fluctuations is zero at the critical point where the classical fluctuations diverge. However, the mean-field part of the density matrix remains pure.

We cannot perform the same procedure in the ordered phase, as discussed in Sec. 7.1.2. However, a simple analysis shows that the entropy is dominated by the mean-field contribution which is $O(N)$, i.e. volume law. This is easily seen through

$$S_{\mathrm{vN}}(\rho_{\mathrm{MF}}^{\otimes N}) = N\, S_{\mathrm{vN}}(\rho_{\mathrm{MF}})\,, \tag{7.18}$$

which is proportional to N. While the entropy does transition from "area law" ($S_{vN} \sim O(1)$) in the normal phase to volume law in the ordered phase, this is distinct from the entanglement phase transitions studied recently which identify this transition at the level of individual quantum trajectories as opposed to the density matrix [126, 127, 131, 132]. We believe that, the volume law observed here is due to the infinite-range interactions. Furthermore, the steady state becomes increasingly mixed in the ordered phase. The mean-field prediction of the purity is $\mu(\rho_{\mathrm{MF}}) = \frac{1}{2}(1 + s^2) < 1$, with $s = S/N = \sqrt{\langle S_x\rangle^2 + \langle S_y\rangle^2 + \langle S_z\rangle^2}/N$. Inserting the steady state solutions of the mean-field equations from Eq. (3.7), we find

$$\mu(\rho_{\mathrm{MF}}) = \frac{2\Gamma^2(\Gamma_c^2 - \Gamma^2) + 16\Delta^2\Gamma_c^2 + 512J\Delta^2(2J + \Delta)}{2048J^2\Delta^2}\,. \tag{7.19}$$

In the ordered phase, $\mu(\rho_{\mathrm{MF}}) < 1$ such that the mean-field solution predicts a mixed steady state. The purity reaches its minimum, $\mu = 1/2$, when $\Gamma, \Delta \to 0$.

Another interesting quantity is the mutual information [126, 130, 133],

$$I_{AB} = S_{\mathrm{vN},A} + S_{\mathrm{vN},B} - S_{\mathrm{vN},AB} \tag{7.20}$$

which captures the total correlations between two subsystems A and B. This quantity has been used as a signal for phase transitions at finite temperature [126, 130, 133]. We can calculate it

analytically in the normal phase by using Eq. (7.8), in combination with Eq. (7.13). To obtain the subsystem entropy, we construct the subsystem covariance matrices from Eq. (7.8),

$$\sigma^A = \sigma^B = \begin{pmatrix} X_{11} & K_{11} \\ K_{11} & P_{11} \end{pmatrix}, \tag{7.21}$$

where the matrix elements are given by Eq. (7.9). The two matrices are equal due to the permutation symmetry of the model, and the fact that we have split the system in half.

We can now determine the symplectic eigenvalues of these covariance matrices,

$$\nu^A = \nu^B = \sqrt{1 + \frac{12J^2}{\Gamma^2 - \Gamma_c^2}}\,. \tag{7.22}$$

These eigenvalues, as expected, are rather similar to the symplectic eigenvalue of the total system covariance matrix ν given by Eq. (7.14). Plugging these eigenvalues into Eqs. (7.13) and (7.20), we find the mutual information for the driven-dissipative Ising model in the normal phase. Similar to the von Neumann entropy, the mutual information diverges logarithmically at the phase boundary as $I_{AB} \sim \frac{1}{2}\log\gamma$. Therefore, it also grows logarithmically with the system size,

$$I_{AB} \sim \frac{1}{4}\log N\,, \tag{7.23}$$

with the same coefficient as the von Neumann entropy.

In Fig. 7.2.1, we see that the mutual information does not grow with the system size in the normal phase, where $\Gamma > \Gamma_c = 4$. As predicted in Eq. (7.23), it grows logarithmically at the phase boundary (see the inset). The discrepancy in the numerically predicted coefficient $\sim 0.36\log N$ from the theoretically predicted value of $\frac{1}{4}\log N$ is due to finite-size effects, as well as the total evolution time growing as $\sqrt{N}$ at the critical point [94]. Specifically, it is difficult to numerically access the late times necessary to guarantee we are in the steady state, in addition to the fact that the memory cost of storing the density matrix over longer time-scales and larger system sizes grows to be prohibitive. Taking these details into account, we performed these simulations with a time step of $\delta t = .001$ over 2000 trajectories, and we averaged over the last 100 time steps, skipping every 5, of the mutual information dynamics. At the critical point, the total evolution time was $t_f = 10\Gamma^{-1}\sqrt{N}$ to account for the finite-size scaling of the critical dynamics.

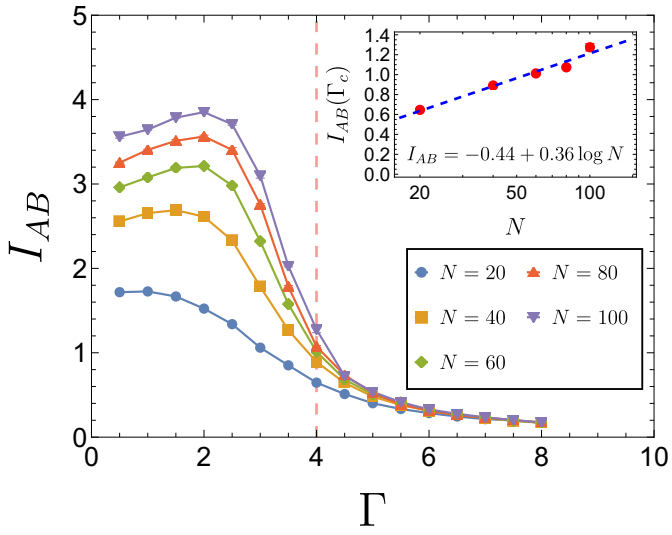

Figure 7.2.1 The mutual information as a function of Γ for various system sizes, with $J = 1, \Delta = 1$. At the critical point, I_{AB} gorws logarithmically with the system size as shown in the inset. In the ordered phase, the mutual information surprisingly further grows with system size. This could be due to the permutation symmetry of the model; see the text for further explanation.

In the ordered phase we rely on numerics to calculate the mutual information, where now the total evolution time is $t_f = 10\Gamma^{-1} \log N$. Figure 7.2.1 indicates that the mutual information grows with the system size inside the ordered phase where $\Gamma < \Gamma_c = 4$. This is at odds with the conventional wisdom that the mutual information peaks at the critical point. We speculate that this follows from the contribution of different total angular momentum sectors. In general, an Ising phase transition would contribute an additional constant of log 2 to the mutual information at any finite system size. However, the permutation of the symmetry of the model leads to a mixture of different total angular momentum sectors in the density matrix [41, 42], and each sector may contribute to the ordering, hence the nontrivial behavior of the mutual information.

7.3 Entanglement Measures

In this section, we investigate three prominent measures of quantum entanglement: logarithmic negativity, quantum Fisher information, and spin squeezing. Each of these quantities characterizes a particular aspect of the entanglement features of the system. Using numerical simulation, and theoretical techniques established in [98, 128] and supplemented in Appendices A and B, we

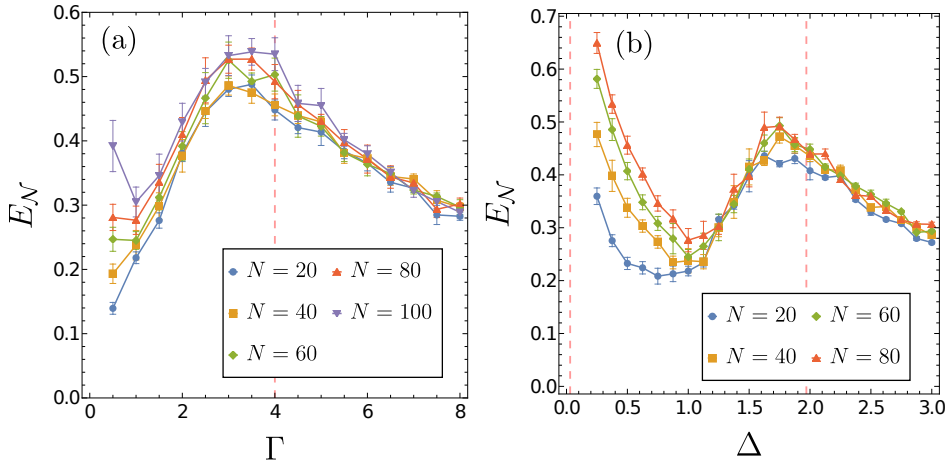

Figure 7.3.1 (a) Logarithmic negativity as a function of Γ with $J = 1, \Delta = 1$. We see that $E_{\mathcal{N}}$ peaks near the phase boundary at $\Gamma_c = 4$, close to the predicted value of $E_{\mathcal{N}} = 1/2$. The logarithmic negativity appears to increase with system size at small Γ, as quantum trajectories require long evolution times ($\sim 1/\Gamma$) that are not accessible in this regime. (b) A plot of $E_{\mathcal{N}}$ vs. Δ at $J = 1, \Gamma = 1$. The peak occurs near $\Delta_c = 1.97$, and is near the predicted value of $E_{\mathcal{N}} = 1/2$. The growing negativity at small Δ could be an artifact of quantum trajectories; see the text.

calculate each of these quantities throughout the phase diagram.

7.3.1 Logarithmic Negativity

To better understand the nature of quantum correlations, or entanglement, in the nonequilibrium steady state, we may consider the logarithmic negativity [111, 134]

$$E_{\mathcal{N}} = \log \mathrm{Tr}(|\rho^{T_B}|_1)\,, \tag{7.24}$$

where T_B denotes the partial transpose of a subsystem B, and $|\bullet|_1$ signifies the trace norm. The partial transpose only affects the coherences of the density matrix, which could violate its positivity and lead to negative eigenvalues. The logarithmic negativity then captures the degree to which positivity is violated due to the entanglement of A and B subsystems. This quantity can also be used to detect phase transitions and critical phenomena in many-body systems [135, 136] when they are driven by quantum fluctuations.

Equation (7.24) is useful when one has access to the full density matrix and can compute its singular values; however, we can also calculate this quantity for Guassian states using the covariance

matrix formalism. This requires that the system be split into subsystems, meaning we will use Eq. (7.8) where we have split the system in half. In terms of the symplectic eigenvalues of the covariance matrix, the logarithmic negativity can be computed as [122, 135]

$$E_{\mathcal{N}} = -\sum_i \log_2 \left(\min(\tilde{\nu}_i, 1)\right) , \tag{7.25}$$

where $\tilde{\nu}_i$s are the symplectic eigenvalues upon partial transposition of the density matrix, which is equivalent to sending $p_B \to -p_B$ in the covariance matrix [122, 135]. The violation of positivity in the density matrix is equivalent to the violation of the bound $\nu \geq 1$. Computing these new symplectic eigenvalues, we find only one that satisfies $\tilde{\nu} < 1$,

$$\tilde{\nu} = \sqrt{1 + \frac{4J(4J - \sqrt{\Gamma^2 + 16(J-\Delta)^2})}{\Gamma^2 - 16\Delta(2J - \Delta)}} . \tag{7.26}$$

Plugging this into Eq. (7.25), we find that $E_{\mathcal{N}}$ is indeed *finite* throughout the normal phase. Taking the limit $\Gamma \to \Gamma_c$, the symplectic eigenvalue approaches $\tilde{\nu} \to 1/\sqrt{2}$ which leads to $E_{\mathcal{N}} = \log_2 \sqrt{2} = 1/2$. Therefore, the logarithmic negativity does not diverge. This indicates that while quantum correlations do not govern the phase transition, they are still present; this should be contrasted with divergent quantum fluctuations of the Hamiltonian system at zero temperature [135]. Our results show that, despite being a mean-field model, the DDIM nonequilibrium steady state is an entangled many-body state.

In the ordered phase we rely numerics to calculate the logarithmic negativity. In Fig. 7.3.1, we first see that the peak in the negativity is slightly shifted from the critical point at $\Gamma = 4$, due to finite-size effects. Furthermore, the numerics show that the peak at the phase boundary is close to the theoretically predicted value in the thermodynamic limit of $E_{\mathcal{N}} = 1/2$. Despite the fact that the steady state becomes increasingly mixed, we still have a finite logarithmic negativity and the system appears to be entangled at finite system sizes. From Fig. 7.3.1(a) it might appear that the logarithmic negativity grows with system size when $\Gamma \ll J$, however, this is merely an effect of the quantum trajectories simulation. Small Γ necessitates longer evolution times and storage of a longer density matrix history, which become inaccessible in this regime. Similar to the mutual information simulations, we evolved 2000 trajectories for a total time of $t_f = 10\Gamma^{-1} \log N$ in the

ordered phase, with time step size $\delta t = .001$. To calculate the logarithmic negativity, we averaged over the last 100 time steps of the dynamics while skipping every 5 time steps. Furthermore, the logarithmic negativity in Fig. 7.3.1(b) grows as we approach the other side of the phase boundary near $\Delta = 0$. While a peak near the boundary is expected, the large growth with the system size is not, and is likely an artifact of quantum trajectories for $\Delta \ll J$. Indeed, the model at $\Delta = 0$ does not support correlations spreading in the system [47], while the non-Hermitian Hamiltonian employed in quantum trajectories becomes a complex-valued transverse-field Ising model and leads to the propagation of correlations; this is an artifact of quantum trajectories where the jump terms and the non-Hermitian Hamiltonian are treated on different footings. Convergence may require a very large number of quantum trajectories that is not accessible in our numerics.

7.3.2 Quantum Fisher Information

The quantum Fisher information F, although typically used in quantum metrology, is a useful measure of entanglement in spin systems [112–116]. This quantity bounds the precision one can attain when performing a phase estimation measurement corresponding to the transformation $U = \exp(i\theta O)$ with the phase θ and operator O. To saturate this bound the system needs to be entangled [105, 112–116]. For a spin system, it has been shown that the quantum Fisher information density of a total spin operator $S_{\mathbf{n}} = \frac{1}{2}\sum_i \mathbf{n}\cdot\boldsymbol{\sigma}_i$ (where $\boldsymbol{\sigma}_i = (\sigma_i^x, \sigma_i^y, \sigma_i^z)^T$) pointed along the unit vector $\mathbf{n} = (n_x, n_y, n_z)$, can indicate whether or not a state is k-partical entangled [112–116]. Specifically, a state of N spin-$\frac{1}{2}$ particles is at least $(m+1)$-partite entangled if

$$\frac{F}{N} = f > m\,, \tag{7.27}$$

for m a divisor of N. This bound provides a direct way to determine the presence of entanglement from the quantum Fisher information density.

The quantum Fisher information of a density matrix ρ with respect to the transformation generator O is defined as

$$F(\rho, O) = 2\sum_{i,j}\frac{(\lambda_i - \lambda_j)^2}{\lambda_i + \lambda_j}|\langle i|\, O\, |j\rangle|^2\,, \tag{7.28}$$

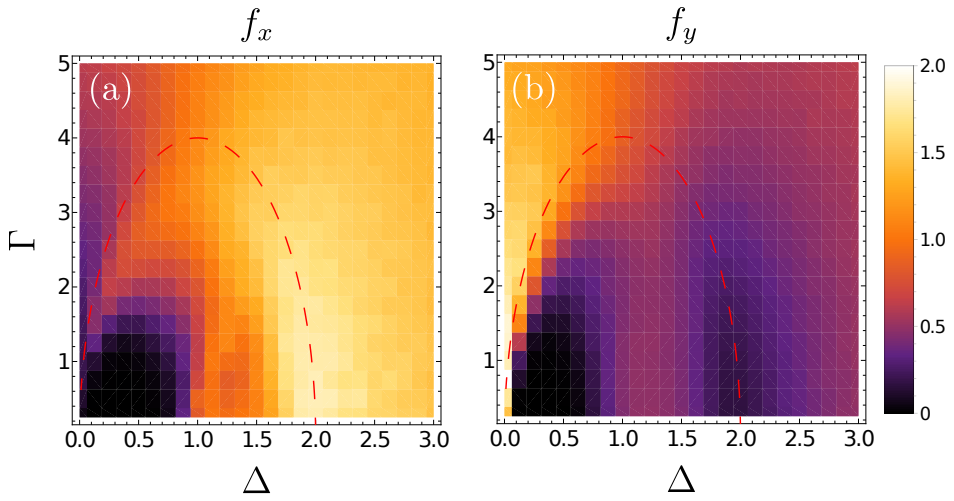

Figure 7.3.2 Numerical density plots of the quantum Fisher information density measured with respect to $S_x/2$ and $S_y/2$; we have set $J = 1$. (a) The quantity f_x is maximal in the $\Delta \to 2, \Gamma \to 0$ limit, where the theoretically predicted value is $f_x = 2$. (b) We see that f_y approaches its theoretically predicted maximum value of $f_y = 2$ when $\Delta \to 0, \Gamma \to 0$. In both cases, the quantum Fisher information is vanishing in a corner of the ordered phase as $\Delta, \Gamma \to 0$.

which is useful for numerical computations where the eigenvalues λ_i and eigenvectors $|i\rangle$ of the density matrix are accesible. However, these quantities are difficult to obtain analytically. Conveniently, for Gaussian states there exists an analytical form of the quantum Fisher information in terms of the covariance matrix and the displacement vector [125]. For a generator of the transformation that is a collective spin operator in the x-y plane, we can write the unitary in the form

$$U(\theta) = e^{i\mathbf{r}^T \Omega \boldsymbol{\gamma}(\theta)}\,, \tag{7.29}$$

where $\boldsymbol{\gamma}(\theta) = \sqrt{\frac{N}{2}}\theta(n_y, n_x)$; we recall that $\frac{1}{2}S_x = \sqrt{N/2}x$, $\frac{1}{2}S_y = -\sqrt{N/2}p$, and $\mathbf{r} = (x, p)$. The factor of $1/2$ in front of the collective operators is introduced so that the spin operators have a spectrum of unit width. The above unitary transformation merely shifts the displacement vector,

$$\mathbf{d}(\theta) = \mathbf{d} + \boldsymbol{\gamma}(\theta)\,. \tag{7.30}$$

For a transformation of this type, linear in the canonical operators, F was shown to be given by [125]

$$F = \dot{\boldsymbol{\gamma}}^T(\theta)\sigma^{-1}\dot{\boldsymbol{\gamma}}(\theta)\,, \tag{7.31}$$

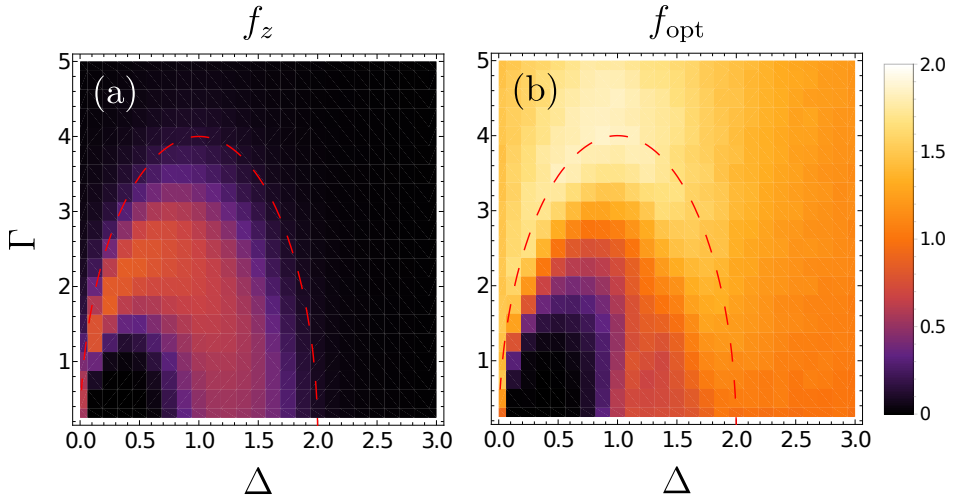

Figure 7.3.3 Numerical density plots of the quantum Fisher information measured with respect to $S_z/2$ and the optimal quantum Fisher information, with $J = 1$. (a) f_z is only finite in the ordered phase where the collective spin is no longer fully polarized along the z direction, allowing for nontrivial fluctuations in S_z. (b) The optimal Fisher information density finds a maximal value of $f_{\text{opt}} = 2$ along the phase boundary. Deviations from this exact value along the phase boundary are due to finite-size effects and the uncertainties involving quantum trajectories. The optical Fisher information too is vanishing in the ordered phase near $\Delta, \Gamma \to 0$.

where the dot denotes a derivative with respect to θ. For the transformation operators $\frac{1}{2}S_x$ and $\frac{1}{2}S_y$, we have $n_x = 0$ and $n_y = 0$ respectively. Plugging Eq. (7.5) into Eq. (7.31), we find for these two limits the quantum Fisher information densities

$$f_x = \frac{\Gamma^2 - 16\Delta(J-\Delta)}{\Gamma^2 + 16(J-\Delta)^2}\,, \tag{7.32}$$

$$f_y = 1 + \frac{16J(J-\Delta)}{\Gamma^2 + 16(J-\Delta)^2}\,, \tag{7.33}$$

which are valid throughout the normal phase. Interestingly, each of these quantities is bounded from above by $f_x, f_y \leq 2$. In fact, $f_x + f_y = 2$ is an exact relation, even at the phase boundary. Furthermore, through the bound given by Eq. (7.27), we can conclude that the system is at least bipartite entangled, hence our mean-field type model hosts a nontrivial many-body entanglement. The quantum Fisher information density along the z-direction is zero in the thermodynamic limit in the normal phase, as the collective spin is fully polarized in this direction so there are no fluctuations along z.

These results suggest that there is an optimal direction $\mathbf{n}$ with which to calculate F. This optimal

direction can be determined by solving for the n_x, n_y that maximizes F, which are found to be

$$n_x^* = \sqrt{\frac{1}{2} - \frac{2(J-\Delta)}{\sqrt{\Gamma^2 + 16(J-\Delta)^2}}}\,, \tag{7.34}$$

$$n_y^* = -\frac{\Gamma}{\sqrt{4(\Gamma^2 + 16(J-\Delta)^2)n_x^{*2}}}\,. \tag{7.35}$$

These coefficients are properly normalized, and there is also a solution with the unit vector pointing in the opposite direction. Plugging this into Eq. (7.31), we find the optimal quantum Fisher information density one can achieve in the normal phase,

$$f^* = 1 + \frac{4J}{\sqrt{\Gamma^2 + 16(J-\Delta)^2}}\,. \tag{7.36}$$

From the above equation we see that $1 \leq f^* \leq 2$ throughout the normal phase. In fact, it only saturates the upper bound at the phase transition. These bounds show that the steady state is at least 2-partite entangled throughout most of the normal phase [112–116]. At criticality the optimal direction coincides exactly with the "gapless mode" of the system (i.e. the critical mode), which are given by $\mathbf{n}_\phi = (\sqrt{\Delta}, -\sqrt{2J-\Delta})/\sqrt{2J}$, as shown in a previous work by some of the authors [128]. The quantum Fisher information density in this case is $f_\phi = 2$ along the entire phase boundary. Along the "gapped" direction, $\mathbf{n}_\zeta = (\sqrt{2J-\Delta}, \sqrt{\Delta})/\sqrt{2J}$, we instead have $f_\zeta = 0$. These results are intuitive as the quantum Fisher information is sensitive to fluctuations, a useful feature for quantum metrology [104, 105]; it is precisely the gapless mode that exhibits the largest (in fact, divergent) fluctuations criticality. On the other hand, the gapped mode has negligible fluctuations, which leads to its zero quantum Fisher information density. An alternative interpretation is that the steady state density matrix is a squeezed state, where the gapped mode is completely squeezed as we shall discuss in the next section.

Interestingly, previous work [113] has shown that a saturation of the bound in Eq. (7.27) implies that the state is a m-particle GHZ state. In the steady state discussed here, the optimal quantum Fisher information saturates this bound at the phase boundary with $m = 2$, implying that the steady state at criticality is a 2-particle GHZ state. However, we know that this cannot be the case as a product of 2-particle GHZ states is not permutation symmetric. Instead, it is possible that the

state is a mixture of all permutations of 2-particle GHZ states such that the steady state respects the permutation symmetry of the model, but this requires further investigation. Our results are particularly interesting for metrological or entanglement studies of critical systems in the future, where the role of gapless and gapped modes can be further elucidated.

To investigate the ordered phase, we once again employ numerics. The quantum trajectory simulations were evolved for a total time $t_f = 10\Gamma^{-1}$ with time step $\delta t = .1$ and 1000 trajectories. For each data point, the quantum Fisher information density was averaged over the last ten time steps of the dynamics. As shown in Fig. 7.3.3(a) we have that f_z becomes finite in the ordered phase, as the spin is no longer fully polarized in the z-direction which introduces fluctuations in S_z. However, all four begin to deplete as $\Gamma, \Delta \to 0$ where the state becomes increasingly mixed. This mixture is easily seen by the fact that $\mu(\rho_{\mathrm{MF}}) = \frac{1}{2}(1 + s^2) < 1$, with $s = S/N = \sqrt{\langle S_x\rangle^2 + \langle S_y\rangle^2 + \langle S_z\rangle^2}/N$. From Eq. (7.28), it is clear that the quantum Fisher information density vanishes for completely mixed states, so it is reasonable to expect that states sufficiently close to being completely mixed would have small quantum Fisher information density.

7.3.3 Spin Squeezing

Squeezed states are extensively studied in the field of metrology as they are useful for surpassing the quantum limit in high-precision measurements [117–119]. They are states in which the variance of one or more quadratures is less than that of states with symmetric quadrature variances. An example of such symmetric states are the coherent states. Squeezing of spin operators is characterized by the squeezing parameter

$$\xi = \frac{\min(\Delta S^2_{\mathbf{s}_\perp})}{N}, \tag{7.37}$$

where $\Delta O^2 = \langle O^2\rangle - \langle O\rangle^2$ is the variance of operator O, and $\mathbf{s}_\perp$ defines an axis perpendicular to the direction $\mathbf{s}$ of the mean total spin. The minimization is performed over all directions perpendicular to $\mathbf{s}$. We take this definition such that $\xi < 1$ for a squeezed state and $\xi = 1$ for a coherent spin state. The squeezing parameter, ξ, is related to the quantum Fisher information as they both depend on the fluctuations in the system and can indicate the presence of entanglement [117, 119]. Furthermore,

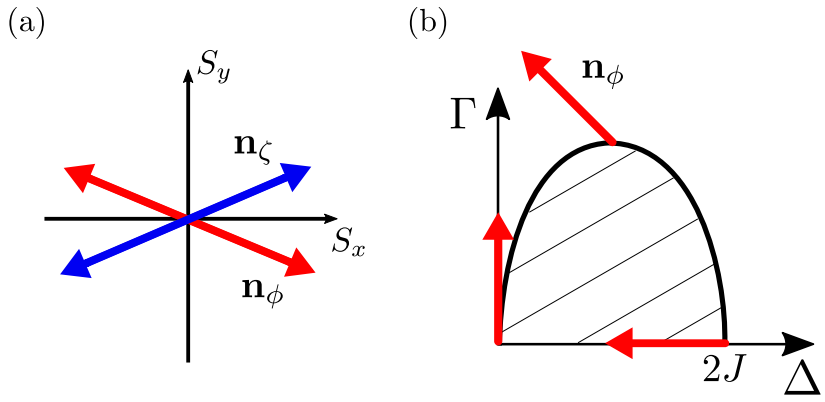

Figure 7.3.4 (a) A schematic diagram depicting the direction of the gapless ($\mathbf{n}_\phi$) and gapped ($\mathbf{n}_\zeta$) modes with respect to those defined by S_x and S_y. The vectors are shown pointing in both directions as they can be defined up to an overall sign. (b) The depiction of the gapless mode along the phase boundary. The corresponding vector $\mathbf{n}_\phi$ rotates from vertical to horizontal as the phase boundary is traversed from left to right.

the squeezing parameter is directly related to the concurrence, and if $\xi < 1$ then the state is not only squeezed, but it also entangled [119].

Using the formalism described in Appendix 7.B, we are able to calculate the correlations for all of the quadratures throughout the entire phase diagram analytically. We always take $\mathbf{s}$ to be pointing along the z-direction, hence, we can write the perpendicular spin as $S_{\mathbf{s}_\perp} = \tilde{\mathbf{S}} \cdot \mathbf{s}_\perp = \cos(\phi)\tilde{S}_x + \sin(\phi)\tilde{S}_y$ and minimize Eq. (7.37) with respect to ϕ. The tilde indicates that they are in the rotated frame such that $\tilde{S}_z = S$, with S the mean total spin.

In the normal phase the covariance matrix in Eq. (7.5) already provides us with the necessary ingredients to write Eq. (7.37) as

$$\xi = \min_\phi(\sigma_{11}\sin^2\phi + \sigma_{22}\cos^2\phi - 2\sigma_{12}\cos\phi\sin\phi)\,. \tag{7.38}$$

We have used the fact that $\tilde{S}_{x,y} = -S_{y,x}$ in the normal phase, and identified $x = S_x/\sqrt{2N}$ and $p = -Sy/\sqrt{2N}$. Recall that the covariance matrix elements are defined as $\sigma_{11} = \langle\{x,x\}\rangle = \langle S_x^2/N\rangle$ and similarly for σ_{22}. The cross correlation takes the form $\sigma_{12} = \langle\{x,p\}\rangle = -\langle\{S_x,S_y\}\rangle/2N$, hence, the multiplicative factor of -2 in the last term of Eq. (7.38). At the phase boundary, we solve for ϕ that minimizes the above expression and find the unit vector $\mathbf{s}_\perp^* = (\sqrt{\Delta}, \sqrt{2J-\Delta})/\sqrt{2J}$, which exactly coincides with the direction of the gapped mode $\mathbf{n}_\zeta = (\sqrt{2J-\Delta}, \sqrt{\Delta})/\sqrt{2J}$ in the

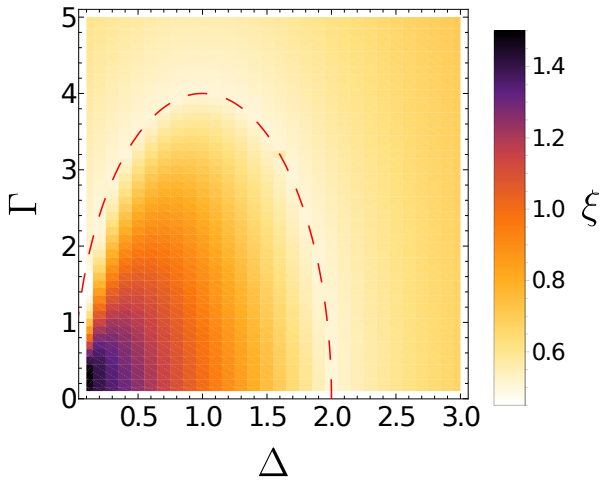

Figure 7.3.5 Squeezing parameter ξ over the phase space in the phase diagram; we have set $J = 1$. The steady state is most squeezed along the phase boundary, where the fluctuations of the gapless mode diverge while the gapped mode is squeezed. In the corner region within the ordered phase, the steady state is not squeezed as it becomes increasingly mixed.

original frame. Interestingly, we find that all along the phase boundary $\xi = 1/2$ exactly.

In the ordered phase, we cannot find analytical expressions for the correlation functions, but we can numerically evaluate the formal expressions we obtained in Appendix 7.B. With this, we produce a density plot throughout the phase diagram in Fig. 7.3.5. From this figure, it is clear that the nonequilibrium steady state is most squeezed at the phase boundary. Furthermore, the steady state transitions to being not squeezed ($\xi \geq 1$) deep inside the ordered phase where $\Delta, \Gamma \ll J = 1$. As discussed in Sec. 7.3.2, this is the region where the state becomes increasingly mixed. These results enforce the conclusions in the previous sections that fluctuations are particularly suppressed in this region of the ordered phase.

APPENDIX

7.A Split system covariance matrix

In this appendix we show how to obtain Eq. (7.8), starting from the exact field theoretical description of Eq. (3.5) as derived in Sec. 3.4. Using an exact quantum-to-classical mapping, the non-equilibrium partition function of the steady state $Z = \lim_{t\to\infty} \mathrm{Tr}(\exp(t\mathcal{L})[\rho_0])$ can be mapped to a path integral over a pair of real fields m_c, m_q,

$$Z = \int \mathcal{D}[m_c, m_q] e^{iS[m_c,m_q]} \,. \tag{7.39}$$

The action S is given by

$$S = -2JN \int_t m_c(t) m_q(t) - iN \ln \mathrm{Tr}\left[\mathcal{T} e^{\int_t \mathbb{T}(m_{c/q}(t))}\right], \tag{7.40}$$

where m_c, the "classical" field, captures the order parameter, and m_q, the "quantum" field, is related to quantum fluctuations and noise.

Connected correlation functions can be obtained by introducing source fields h_i coupled to the desired observables to Eq. (3.5) [4, 13, 98]. After integration of the fields m_c, m_q, one obtains the generating functional $W[\{h_i\}] = i \ln Z$ which is given in terms of the desired Green's functions. We wish to obtain correlation functions for S_x and S_y within the same subsystem and between two different subsystems. Therefore, we define $S_{\alpha,A} = \sum_{i=1}^{N/2} \sigma_i^\alpha$ to be the collective spin operator for one half of the system, while $S_{\alpha,B} = \sum_{i=N/2+1}^{N} \sigma_i^\alpha$ for the other half. We introduce source fields $\mathbf{h}^{(u/l)} = (\alpha_A^{(u/l)}, \alpha_B^{(u/l)}, \beta_A^{(u/l)}, \beta_B^{(u/l)})$ coupled to the operators $\mathbf{S}^{(u/l)} = (S_{x,A}^{(u/l)}, S_{x,B}^{(u/l)}, \mp S_{y,A}^{(u/l)}, \mp S_{y,B}^{(u/l)})/\sqrt{N}$, where u/l denote if the operator is acting to the left or the right of the density matrix in Eq. (3.5). This modifies the vectorized Louvillian $\mathbb{L}$ (found through the transformation $A \bullet B \to A \otimes B^T = A^{(u)} B^{(l)T}$ for operators A, B) by

$$\mathbb{L}' = \mathbb{L} + i\mathbf{h}^{(u)} \cdot \mathbf{S}^{(u)} - i\mathbf{h}^{(l)} \cdot \mathbf{S}^{(l)} \,. \tag{7.41}$$

Following the mapping to the path integral, this modifies the action in the following way,

$$S = -2JN \int_t m_c(t) m_q(t) - i\frac{N}{2} \ln \mathrm{Tr}\left[\mathcal{T} e^{\int_t \mathbb{T}_A(m_{c/q}(t))}\right] - i\frac{N}{2} \ln \mathrm{Tr}\left[\mathcal{T} e^{\int_t \mathbb{T}_B(m_{c/q}(t))}\right], \tag{7.42}$$

where

$$\mathbb{T}_A = \mathbb{T} + i\mathbf{h}_A^{(u)} \cdot \mathbf{s}_A^{(u)} - i\mathbf{h}_A^{(l)} \cdot \mathbf{s}_A^{(l)} \,, \tag{7.43}$$

and similarly for $\mathbb{T}_B$. The vectors with subsystem subscripts only contain fields/operators from that subsytem, and we have also defined the single spin vectors $\mathbf{s}_{A/B}^{(u/l)} = (\sigma_{A/B}^{x(u/l)}, \mp\sigma_{A/B}^{y(u/l)})/\sqrt{N}$.

We can now expand Eq. (7.42) to second order in fluctuations around $m_{c/q} = 0, \mathbf{h}_{c/q} = 0$, where we have performed the Keldysh rotation on the source fields $\mathbf{h}_{c/q} = (\mathbf{h}^{(u)} \pm \mathbf{h}^{(l)})/\sqrt{2}$. This yields an action of the form

$$\mathcal{S}^{(2)} = \frac{1}{2}\int_{t,t'} \mathbf{v}^T(t)\hat{P}(t-t')\mathbf{v}(t') \,, \tag{7.44}$$

where

$$\mathbf{v} = (m_c, m_q, \alpha_{c,A}, \alpha_{q,A}, \alpha_{c,B}, \alpha_{q,B}, \beta_{c,A}, \beta_{q,A}, \beta_{c,B}, \beta_{q,B}) \,,$$

(in an abuse of notation we denote the fluctuations with the original field labels), and the kernel P is a block matrix:

$$\hat{P} = \begin{pmatrix} \hat{P}_m & \hat{P}_{m,\alpha} & \hat{P}_{m,\alpha} & \hat{P}_{m,\beta} & \hat{P}_{m,\beta} \\ \hat{P}_{\alpha,m} & \hat{P}_\alpha & 0 & \frac{1}{2J}\hat{P}_{m,\beta} & 0 \\ \hat{P}_{\alpha,m} & 0 & \hat{P}_\alpha & 0 & \frac{1}{2J}\hat{P}_{m,\beta} \\ \hat{P}_{\beta,m} & \frac{1}{2J}\hat{P}_{\beta,m} & 0 & \hat{P}_\alpha & 0 \\ \hat{P}_{\beta,m} & 0 & \frac{1}{2J}\hat{P}_{\beta,m} & 0 & \hat{P}_\alpha \end{pmatrix} . \tag{7.45}$$

Each of the submatrices has the typical Keldysh structure,

$$\hat{P}_m = \begin{pmatrix} 0 & P_m^A \\ P_m^R & P_m^K \end{pmatrix} . \tag{7.46}$$

The list of elements in the time domain are

$$P_m^{A/R}(t) = -2J\delta(t) + \Theta(\mp t)\left(8J^2 e^{-\frac{\Gamma}{2}|t|}\sin(2\Delta|t|)\right) \,, \tag{7.47}$$

$$P_m^K(t) = i8J^2 e^{-\frac{\Gamma}{2}|t|}\cos(2\Delta|t|) \,, \tag{7.48}$$

$$P_\alpha^{A/R}(t) = \frac{1}{8J^2}\left(P_m^{A/R}(t) + 2J\delta(t)\right) \,, \tag{7.49}$$

$$P_\alpha^K(t) = \frac{1}{8J^2}P_m^K(t) \,, \tag{7.50}$$

$$P_{\beta,m}^{A/R}(t) = \mp\Theta(\mp t)\left(2Je^{-\frac{\Gamma}{2}|t|}\cos(2\Delta|t|)\right) \,, \tag{7.51}$$

$$P_{\beta,m}^K(\delta t) = \mathrm{sgn}(t)\left(-i2Je^{-\frac{\Gamma}{2}|\delta t|}\sin(2\Delta|\delta t|)\right) \,, \tag{7.52}$$

and the submatrices obey the following relations,

$$[\hat{P}_m]^T(-t) = \hat{P}_m(t)\,, \quad [\hat{P}_\alpha]^T(-t) = \hat{P}_\alpha(t)\,, \tag{7.53}$$

$$\hat{P}_{m,\alpha}(t) = 2J\hat{P}_\alpha\,, \quad \hat{P}_{m,\alpha}(t) = \hat{P}_{\alpha,m}(t)\,, \tag{7.54}$$

$$[\hat{P}_{\beta,m}]^T(-t) = \hat{P}_{m,\beta}(t)\,. \tag{7.55}$$

The final step is to integrate out the fields $m_{c/q}$ such that we are left with the generating functional. This integration is easily done in the frequency domain using functional Gaussian integration rules [13], which leads to a generating functional of the form

$$\begin{aligned} W[\mathbf{h}] =& \frac{1}{2}\int_\omega \left(\mathbf{h}^T_{\alpha_A}\hat{G}_{xx}(\omega)\mathbf{h}_{\alpha_A} + \mathbf{h}^T_{\beta_A}\hat{G}_{pp}(\omega)\mathbf{h}_{\beta_A} + 2\mathbf{h}^T_{\alpha_A}\hat{G}_{xp}(\omega)\mathbf{h}_{\beta_A}\right) \\ &+ 2\int_\omega \left(\mathbf{h}^T_{\alpha_A}\hat{G}^{AB}_{xx}(\omega)\mathbf{h}_{\alpha_B} + \mathbf{h}^T_{\beta_A}\hat{G}^{AB}_{pp}(\omega)\mathbf{h}_{\beta_B} + \mathbf{h}^T_{\alpha_A}\hat{G}^{AB}_{xp}(\omega)\mathbf{h}_{\beta_B}\right) + \dots \end{aligned} \tag{7.56}$$

where we have suppressed the frequency dependence of the fields for compactness, $\mathbf{h}_{\alpha_A} = (\alpha_{c,A}, \alpha_{q,A})$ (similarly for the other fields), and the $\dots$ signify the rest of the terms which can be found by swapping $A \to B$. The Green's functions have a Keldysh structure,

$$\hat{G}_{ij} = \begin{pmatrix} 0 & G^A_{ij} \\ G^R_{ij} & G^K_{ij} \end{pmatrix}, \tag{7.57}$$

where G^R_{ij} is the retarded response function, and the Keldysh Green's function $G^K_{ij}(t) = C_{ij}(t) = \langle\{\delta O_i(t), \delta O_j(0)\}\rangle$ is the connected correlation function for operators $O_{i/j}$, i.e. the quantity of interest. In terms of the submatrices given in Eq. (7.45), we have

$$\hat{G}_{xx} = \hat{P}_{\alpha,m}(\omega)\hat{P}^{-1}_m(\omega)\hat{P}_{m,\alpha}(\omega) - \hat{P}_\alpha(\omega) \tag{7.58}$$

$$\hat{G}_{pp} = \hat{P}_{\beta,m}(\omega)\hat{P}^{-1}_m(\omega)\hat{P}_{m,\beta}(\omega) - \hat{P}_\alpha(\omega) \tag{7.59}$$

$$\hat{G}_{xp} = \hat{P}_{\beta,m}(\omega)\hat{P}^{-1}_m(\omega)\hat{P}_{m,\beta}(\omega) - 2\hat{P}_{\beta,\alpha}(\omega) \tag{7.60}$$

$$\hat{G}^{AB}_{xx} = \hat{P}_{\alpha,m}(\omega)\hat{P}^{-1}_m(\omega)\hat{P}_{m,\alpha}(\omega) \tag{7.61}$$

$$\hat{G}^{AB}_{pp} = \hat{P}_{\beta,m}(\omega)\hat{P}^{-1}_m(\omega)\hat{P}_{m,\beta}(\omega) \tag{7.62}$$

$$\hat{G}^{AB}_{xp} = \hat{P}_{\alpha,m}(\omega)\hat{P}^{-1}_m(\omega)\hat{P}_{m,\beta}(\omega)\,. \tag{7.63}$$

Taking only the Keldysh Green's function from each of these matrices, and integrating them over the frequency domain to obtain the correlation function at equal times, we retrieve the expressions

for the split-system covariance matrix as shown in Eq. (7.8). The identification between these results and the covariance matrix elements are

$$X = \begin{pmatrix} C_{xx} & C_{xx}^{AB} \\ C_{xx}^{AB} & C_{xx} \end{pmatrix}, \quad K = \begin{pmatrix} C_{xp} & C_{xp}^{AB} \\ C_{xp}^{AB} & C_{xp} \end{pmatrix}, \quad P = \begin{pmatrix} C_{pp} & C_{pp}^{AB} \\ C_{pp}^{AB} & C_{pp} \end{pmatrix}. \tag{7.64}$$

We have used the fact that these correlation functions are symmetric under swap of x and p.

7.B Ordered phase calculations

Calculating the covariance matrix in the ordered phase, entire or split system, is mostly identical to how it was done in Appendix A. The main differences are how the matrix elements in Eq. (7.47) are calculated, and the introduction of a source for S_z as there are now relevant fluctuations in the z-direction. In addition, we will rotate the total spin operator such that it points along the z-direction in the new reference frame. This is to ensure that the $\tilde{S}_x/\sqrt{2S}$ and $\tilde{S}_y/\sqrt{2S}$ (in an abuse of notation we set $S = |\mathbf{S}|$) in the new frame satisfy the canonical commutation relations, as discussed in Sec. 7.1.2. Here we will show how to perform the calculation without splitting the system in half.

We begin by inserting the source field $\mathbf{h}^{(u/l)} = (\alpha^{(u/l)}, \beta^{(u/l)}, \gamma^{(u/l)})$ which couples to the spin vector $\mathbf{S}^{(u/l)} = (S_x^{(u/l)}, \pm S_y^{(u/l)}, S_z^{(u/l)})/\sqrt{N}$. This modifies the matrix $\mathbb{T}$ in Eq. (7.40),

$$\mathbb{T}' = \mathbb{T} + i\mathbf{h}^{(u)} \cdot \boldsymbol{\sigma}^{(u)} - i\mathbf{h}^{(l)} \cdot \boldsymbol{\sigma}^{(l)}, \tag{7.65}$$

where the individual spin vector is $\boldsymbol{\sigma}^{(u/l)} = (\sigma^{x(u/l)}, \pm\sigma^{y(u/l)}, \sigma^{z(u/l)})/\sqrt{N}$. The expansion of the exact action is now performed around the saddle-point solution, $m_c = m = \sqrt{32J\Delta - 16\Delta^2 - \Gamma^2}/4J$, $m_q = 0, \mathbf{h}_{c/q} = 0$, where we have performed the Keldysh rotation on the source fields $\mathbf{h}_{c/q} = (\mathbf{h}^{(u)} \pm \mathbf{h}^{(l)})/\sqrt{2}$. Defining the matrices $T_{\mu_i} = \partial_{\mu_i}\mathbb{T}$, with $\mu \in \{m, \alpha, \beta, \gamma\}, i \in \{c, q\}$, we have that

$$\begin{aligned} \frac{\delta^2 \log \mathrm{Tr}(\mathcal{T} e^{\int_t \mathbb{T}})}{\delta\mu_i(t)\delta\nu_j(t')}|_{\text{s.p.}} = \Theta(t-t') \langle\langle I| T_{\mu_i} e^{t\mathbb{T}_m} T_{\nu_j} |\rho_{\text{ss}}\rangle\rangle + \Theta(t'-t) \langle\langle I| T_{\nu_j} e^{t\mathbb{T}_m} T_{\mu_i} |\rho_{\text{ss}}\rangle\rangle \\ - \langle\langle I| T_{\mu_i} |\rho_{\text{ss}}\rangle\rangle \langle\langle I| T_{\nu_i} |\rho_{\text{ss}}\rangle\rangle, \end{aligned} \tag{7.66}$$

where we have evaluated the left-hand side at the saddle-point solution. We have used the fact that $\mathbb{T}$ is a vectorized single-spin Liouvillian and has a steady state given by the vectors $\langle\langle I|$ and $|\rho\text{ss}\rangle\rangle$. These are the left and right eigenvectors of $\mathbb{T}_m = \mathbb{T}|_{\text{s.p}}$ respectively and satisfy $\mathbb{T}_m |\rho_{\text{ss}}\rangle\rangle = 0$

(and similarly for $\langle\langle I|$). We have also used the fact that $\mathrm{Tr}(e^{\infty\mathbb{T}_m}) = 1$. The retarded elements of the expansion correspond to when $i = q, j = c$ and the Keldysh elements correspond to when $i = q, j = q$. Therefore we have generally

$$P^R_{\mu\nu}(t) = -2J\delta(t)\delta_{\mu,m}\delta_{\nu,m} - iN\Theta(t)\,\langle\langle I|\,T_{\mu_q}e^{t\mathbb{T}_m}T_{\nu_c}\,|\rho_{\mathrm{ss}}\rangle\rangle \tag{7.67}$$

$$P^K_{\mu\nu}(t) = -iN\Theta(t)\,\langle\langle I|\,T_{\mu_q}e^{t\mathbb{T}_m}T_{\nu_q}\,|\rho_{\mathrm{ss}}\rangle\rangle - iN\Theta(-t)\,\langle\langle I|\,T_{\nu_q}e^{t\mathbb{T}_m}T_{\mu_q}\,|\rho_{\mathrm{ss}}\rangle\rangle\ . \tag{7.68}$$

The fact that m is finite makes further expansion of the trace-log in Eq. (**??**) difficult analytically [98]. To simplify this expression, we can rewrite the generator as

$$e^{t\mathbb{T}_m} = |\rho_{\mathrm{ss}}\rangle\rangle\,\langle\langle I| + \sum_{k=1}^{3} e^{t\lambda_k}\,|\lambda^R_k\rangle\rangle\,\langle\langle\lambda^L_k|\ , \tag{7.69}$$

where each of the eigenvalues λ_k are either real or come in complex conjugate pairs with $\mathrm{Re}(\lambda_k) < 0$. We then Fourier transform the result, using the definition $\phi(t) = \frac{1}{2\pi}\int d\omega e^{-i\omega t}\phi(\omega)$ for any field $\phi(t)$. We find

$$P^R_{\mu\nu}(\omega) = -2J\delta_{\mu,m}\delta_{\nu,m} + iN\sum_{k=1}^{3} D_{\mu\nu}(k)\frac{1}{\lambda_k + i\omega} \tag{7.70}$$

$$P^K_{\mu\nu}(\omega) = iN\sum_{k=1}^{3} \tilde{D}_{\mu\nu}(k)\frac{1}{\lambda_k + i\omega} + \tilde{D}_{\nu\mu}(k)\frac{1}{\lambda_k - i\omega}\,, \tag{7.71}$$

where we have defined the coefficients

$$D_{\mu\nu}(k) = \langle\langle I|\,T_{\mu_q}\,|\lambda^R_k\rangle\rangle\,\langle\langle\lambda^L_k|\,T_{\nu_c}\,|\rho_{\mathrm{ss}}\rangle\rangle \tag{7.72}$$

$$\tilde{D}_{\mu\nu}(k) = \langle\langle I|\,T_{\mu_q}\,|\lambda^R_k\rangle\rangle\,\langle\langle\lambda^L_k|\,T_{\nu_q}\,|\rho_{\mathrm{ss}}\rangle\rangle\ , \tag{7.73}$$

for compactness. These are the matrix elements of the submatrices in a block matrix similar to that of Eq. (7.45), except now there are no subsystems and we have new blocks from the γ source field. Following that procedure, we arrive at the Green's functions in the ordered phase,

$$\hat{G}_{\mu\nu} = \hat{P}_{\mu\nu}(\omega)\hat{P}^{-1}_{mm}(\omega)[\hat{P}_{\nu\mu}]^T(-\omega) - 2\hat{P}_{\mu\nu}(\omega) + \delta_{\mu,\nu}\hat{P}_{\mu\mu}\,, \tag{7.74}$$

where $\mu, \nu \in \{\alpha, \beta, \gamma\}$ as we have eliminated the m fields. The correlation functions for $S_{x,y,z}/\sqrt{N}$ are then all given by

$$C_{\mu\nu} = \int_\omega G^K_{\mu\nu}(\omega)\,, \tag{7.75}$$

where the Keldysh component is as defined in Eq. (7.57). The labels μ, ν can now be identified with x, y, z instead of α, β, γ respectively. As mentioned before, it is difficult to obtain an analytical expression for the correlation functions. However, one can numerically evaluate the coefficients $D_{\mu\nu}, \tilde{D}_{\mu\nu}$ and then integrate $G^K_{\mu\nu}$ over its ω dependence to obtain a numerical value for the correlation functions.

To obtain a representation in terms of canonical variables as we did in the normal phase, we rotate the spin observables such that $\tilde{S}_z$, the rotated spin operator, points along $\mathbf{n} = \mathbf{S}/|\mathbf{S}|$. This is done using the transformation matrix [34]

$$R(\theta, \phi) = \begin{pmatrix} \cos\theta\cos\phi & \cos\theta\sin\phi & -\sin\theta \\ -\sin\phi & \cos\phi & 0 \\ \sin\theta\cos\phi & \sin\theta\sin\phi & \cos\theta \end{pmatrix}, \tag{7.76}$$

which defines the new spin variables

$$\tilde{\mathbf{S}} = R(\theta, \phi)\mathbf{S}\,. \tag{7.77}$$

The angles θ, ϕ that achieve the desired rotation are given by

$$\theta = \cos^{-1}\left(\frac{Z}{s}\right), \quad \phi = \cot^{-1}\left(\frac{X}{Y}\right), \tag{7.78}$$

where X, Y, Z are the mean-field solutions defined in Eq. (3.7), and $s = \sqrt{X^2 + Y^2 + Z^2}$. This rotation gives the new spin operators in terms of the old ones, which means we also know what the correlation functions of the new variables are in terms of the old ones.

BIBLIOGRAPHY

BIBLIOGRAPHY

[1] J. J. Sakurai and Jim Napolitano. *Modern Quantum Mechanics*. September 2020. doi: 10.1017/9781108587280. URL https://www.cambridge.org/highereducation/books/modern-quantum-mechanics/DF43277E8AEDF83CC12EA62887C277DC. ISBN: 9781108587280 Publisher: Cambridge University Press.

[2] Michael A. Nielsen and Isaac L. Chuang. *Quantum Computation and Quantum Information: 10th Anniversary Edition*. December 2010. doi: 10.1017/CBO9780511976667. URL https://www.cambridge.org/highereducation/books/quantum-computation-and-quantum-information/01E10196D0A682A6AEFFEA52D53BE9AE. ISBN: 9780511976667 Publisher: Cambridge University Press.

[3] Heinz-Peter Breuer and Francesco Petruccione. *The Theory of Open Quantum Systems*. 2002. ISBN 978-0-19-852063-4.

[4] Alex Kamenev. *Field Theory of Non-Equilibrium Systems*. 2011.

[5] Crispin Gardiner and Peter Zoller. *Quantum Noise: A Handbook of Markovian and Non-Markovian Quantum Stochastic Methods with Applications to Quantum Optics*. Springer Berlin, 3 edition, 2004. ISBN 978-3-540-22301-6. URL https://www.springer.com/us/book/9783540223016.

[6] Stanislaw Kryszewski and Justyna Czechowska-Kryszk. Master equation - tutorial approach, January 2008. URL http://arxiv.org/abs/0801.1757. arXiv:0801.1757 [quant-ph].

[7] Claude Cohen-Tannoudji, Jacques Dupont-Roc, and Gilbert Grynberg. *Atom-Photon Interactions: Basic Processes and Applications*. Wiley-VCH, New York, March 1998. ISBN 978-0-471-29336-1.

[8] Kristian Baumann, Christine Guerlin, Ferdinand Brennecke, and Tilman Esslinger. Dicke quantum phase transition with a superfluid gas in an optical cavity. *Nature*, 464(7293): 1301–1306, July 2010. ISSN 1476-4687. doi: 10.1038/nature09009. URL https://www.nature.com/articles/nature09009.

[9] Markus P. Baden, Kyle J. Arnold, Arne L. Grimsmo, Scott Parkins, and Murray D. Barrett. Realization of the Dicke Model Using Cavity-Assisted Raman Transitions. *Phys. Rev. Lett.*, 113(2):020408, July 2014. doi: 10.1103/PhysRevLett.113.020408. URL https://link.aps.org/doi/10.1103/PhysRevLett.113.020408.

[10] Juan A. Muniz, Diego Barberena, Robert J. Lewis-Swan, Dylan J. Young, Julia R. K. Cline, Ana Maria Rey, and James K. Thompson. Exploring dynamical phase transitions with

cold atoms in an optical cavity. *Nature*, 580(7805):602–607, April 2020. ISSN 1476-4687. doi: 10.1038/s41586-020-2224-x. URL https://www.nature.com/articles/s41586-020-2224-x.

[11] Mattias Fitzpatrick, Neereja M. Sundaresan, Andy C.Y. Li, Jens Koch, and Andrew A. Houck. Observation of a Dissipative Phase Transition in a One-Dimensional Circuit QED Lattice. *Phys. Rev. X*, 7(1):011016, February 2017. ISSN 2160-3308. doi: 10.1103/PhysRevX.7.011016. URL https://link.aps.org/doi/10.1103/PhysRevX.7.011016.

[12] Philip Pearle. Simple Derivation of the Lindblad Equation. *Eur. J. Phys.*, 33(4):805–822, July 2012. ISSN 0143-0807, 1361-6404. doi: 10.1088/0143-0807/33/4/805. URL http://arxiv.org/abs/1204.2016. arXiv:1204.2016 [math-ph, physics:quant-ph].

[13] L. M. Sieberer, M. Buchhold, and S. Diehl. Keldysh field theory for driven open quantum systems. *Rep. Prog. Phys.*, 79(9):096001, August 2016. ISSN 0034-4885. doi: 10.1088/0034-4885/79/9/096001. URL https://doi.org/10.1088%2F0034-4885%2F79%2F9%2F096001.

[14] Emanuele G. Dalla Torre, Sebastian Diehl, Mikhail D. Lukin, Subir Sachdev, and Philipp Strack. Keldysh approach for nonequilibrium phase transitions in quantum optics: Beyond the Dicke model in optical cavities. *Phys. Rev. A*, 87(2):023831, February 2013. doi: 10.1103/PhysRevA.87.023831. URL https://link.aps.org/doi/10.1103/PhysRevA.87.023831.

[15] Sei Suzuki, Jun-ichi Inoue, and Bikas K. Chakrabarti. *Quantum Ising Phases and Transitions in Transverse Ising Models*. Lecture Notes in Physics. Springer-Verlag, Berlin Heidelberg, 2 edition, 2013. ISBN 978-3-642-33038-4. URL https://www.springer.com/us/book/9783642330384.

[16] Garraway Barry M. The Dicke model in quantum optics: Dicke model revisited. *Philosophical Transactions of the Royal Society A: Mathematical, Physical and Engineering Sciences*, 369(1939):1137–1155, March 2011. doi: 10.1098/rsta.2010.0333. URL https://royalsocietypublishing.org/doi/full/10.1098/rsta.2010.0333.

[17] Peter Kirton, Mor M. Roses, Jonathan Keeling, and Emanuele G. Dalla Torre. Introduction to the Dicke model: from equilibrium to nonequilibrium, and vice versa. *Adv. Quantum Technol.*, 2(1-2):1800043, February 2019. ISSN 25119044. doi: 10.1002/qute.201800043. URL http://arxiv.org/abs/1805.09828. arXiv: 1805.09828.

[18] K. Rzażewski, K. Wódkiewicz, and W. Żakowicz. Phase Transitions, Two-Level Atoms, and the ${A}^{2}$ Term. *Phys. Rev. Lett.*, 35(7):432–434, August 1975. doi: 10.1103/PhysRevLett.35.432. URL https://link.aps.org/doi/10.1103/PhysRevLett.35.432. Publisher: American Physical Society.

[19] F. Dimer, B. Estienne, A. S. Parkins, and H. J. Carmichael. Proposed realization of the

Dicke-model quantum phase transition in an optical cavity QED system. *Phys. Rev. A*, 75 (1):013804, January 2007. doi: 10.1103/PhysRevA.75.013804. URL https://link.aps.org/doi/10.1103/PhysRevA.75.013804.

[20] Zhang Zhiqiang, Chern Hui Lee, Ravi Kumar, K. J. Arnold, Stuart J. Masson, A. S. Parkins, and M. D. Barrett. Nonequilibrium phase transition in a spin-1 Dicke model. *Optica, OPTICA*, 4(4):424–429, April 2017. ISSN 2334-2536. doi: 10.1364/OPTICA.4.000424. URL https://www.osapublishing.org/optica/abstract.cfm?uri=optica-4-4-424.

[21] K. Baumann, R. Mottl, F. Brennecke, and T. Esslinger. Exploring Symmetry Breaking at the Dicke Quantum Phase Transition. *Phys. Rev. Lett.*, 107(14):140402, September 2011. doi: 10.1103/PhysRevLett.107.140402. URL https://link.aps.org/doi/10.1103/PhysRevLett.107.140402.

[22] Emanuele G. Dalla Torre, Yulia Shchadilova, Eli Y. Wilner, Mikhail D. Lukin, and Eugene Demler. Dicke phase transition without total spin conservation. *Phys. Rev. A*, 94(6):061802, December 2016. ISSN 2469-9926, 2469-9934. doi: 10.1103/PhysRevA.94.061802. URL https://link.aps.org/doi/10.1103/PhysRevA.94.061802.

[23] Rex Lundgren, Alexey V. Gorshkov, and Mohammad F. Maghrebi. Nature of the nonequilibrium phase transition in the non-Markovian driven Dicke model. *Phys. Rev. A*, 102(3):032218, September 2020. doi: 10.1103/PhysRevA.102.032218. URL https://link.aps.org/doi/10.1103/PhysRevA.102.032218.

[24] Peter Kirton and Jonathan Keeling. Superradiant and lasing states in driven-dissipative Dicke models. *New J. Phys.*, 20(1):015009, January 2018. ISSN 1367-2630. doi: 10.1088/1367-2630/aaa11d. URL https://doi.org/10.1088%2F1367-2630%2Faaa11d.

[25] Peter Kirton and Jonathan Keeling. Suppressing and Restoring the Dicke Superradiance Transition by Dephasing and Decay. *Phys. Rev. Lett.*, 118(12):123602, March 2017. doi: 10.1103/PhysRevLett.118.123602. URL https://link.aps.org/doi/10.1103/PhysRevLett.118.123602.

[26] Victor V. Albert and Liang Jiang. Symmetries and conserved quantities in Lindblad master equations. *Phys. Rev. A*, 89(2):022118, February 2014. doi: 10.1103/PhysRevA.89.022118. URL https://link.aps.org/doi/10.1103/PhysRevA.89.022118.

[27] François Damanet, Andrew J. Daley, and Jonathan Keeling. Atom-only descriptions of the driven-dissipative Dicke model. *Phys. Rev. A*, 99(3):033845, March 2019. doi: 10.1103/PhysRevA.99.033845. URL https://link.aps.org/doi/10.1103/PhysRevA.99.033845.

[28] Arnab Das, K. Sengupta, Diptiman Sen, and Bikas K. Chakrabarti. Infinite-range Ising ferromagnet in a time-dependent transverse magnetic field: Quench and ac dynamics near the quantum critical point. *Phys. Rev. B*, 74(14):144423, October 2006. doi: 10.1103/PhysRevB.

74.144423. URL https://link.aps.org/doi/10.1103/PhysRevB.74.144423.

[29] Feng Pan and J. P. Draayer. Analytical solutions for the LMG model. *Physics Letters B*, 451(1):1–10, April 1999. ISSN 0370-2693. doi: 10.1016/S0370-2693(99)00191-4. URL http://www.sciencedirect.com/science/article/pii/S0370269399001914.

[30] Hiroyuki Morita, Hiromasa Ohnishi, João da Providência, and Seiya Nishiyama. Exact solutions for the LMG model Hamiltonian based on the Bethe ansatz. *Nucl. Phys. B*, 737 (3):337–350, March 2006. ISSN 0550-3213. doi: 10.1016/j.nuclphysb.2006.01.015. URL http://www.sciencedirect.com/science/article/pii/S0550321306000289.

[31] R. Botet, R. Jullien, and P. Pfeuty. Size Scaling for Infinitely Coordinated Systems. *Phys. Rev. Lett.*, 49(7):478–481, August 1982. ISSN 0031-9007. doi: 10.1103/PhysRevLett.49.478. URL https://link.aps.org/doi/10.1103/PhysRevLett.49.478.

[32] Jan C. Louw, Johannes N. Kriel, and Michael Kastner. Thermalization of a Lipkin-Meshkov-Glick model coupled to a bosonic bath. *Phys. Rev. A*, 100(2):022115, August 2019. doi: 10.1103/PhysRevA.100.022115. URL https://link.aps.org/doi/10.1103/PhysRevA.100.022115.

[33] Paraj Titum and Mohammad F. Maghrebi. Nonequilibrium Criticality in Quench Dynamics of Long-Range Spin Models. *Phys. Rev. Lett.*, 125(4):040602, July 2020. doi: 10.1103/PhysRevLett.125.040602. URL https://link.aps.org/doi/10.1103/PhysRevLett.125.040602.

[34] Alessio Lerose, Bojan Žunkovič, Jamir Marino, Andrea Gambassi, and Alessandro Silva. Impact of nonequilibrium fluctuations on prethermal dynamical phase transitions in long-range interacting spin chains. *Phys. Rev. B*, 99(4):045128, January 2019. doi: 10.1103/PhysRevB.99.045128. URL https://link.aps.org/doi/10.1103/PhysRevB.99.045128.

[35] Andrew J. Daley. Quantum trajectories and open many-body quantum systems. *Advances in Physics*, 63(2):77–149, March 2014. ISSN 0001-8732. doi: 10.1080/00018732.2014.933502. URL https://doi.org/10.1080/00018732.2014.933502. Publisher: Taylor & Francis _eprint: https://doi.org/10.1080/00018732.2014.933502.

[36] John D. Dixon and Brian Mortimer. *Permutation Groups*, volume 163 of *Graduate Texts in Mathematics*. Springer, New York, NY, 1996. ISBN 978-1-4612-6885-7 978-1-4612-0731-3. doi: 10.1007/978-1-4612-0731-3. URL http://link.springer.com/10.1007/978-1-4612-0731-3.

[37] P. D. Nation. Steady-state solution methods for open quantum optical systems. *arXiv:1504.06768*, April 2015. URL http://arxiv.org/abs/1504.06768.

[38] A. Schwarzenberg-Czerny. On matrix factorization and efficient least squares solution. *Astronomy and Astrophysics Supplement Series*, 110:405, April 1995. ISSN 0365-0138.

URL https://ui.adsabs.harvard.edu/abs/1995A&AS..110..405S/abstract.

[39] H. A. van der Vorst. Bi-CGSTAB: A Fast and Smoothly Converging Variant of Bi-CG for the Solution of Nonsymmetric Linear Systems. *SIAM J. Sci. and Stat. Comput.*, 13(2):631–644, March 1992. ISSN 0196-5204. doi: 10.1137/0913035. URL https://epubs.siam.org/doi/10.1137/0913035. Publisher: Society for Industrial and Applied Mathematics.

[40] Yuan Zhang, Yu-Xiang Zhang, and Klaus Mølmer. Monte-Carlo simulations of superradiant lasing. 20(11):112001, November 2018. ISSN 1367-2630. doi: 10.1088/1367-2630/aaec36. URL https://doi.org/10.1088/1367-2630/aaec36. Publisher: IOP Publishing.

[41] Bradley A. Chase and J. M. Geremia. Collective processes of an ensemble of spin-$1/2$ particles. *Phys. Rev. A*, 78(5):052101, November 2008. doi: 10.1103/PhysRevA.78.052101. URL https://link.aps.org/doi/10.1103/PhysRevA.78.052101. Publisher: American Physical Society.

[42] Ben Q. Baragiola, Bradley A. Chase, and JM Geremia. Collective uncertainty in partially polarized and partially decohered spin-$\frac{1}{2}$ systems. *Phys. Rev. A*, 81(3):032104, March 2010. doi: 10.1103/PhysRevA.81.032104. URL https://link.aps.org/doi/10.1103/PhysRevA.81.032104. Publisher: American Physical Society.

[43] P. M. Chaikin and T. C. Lubensky. *Principles of Condensed Matter Physics*. Cambridge University Press, September 2000. ISBN 978-0-521-79450-3. Google-Books-ID: P9YjNjzr9OIC.

[44] Jan Gelhausen, Michael Buchhold, and Philipp Strack. Many-body quantum optics with decaying atomic spin states: ($\ensuremath{\gamma}, \ensuremath{\kappa}$) Dicke model. *Phys. Rev. A*, 95(6):063824, June 2017. doi: 10.1103/PhysRevA.95.063824. URL https://link.aps.org/doi/10.1103/PhysRevA.95.063824.

[45] Alessio Chiocchetta, Marco Tavora, Andrea Gambassi, and Aditi Mitra. Short-time universal scaling in an isolated quantum system after a quench. *Phys. Rev. B*, 91(22):220302, June 2015. doi: 10.1103/PhysRevB.91.220302. URL https://link.aps.org/doi/10.1103/PhysRevB.91.220302.

[46] D. Adu Smith, M. Gring, T. Langen, M. Kuhnert, B. Rauer, R. Geiger, T. Kitagawa, I. Mazets, E. Demler, and J. Schmiedmayer. Prethermalization revealed by the relaxation dynamics of full distribution functions. *New J. Phys.*, 15(7):075011, July 2013. ISSN 1367-2630. doi: 10.1088/1367-2630/15/7/075011. URL https://doi.org/10.1088%2F1367-2630%2F15%2F7%2F075011.

[47] Michael Foss-Feig, Jeremy T. Young, Victor V. Albert, Alexey V. Gorshkov, and Mohammad F. Maghrebi. Solvable Family of Driven-Dissipative Many-Body Systems. *Phys. Rev. Lett.*, 119(19):190402, November 2017. doi: 10.1103/PhysRevLett.119.190402. URL https://link.aps.org/doi/10.1103/PhysRevLett.119.190402.

[48] Uwe C. Täuber. *Critical Dynamics: A Field Theory Approach to Equilibrium and Non-Equilibrium Scaling Behavior*. March 2014. ISBN 978-1-139-86720-7.

[49] R. Botet and R. Jullien. Large-size critical behavior of infinitely coordinated systems. *Phys. Rev. B*, 28(7):3955–3967, October 1983. doi: 10.1103/PhysRevB.28.3955. URL https://link.aps.org/doi/10.1103/PhysRevB.28.3955.

[50] John Cardy. *Scaling and Renormalization in Statistical Physics*. April 1996. ISBN 978-0-521-49959-0.

[51] Daniel A. Paz and Mohammad F. Maghrebi. Critical Dynamics of Weakly-Dissipative Driven Systems. *arXiv:1906.08278 [cond-mat, physics:physics, physics:quant-ph]*, June 2019. URL http://arxiv.org/abs/1906.08278. arXiv: 1906.08278.

[52] Subir Sachdev. Quantum Phase Transitions, April 2011. URL /core/books/quantum-phase-transitions/33C1C81500346005E54C1DE4223E5562.

[53] Florian Lange, Zala Lenarčič, and Achim Rosch. Pumping approximately integrable systems. *Nat. Commun.*, 8:15767, June 2017. ISSN 2041-1723. doi: 10.1038/ncomms15767. URL https://www.nature.com/articles/ncomms15767.

[54] Florian Lange, Zala Lenarčič, and Achim Rosch. Time-dependent generalized Gibbs ensembles in open quantum systems. *Phys. Rev. B*, 97(16):165138, April 2018. doi: 10.1103/PhysRevB.97.165138. URL https://link.aps.org/doi/10.1103/PhysRevB.97.165138.

[55] Zala Lenarčič, Florian Lange, and Achim Rosch. Perturbative approach to weakly driven many-particle systems in the presence of approximate conservation laws. *Phys. Rev. B*, 97(2):024302, January 2018. doi: 10.1103/PhysRevB.97.024302. URL https://link.aps.org/doi/10.1103/PhysRevB.97.024302.

[56] Tatsuhiko Shirai and Takashi Mori. Thermalization in open many-body systems based on eigenstate thermalization hypothesis. *Phys. Rev. E*, 101(4):042116, April 2020. doi: 10.1103/PhysRevE.101.042116. URL https://link.aps.org/doi/10.1103/PhysRevE.101.042116.

[57] Suhk Kun Oh and Kang, Hee Jae. Monte Carlo steps per spin vs. time in the master equation: Glauber kinetics for the infinite-range ising model. *J. Korean Phy. Soc.*, 47(1):6–12, 2005. ISSN ISSN 0374-4884. URL http://inis.iaea.org/Search/search.aspx?orig_q=RN:42074612.

[58] P. C. Hohenberg and B. I. Halperin. Theory of dynamic critical phenomena. *Rev. Mod. Phys.*, 49(3):435–479, July 1977. doi: 10.1103/RevModPhys.49.435. URL https://link.aps.org/doi/10.1103/RevModPhys.49.435.

[59] Mohammad F. Maghrebi and Alexey V. Gorshkov. Nonequilibrium many-body steady states via Keldysh formalism. *Phys. Rev. B*, 93(1):014307, January 2016. doi: 10.1103/PhysRevB.93.014307. URL https://link.aps.org/doi/10.1103/PhysRevB.93.014307.

[60] E. T. Owen, J. Jin, D. Rossini, R. Fazio, and M. J. Hartmann. Quantum correlations and limit cycles in the driven-dissipative Heisenberg lattice. *New J. Phys.*, 20(4):045004, April 2018. ISSN 1367-2630. doi: 10.1088/1367-2630/aab7d3. URL https://doi.org/10.1088%2F1367-2630%2Faab7d3.

[61] Ching-Kit Chan, Tony E. Lee, and Sarang Gopalakrishnan. Limit-cycle phase in driven-dissipative spin systems. *Phys. Rev. A*, 91(5):051601, May 2015. doi: 10.1103/PhysRevA.91.051601. URL https://link.aps.org/doi/10.1103/PhysRevA.91.051601.

[62] Ryan M. Wilson, Khan W. Mahmud, Anzi Hu, Alexey V. Gorshkov, Mohammad Hafezi, and Michael Foss-Feig. Collective phases of strongly interacting cavity photons. *Phys. Rev. A*, 94(3):033801, September 2016. doi: 10.1103/PhysRevA.94.033801. URL https://link.aps.org/doi/10.1103/PhysRevA.94.033801.

[63] Alexandre Le Boité, Giuliano Orso, and Cristiano Ciuti. Steady-State Phases and Tunneling-Induced Instabilities in the Driven Dissipative Bose-Hubbard Model. *Phys. Rev. Lett.*, 110 (23):233601, June 2013. doi: 10.1103/PhysRevLett.110.233601. URL https://link.aps.org/doi/10.1103/PhysRevLett.110.233601.

[64] M. Foss-Feig, P. Niroula, J. T. Young, M. Hafezi, A. V. Gorshkov, R. M. Wilson, and M. F. Maghrebi. Emergent equilibrium in many-body optical bistability. *Phys. Rev. A*, 95(4): 043826, April 2017. doi: 10.1103/PhysRevA.95.043826. URL https://link.aps.org/doi/10.1103/PhysRevA.95.043826.

[65] Filippo Vicentini, Fabrizio Minganti, Riccardo Rota, Giuliano Orso, and Cristiano Ciuti. Critical slowing down in driven-dissipative Bose-Hubbard lattices. *Phys. Rev. A*, 97(1): 013853, January 2018. doi: 10.1103/PhysRevA.97.013853. URL https://link.aps.org/doi/10.1103/PhysRevA.97.013853.

[66] Vincent R. Overbeck, Mohammad F. Maghrebi, Alexey V. Gorshkov, and Hendrik Weimer. Multicritical behavior in dissipative Ising models. *Phys. Rev. A*, 95(4):042133, April 2017. doi: 10.1103/PhysRevA.95.042133. URL https://link.aps.org/doi/10.1103/PhysRevA.95.042133.

[67] Aditi Mitra, So Takei, Yong Baek Kim, and A. J. Millis. Nonequilibrium Quantum Criticality in Open Electronic Systems. *Phys. Rev. Lett.*, 97(23):236808, December 2006. doi: 10.1103/PhysRevLett.97.236808. URL https://link.aps.org/doi/10.1103/PhysRevLett.97.236808.

[68] M. Wouters and I. Carusotto. Absence of long-range coherence in the parametric emission of photonic wires. *Phys. Rev. B*, 74(24):245316, December 2006. doi: 10.1103/PhysRevB.

74.245316. URL https://link.aps.org/doi/10.1103/PhysRevB.74.245316.

[69] Jeremy T. Young, Alexey V. Gorshkov, Michael Foss-Feig, and Mohammad F. Maghrebi. Nonequilibrium Fixed Points of Coupled Ising Models. *Phys. Rev. X*, 10(1):011039, February 2020. doi: 10.1103/PhysRevX.10.011039. URL https://link.aps.org/doi/10.1103/PhysRevX.10.011039.

[70] Jamir Marino and Sebastian Diehl. Quantum dynamical field theory for nonequilibrium phase transitions in driven open systems. *Phys. Rev. B*, 94(8):085150, August 2016. doi: 10.1103/PhysRevB.94.085150. URL https://link.aps.org/doi/10.1103/PhysRevB.94.085150. Publisher: American Physical Society.

[71] Riccardo Rota, Fabrizio Minganti, Cristiano Ciuti, and Vincenzo Savona. Quantum Critical Regime in a Quadratically Driven Nonlinear Photonic Lattice. *Phys. Rev. Lett.*, 122(11):110405, March 2019. doi: 10.1103/PhysRevLett.122.110405. URL https://link.aps.org/doi/10.1103/PhysRevLett.122.110405.

[72] Hannes Risken. *The Focker-Planck Equation*. Springer, Berlin, Heidelberg. ISBN 978-3-540-61530-9.

[73] Alessio Lerose, Jamir Marino, Bojan Žunkovič, Andrea Gambassi, and Alessandro Silva. Chaotic Dynamical Ferromagnetic Phase Induced by Nonequilibrium Quantum Fluctuations. *Phys. Rev. Lett.*, 120(13):130603, March 2018. doi: 10.1103/PhysRevLett.120.130603. URL https://link.aps.org/doi/10.1103/PhysRevLett.120.130603.

[74] Bihui Zhu, Jamir Marino, Norman Y. Yao, Mikhail D. Lukin, and Eugene A. Demler. Dicke time crystals in driven-dissipative quantum many-body systems. *New J. Phys.*, 21(7):073028, July 2019. ISSN 1367-2630. doi: 10.1088/1367-2630/ab2afe. URL https://doi.org/10.1088%2F1367-2630%2Fab2afe.

[75] Robert Zwanzig. *Nonequilibrium Statistical Mechanics*. Oxford University Press, April 2001. ISBN 978-0-19-803215-1. Google-Books-ID: 4cI5136OdoMC.

[76] Mohammad F. Maghrebi, Matthias Krüger, and Mehran Kardar. Flight of a heavy particle nonlinearly coupled to a quantum bath. *Phys. Rev. B*, 93(1):014309, January 2016. doi: 10.1103/PhysRevB.93.014309. URL https://link.aps.org/doi/10.1103/PhysRevB.93.014309. Publisher: American Physical Society.

[77] S.R. De Groot and P. Mazur. *Non-equilibrium thermodynamics*. Dover Publications, 1984.

[78] Robert Zwanzig. *Nonequilibrium statistical mechanics*. Oxford University Press, 2001.

[79] G. S. Agarwal. Open quantum Markovian systems and the microreversibility. *Z. Physik*, 258(5):409–422, October 1973. ISSN 0939-7922. doi: 10.1007/BF01391504. URL https://doi.org/10.1007/BF01391504.

[80] HJ Carmichael and DF Walls. Detailed balance in open quantum markoffian systems. *Z. Phys. B*, 23(3):299–306, 1976. doi: 10.1007/BF01318974.

[81] Robert Alicki and K. Lendi. *Quantum Dynamical Semigroups and Applications*. Lecture Notes in Physics. Springer-Verlag, Berlin Heidelberg, 2007. ISBN 978-3-540-70860-5. doi: 10.1007/3-540-70861-8. URL https://www.springer.com/gp/book/9783540708605.

[82] Giulio Biroli. Slow relaxations and nonequilibrium dynamics in classical and quantum systems. In Thierry Giamarchi, Andrew J Millis, Olivier Parcollet, Hubert Saleur, and Leticia F Cugliandolo, editors, *Strongly Interacting Quantum Systems out of Equilibrium: Lecture Notes of the Les Houches Summer School: Volume 99, August 2012*, volume 99, chapter 3, pages 207–264. Oxford University Press, 2016. doi: 10.1093/acprof:oso/9780198768166.001.0001.

[83] A. Denisov, H. M. Castro-Beltran, and H. J. Carmichael. Time-Asymmetric Fluctuations of Light and the Breakdown of Detailed Balance. *Phys. Rev. Lett.*, 88(24):243601, May 2002. doi: 10.1103/PhysRevLett.88.243601. URL https://link.aps.org/doi/10.1103/PhysRevLett.88.243601.

[84] Ehud Altman, Lukas M. Sieberer, Leiming Chen, Sebastian Diehl, and John Toner. Two-dimensional superfluidity of exciton polaritons requires strong anisotropy. *Phys. Rev. X*, 5:011017, Feb 2015. doi: 10.1103/PhysRevX.5.011017. URL https://link.aps.org/doi/10.1103/PhysRevX.5.011017.

[85] Jamir Marino and Sebastian Diehl. Driven markovian quantum criticality. *Phys. Rev. Lett.*, 116:070407, Feb 2016. doi: 10.1103/PhysRevLett.116.070407. URL https://link.aps.org/doi/10.1103/PhysRevLett.116.070407.

[86] H. F. H. Cheung, Y. S. Patil, and M. Vengalattore. Emergent phases and critical behavior in a non-markovian open quantum system. *Phys. Rev. A*, 97:052116, May 2018. doi: 10.1103/PhysRevA.97.052116. URL https://link.aps.org/doi/10.1103/PhysRevA.97.052116.

[87] Emanuele G Dalla Torre, Eugene Demler, Thierry Giamarchi, and Ehud Altman. Quantum critical states and phase transitions in the presence of non-equilibrium noise. *Nat. Phys.*, 6(10):806–810, 2010. doi: 10.1038/nphys1754.

[88] Tony E. Lee, Sarang Gopalakrishnan, and Mikhail D. Lukin. Unconventional magnetism via optical pumping of interacting spin systems. *Phys. Rev. Lett.*, 110:257204, Jun 2013. doi: 10.1103/PhysRevLett.110.257204. URL https://link.aps.org/doi/10.1103/PhysRevLett.110.257204.

[89] Mohammad F. Maghrebi and Alexey V. Gorshkov. Nonequilibrium many-body steady states via Keldysh formalism. *Phys. Rev. B*, 93(1):014307, January 2016. doi: 10.1103/PhysRevB.

93.014307. URL https://link.aps.org/doi/10.1103/PhysRevB.93.014307.

[90] Luca Peliti. *Statistical mechanics in a nutshell*, volume 10. Princeton University Press, 2011. doi: 10.1515/9781400839360.

[91] H. K. Janssen. On the renormalized field theory of nonlinear critical relaxation. In *From Phase Transitions to Chaos*, pages 68–91. WORLD SCIENTIFIC, April 1992. ISBN 978-981-02-0938-4. doi: 10.1142/9789814355872_0007. URL https://www.worldscientific.com/doi/abs/10.1142/9789814355872_0007.

[92] Ferdinand Brennecke, Rafael Mottl, Kristian Baumann, Renate Landig, Tobias Donner, and Tilman Esslinger. Real-time observation of fluctuations at the driven-dissipative dicke phase transition. *Proceedings of the National Academy of Sciences*, 110(29):11763–11767, 2013. ISSN 0027-8424. doi: 10.1073/pnas.1306993110. URL http://www.pnas.org/content/110/29/11763.

[93] Dainius Kilda and Jonathan Keeling. Fluorescence Spectrum and Thermalization in a Driven Coupled Cavity Array. *Phys. Rev. Lett.*, 122(4):043602, February 2019. ISSN 0031-9007, 1079-7114. doi: 10.1103/PhysRevLett.122.043602. URL https://link.aps.org/doi/10.1103/PhysRevLett.122.043602.

[94] Daniel A. Paz and Mohammad F. Maghrebi. Driven-dissipative Ising model: Dynamical crossover at weak dissipation. *arXiv:1906.08278*, January 2021. URL http://arxiv.org/abs/1906.08278.

[95] L. M. Sieberer, A. Chiocchetta, A. Gambassi, U. C. Täuber, and S. Diehl. Thermodynamic equilibrium as a symmetry of the Schwinger-Keldysh action. *Phys. Rev. B*, 92(13):134307, October 2015. doi: 10.1103/PhysRevB.92.134307. URL https://link.aps.org/doi/10.1103/PhysRevB.92.134307.

[96] Camille Aron, Giulio Biroli, and Leticia F. Cugliandolo. (Non) equilibrium dynamics: a (broken) symmetry of the Keldysh generating functional. *SciPost Phys.*, 4:008, 2018. doi: 10.21468/SciPostPhys.4.1.008. URL https://scipost.org/10.21468/SciPostPhys.4.1.008.

[97] H.J. Carmichael. Breakdown of Photon Blockade: A Dissipative Quantum Phase Transition in Zero Dimensions. *Phys. Rev. X*, 5(3):031028, September 2015. doi: 10.1103/PhysRevX.5.031028. URL https://link.aps.org/doi/10.1103/PhysRevX.5.031028.

[98] Daniel A. Paz and Mohammad F. Maghrebi. Driven-dissipative Ising Model: An exact field-theoretical analysis. *arXiv:2101.05297*, January 2021. URL http://arxiv.org/abs/2101.05297.

[99] Albert Messiah. *Quantum mechanics: volume II*. North-Holland Publishing Company Amsterdam, 1962.

[100] Ryszard Horodecki, Paweł Horodecki, Michał Horodecki, and Karol Horodecki. Quantum entanglement. *Rev. Mod. Phys.*, 81(2):865–942, June 2009. doi: 10.1103/RevModPhys.81.865. URL https://link.aps.org/doi/10.1103/RevModPhys.81.865. Publisher: American Physical Society.

[101] ShengChao Ding and Zhi Jin. Review on the study of entanglement in quantum computation speedup. *CHINESE SCI BULL*, 52(16):2161–2166, August 2007. ISSN 1861-9541. doi: 10.1007/s11434-007-0324-8. URL https://doi.org/10.1007/s11434-007-0324-8.

[102] He-Liang Huang, Dachao Wu, Daojin Fan, and Xiaobo Zhu. Superconducting quantum computing: a review. *Sci. China Inf. Sci.*, 63(8):180501, July 2020. ISSN 1869-1919. doi: 10.1007/s11432-020-2881-9. URL https://doi.org/10.1007/s11432-020-2881-9.

[103] I.M. Georgescu, S. Ashhab, and Franco Nori. Quantum simulation. *Rev. Mod. Phys.*, 86 (1):153–185, March 2014. doi: 10.1103/RevModPhys.86.153. URL https://link.aps.org/doi/10.1103/RevModPhys.86.153. Publisher: American Physical Society.

[104] Vittorio Giovannetti, Seth Lloyd, and Lorenzo Maccone. Quantum Metrology. *Phys. Rev. Lett.*, 96(1):010401, January 2006. doi: 10.1103/PhysRevLett.96.010401. URL https://link.aps.org/doi/10.1103/PhysRevLett.96.010401. Publisher: American Physical Society.

[105] Vittorio Giovannetti, Seth Lloyd, and Lorenzo Maccone. Advances in quantum metrology. *Nature Photon*, 5(4):222–229, April 2011. ISSN 1749-4893. doi: 10.1038/nphoton.2011.35. URL http://www.nature.com/articles/nphoton.2011.35. Bandiera_abtest: a Cg_type: Nature Research Journals Number: 4 Primary_atype: Reviews Publisher: Nature Publishing Group Subject_term: Optical metrology;Quantum optics Subject_term_id: optical-metrology;quantum-optics.

[106] Hanna Krauter, Christine A. Muschik, Kasper Jensen, Wojciech Wasilewski, Jonas M. Petersen, J. Ignacio Cirac, and Eugene S. Polzik. Entanglement Generated by Dissipation and Steady State Entanglement of Two Macroscopic Objects. *Phys. Rev. Lett.*, 107(8): 080503, August 2011. doi: 10.1103/PhysRevLett.107.080503. URL https://link.aps.org/doi/10.1103/PhysRevLett.107.080503. Publisher: American Physical Society.

[107] S. Zippilli, M. Paternostro, G. Adesso, and F. Illuminati. Entanglement Replication in Driven Dissipative Many-Body systems. *Phys. Rev. Lett.*, 110(4):040503, January 2013. doi: 10.1103/PhysRevLett.110.040503. URL https://link.aps.org/doi/10.1103/PhysRevLett.110.040503. Publisher: American Physical Society.

[108] Y. Lin, J. P. Gaebler, F. Reiter, T. R. Tan, R. Bowler, A. S. Sørensen, D. Leibfried, and D. J. Wineland. Dissipative production of a maximally entangled steady state of two quantum bits. *Nature; London*, 504(7480):415–8, December 2013. ISSN 00280836. URL http://search.proquest.com/docview/1470880215/abstract/96D6BAA3D16D45B1PQ/1.

[109] Y. Liu, S. Shankar, N. Ofek, M. Hatridge, A. Narla, K.M. Sliwa, L. Frunzio, R.J. Schoelkopf, and M.H. Devoret. Comparing and Combining Measurement-Based and Driven-Dissipative Entanglement Stabilization. *Phys. Rev. X*, 6(1):011022, March 2016. doi: 10.1103/PhysRevX.6.011022. URL https://link.aps.org/doi/10.1103/PhysRevX.6.011022. Publisher: American Physical Society.

[110] Mario Boneberg, Igor Lesanovsky, and Federico Carollo. Quantum fluctuations and correlations in open quantum Dicke models. *arXiv:2110.13191 [cond-mat, physics:quant-ph]*, October 2021. URL http://arxiv.org/abs/2110.13191. arXiv: 2110.13191.

[111] M. B. Plenio. Logarithmic Negativity: A Full Entanglement Monotone That is not Convex. *Phys. Rev. Lett.*, 95(9):090503, August 2005. ISSN 0031-9007, 1079-7114. doi: 10.1103/PhysRevLett.95.090503. URL https://link.aps.org/doi/10.1103/PhysRevLett.95.090503.

[112] Jian Ma and Xiaoguang Wang. Fisher information and spin squeezing in the Lipkin-Meshkov-Glick model. *Phys. Rev. A*, 80(1):012318, July 2009. doi: 10.1103/PhysRevA.80.012318. URL https://link.aps.org/doi/10.1103/PhysRevA.80.012318. Publisher: American Physical Society.

[113] Philipp Hyllus, Wiesław Laskowski, Roland Krischek, Christian Schwemmer, Witlef Wieczorek, Harald Weinfurter, Luca Pezzé, and Augusto Smerzi. Fisher information and multiparticle entanglement. *Phys. Rev. A*, 85(2):022321, February 2012. doi: 10.1103/PhysRevA.85.022321. URL https://link.aps.org/doi/10.1103/PhysRevA.85.022321. Publisher: American Physical Society.

[114] Nan Li and Shunlong Luo. Entanglement detection via quantum Fisher information. *Phys. Rev. A*, 88(1):014301, July 2013. ISSN 1050-2947, 1094-1622. doi: 10.1103/PhysRevA.88.014301. URL https://link.aps.org/doi/10.1103/PhysRevA.88.014301.

[115] Géza Tóth. Multipartite entanglement and high-precision metrology. *Phys. Rev. A*, 85(2):022322, February 2012. doi: 10.1103/PhysRevA.85.022322. URL https://link.aps.org/doi/10.1103/PhysRevA.85.022322. Publisher: American Physical Society.

[116] Philipp Hauke, Markus Heyl, Luca Tagliacozzo, and Peter Zoller. Measuring multipartite entanglement through dynamic susceptibilities. *Nature Phys*, 12(8):778–782, August 2016. ISSN 1745-2481. doi: 10.1038/nphys3700. URL https://www.nature.com/articles/nphys3700. Bandiera_abtest: a Cg_type: Nature Research Journals Number: 8 Primary_atype: Research Publisher: Nature Publishing Group Subject_term: Phase transitions and critical phenomena;Quantum information;Quantum metrology;Ultracold gases Subject_term_id: phase-transitions-and-critical-phenomena;quantum-information;quantum-metrology;ultracold-gases.

[117] Géza Tóth and Iagoba Apellaniz. Quantum metrology from a quantum information science perspective. *J. Phys. A: Math. Theor.*, 47(42):424006, October 2014. ISSN 1751-8121. doi:

10.1088/1751-8113/47/42/424006. URL https://doi.org/10.1088/1751-8113/47/42/424006. Publisher: IOP Publishing.

[118] Christian Gross. Spin squeezing, entanglement and quantum metrology with Bose–Einstein condensates. *J. Phys. B: At. Mol. Opt. Phys.*, 45(10):103001, May 2012. ISSN 0953-4075. doi: 10.1088/0953-4075/45/10/103001. URL https://doi.org/10.1088/0953-4075/45/10/103001. Publisher: IOP Publishing.

[119] Jian Ma, Xiaoguang Wang, C. P. Sun, and Franco Nori. Quantum spin squeezing. *Physics Reports*, 509(2):89–165, December 2011. ISSN 0370-1573. doi: 10.1016/j.physrep.2011.08.003. URL https://www.sciencedirect.com/science/article/pii/S0370157311002201.

[120] Ingo Peschel. Calculation of reduced density matrices from correlation functions. *J. Phys. A: Math. Gen.*, 36(14):L205–L208, April 2003. ISSN 0305-4470, 1361-6447. doi: 10.1088/0305-4470/36/14/101. URL http://arxiv.org/abs/cond-mat/0212631.

[121] Alessio Serafini, Fabrizio Illuminati, and Silvio De Siena. Symplectic invariants, entropic measures and correlations of Gaussian states. *J. Phys. B: At. Mol. Opt. Phys.*, 37(2):L21–L28, December 2003. ISSN 0953-4075. doi: 10.1088/0953-4075/37/2/L02. URL https://doi.org/10.1088%2F0953-4075%2F37%2F2%2Fl02.

[122] Gerardo Adesso, Alessio Serafini, and Fabrizio Illuminati. Extremal entanglement and mixedness in continuous variable systems. *Phys. Rev. A*, 70(2):022318, August 2004. doi: 10.1103/PhysRevA.70.022318. URL https://link.aps.org/doi/10.1103/PhysRevA.70.022318.

[123] Ingo Peschel and Viktor Eisler. Reduced density matrices and entanglement entropy in free lattice models. *J. Phys. A: Math. Theor.*, 42(50):504003, December 2009. ISSN 1751-8113, 1751-8121. doi: 10.1088/1751-8113/42/50/504003. URL http://arxiv.org/abs/0906.1663.

[124] Viktor Eisler and Zoltan Zimboras. Entanglement negativity in the harmonic chain out of equilibrium. *New J. Phys.*, 16(12):123020, December 2014. ISSN 1367-2630. doi: http://arxiv.org/abs/0906.1663. URL http://arxiv.org/abs/1406.5474.

[125] Dominik Šafránek and Ivette Fuentes. Optimal probe states for the estimation of Gaussian unitary channels. *Phys. Rev. A*, 94(6):062313, December 2016. doi: 10.1103/PhysRevA.94.062313. URL https://link.aps.org/doi/10.1103/PhysRevA.94.062313. Publisher: American Physical Society.

[126] Yaodong Li, Xiao Chen, and Matthew P. A. Fisher. Measurement-driven entanglement transition in hybrid quantum circuits. *Phys. Rev. B*, 100(13):134306, October 2019. doi: 10.1103/PhysRevB.100.134306. URL https://link.aps.org/doi/10.1103/PhysRevB.100.134306. Publisher: American Physical Society.

[127] Michael J. Gullans and David A. Huse. Dynamical Purification Phase Transition Induced by Quantum Measurements. *Phys. Rev. X*, 10(4):041020, October 2020. doi: 10.1103/PhysRevX.10.041020. URL https://link.aps.org/doi/10.1103/PhysRevX.10.041020. Publisher: American Physical Society.

[128] Daniel A. Paz and Mohammad F. Maghrebi. Time-reversal symmetry breaking and emergence in driven-dissipative Ising models. *arXiv:2105.12747 [cond-mat]*, September 2021. URL http://arxiv.org/abs/2105.12747. arXiv: 2105.12747.

[129] Thomas Barthel, Sébastien Dusuel, and Julien Vidal. Entanglement Entropy beyond the Free Case. *Phys. Rev. Lett.*, 97(22):220402, November 2006. doi: 10.1103/PhysRevLett.97.220402. URL https://link.aps.org/doi/10.1103/PhysRevLett.97.220402.

[130] Johannes Wilms, Julien Vidal, Frank Verstraete, and Sébastien Dusuel. Finite-temperature mutual information in a simple phase transition. *J. Stat. Mech.*, 2012(01):P01023, January 2012. ISSN 1742-5468. doi: 10.1088/1742-5468/2012/01/P01023. URL https://doi.org/10.1088%2F1742-5468%2F2012%2F01%2Fp01023.

[131] Matteo Ippoliti, Michael J. Gullans, Sarang Gopalakrishnan, David A. Huse, and Vedika Khemani. Entanglement Phase Transitions in Measurement-Only Dynamics. *Phys. Rev. X*, 11(1):011030, February 2021. doi: 10.1103/PhysRevX.11.011030. URL https://link.aps.org/doi/10.1103/PhysRevX.11.011030. Publisher: American Physical Society.

[132] Matteo Ippoliti and Vedika Khemani. Postselection-Free Entanglement Dynamics via Spacetime Duality. *Phys. Rev. Lett.*, 126(6):060501, February 2021. doi: 10.1103/PhysRevLett.126.060501. URL https://link.aps.org/doi/10.1103/PhysRevLett.126.060501. Publisher: American Physical Society.

[133] Michael M. Wolf, Frank Verstraete, Matthew B. Hastings, and J. Ignacio Cirac. Area Laws in Quantum Systems: Mutual Information and Correlations. *Phys. Rev. Lett.*, 100(7):070502, February 2008. doi: 10.1103/PhysRevLett.100.070502. URL https://link.aps.org/doi/10.1103/PhysRevLett.100.070502. Publisher: American Physical Society.

[134] G. Vidal and R. F. Werner. Computable measure of entanglement. *Phys. Rev. A*, 65(3):032314, February 2002. doi: 10.1103/PhysRevA.65.032314. URL https://link.aps.org/doi/10.1103/PhysRevA.65.032314.

[135] H. Wichterich, J. Vidal, and S. Bose. Universality of the negativity in the Lipkin-Meshkov-Glick model. *Phys. Rev. A*, 81(3):032311, March 2010. ISSN 1050-2947, 1094-1622. doi: 10.1103/PhysRevA.81.032311. URL http://arxiv.org/abs/0910.1011.

[136] Tsung-Cheng Lu and Tarun Grover. Singularity in Entanglement Negativity Across Finite Temperature Phase Transitions. *Phys. Rev. B*, 99(7):075157, February 2019. ISSN 2469-9950, 2469-9969. doi: 10.1103/PhysRevB.99.075157. URL http://arxiv.org/abs/1808.04381.